ytterbium- & erbium-doped silica for planar waveguide lasers & amplifiers

Dyndgaard, Morten Glarborg

Publication date:
2001

Document Version
Publisher's PDF, also known as Version of record

Ytterbium- and Erbium-Doped Silica for Planar Waveguide Lasers and Amplifiers

Morten Glarborg Dyndgaard

Ph.D. Thesis. March 2001
Research center COM
Technical University of Denmark

Ytterbium- and Erbium-Doped Silica for Planar Waveguide Lasers and Amplifiers

Ph.D Thesis

Morten Glarborg Dyndgaard

March 2001

Research center COM
Technical University of Denmark

The work presented in this thesis was carried out at the Research Center COM (Communications, Optics and Materials) in partial fulfillment of the requirements for the Ph.D. degree from the Technical University of Denmark. The work have been financed by the Danish Technical Research Council under the THOR (Technology by Highy Oriented Research) programme.

Supervisors: Anders Bjarklev, Professor
Jörg Hübner, Associate Professor
Mogens Rysholt Poulsen, Deputy Director

Abstract

The purpose of this work was to demonstrate ytterbium doped planar components, and investigate the possibilities of making erbium/ytterbium codoped planar waveguides in germano-silica glass. Furthermore, tools for modelling lasers and erbium/ytterbium doped amplifiers.

The planar waveguides were fabricated using plasma enhanced chemical vapor deposition (PECVD) and reactive ion etching (RIE). These processes and the control of the film composition is discussed.

Ytterbium doped planar waveguides are demonstrated, and it is shown that codoping with aluminium has a positive influence on the fluorescence intensity of the ytterbium ions. Based on this result ytterbium doped planar waveguides with a net gain of 0.36 dB/cm are made. The glass is sensitive to ultra violet (UV) light, and using UV-writing Bragg gratings are photoimprinted in the waveguides, and a laser is made in a distributed Bragg reflector (DBR) configuration. The laser is shown to have an output power of 19 mW. The results from the laser measurements are in good agreement with the numerical model. The model is then used to propose an improved DBR design optimised with respect to maximum output power.

The influence of ytterbium on the fluorescense of erbium is investigated in germano-siliate and phospho-silicate glass, and it is shown that germano-silicate is inefficient, while phospho-silicate has a very good performance. Based on this conclusion, numerical simulations are made for amplifiers and lasers to estimate the effect of codoping with ytterbium if phospho-silicate glass is used.

Resumé

Formålet med dette Ph.d. projekt var at demonstrere ytterbium doterede planare komponenter, og at undersøge muligheden for at fremstille erbium/ytterbium kodoterede planare bølgeledere i germano-silica glas. Derudover skulle der udvikles værktøjer til at modellere komponenterne.

De planare bølgeledere blev fremstillet vha. PECVD (plasma forstærket deponering fra gasfase) og RIE (ætsning med reaktive ioner). Disse processer samt kontrol af glas sammensætningen bliver diskuteret.

Ytterbium doterede planare bølgeledere bilver demonstreret, og det vises at kodotering med aluminium har en positiv effect på ytterbium ionernes fluorescens intensitet. På baggrund af dette resultat bliver ytterbium doterede planare bølgeledere med et netto gain på 0.36 dB/cm fremstillet. Glasset er følsomt overfor ultra violet (UV) lys, og ved at belyse med UV-lys igennem en fasemaske bliver Bragg gitre indskrevet i bølgelederene, og en laser bliver dermed lavet i en DBR (distribueret Bragg reflektor) konfiguration. Det vises at laserens udgangseffekt er på 19 mW. Resultaterne fra laser målingerne er i god overensstemmelse med relultater opnået med den numeriske model. Modellen bruges dernæst til at optimere desginet af DBR lasere med hensyn til maksimal udgangseffekt.

Indflydelsen af ytterbium på erbium ioners fluorescens bliver undersøgt i germano-silica og phospho-silica, og det vises at germano-silica er ueffektivt mens phospho-silica er særdeles godt. Baseret på denne konklusion, bliver der lavet nummeriske beregninger for forstærkere og lasere med det formål at estimere effekten af at kodotere med ytterbium hvis phospho-silicate glas beliver benyttet.

Acknowledgement

This work was started at the Department of Electromagnetic Systems, and later transferred to Research Center COM. First of all I would like to thank my supervisors Anders Bjarklev, Jörg Hübner and Mogens Rysholt Poulsen for their encouraging and enthusiastic guidance. I also owe great thanks to Thomas Søndergaard for providing the first version of the laser model, and to Martin Ole Berendt and Christian V. Poulsen (IONAS) for many useful discussions on fiber lasers. Christian Laurent-Lund is thanked for helping me with the etching problems, and Søren Guldberg-Kjær for teaching me the ways of the cleanroom and the characterisation lab, and in general for good discussions. Søren also proofread a part of this thesis for which he also deserves great thanks along with the other proof readers Thomas Feuchter and Jesper Arentoft. Furthermore, I would like to thank Andreas Tycho with whom I have shared office and many discussions. I also have to say thank you to the Director of IONAS, Lars Rønn, for directing my attention to this Ph.D. project.

Finally, but most importantly, I would like to thank my family, friends outside DTU, and especially my girlfiend Anikó Zsigri for being so patient with me in the past months where I have been far too busy writing this thesis.

Publications

This thesis is partly based on the work presented in the following international publications.

1. A. Bjarklev, M. G. Dyndgaard, M. O. Berendt, J. Broeng, K. Dridi and J. L. Philipsen, "Spectroscopy of erbium-doped silica", in *Properties, Processing and Applications of Glass and Rare-Earth Doped Glasses for Optical Fibres*, edited by D. Hewak, IEE Books, 1998.

2. M. G. Dyndgaard, T. Søndergaard, J. Broeng, A. Bjarklev, S. Guldberg-Kjær and M. R. Poulsen, "The Effect of Grating Design on the Performance of Erbium-Doped Planar Waveguide Distributed Bragg Reflector Lasers", *Topical Meeting on Optical Amplifiers and Their Applications*, 1999, Paper ThD17.

3. M. G. Dyndgaard, T. Søndergaard, J. Broeng, A. Bjarklev, S. Guldberg-Kjær and M. R. Poulsen, "Design Optimisation of Erbium-Doped Planar Waveguide DBR Lasers", in *OSA Trends in Optics and Photonics (TOPS)*, 1999, vol. 30, pp. 140-146, Optical Society of America.

4. A. Bjarklev, J. Broeng, S. E. Barkou, E. Knudsen, T. Søndergaard, T. W. Berg and M. G. Dyndgaard, "Polarization properties of honeycomb-structured photonic bandgap fibres", Journal of Optics A, vol. 2, no. 6, pp. 584-588, 2000.

5. M. L. Nielsen, M. O. Berendt, A. Bjarklev and M. G. Dyndgaard, "Design of matched cladding fiber with UV-sensitive cladding for minimization of cladding-mode losses in fiber Bragg gratings", Optical Fiber Technology, vol. 6, no. 1, pp. 49-60, 2000.

6. M. G. Dyndgaard, S. Guldberg-Kjær, C. Larent-Lund, M. Rysholt Poulsen and J. Hübner, "Planar waveguide ytterbium laser in Al-doped germanosilicate", *Topical Meeting on Integrated Photonics Research*, 2000, Paper IFH2.

Contents

1 Introduction **1**

2 Ytterbium and Erbium Doped Glass **5**
2.1 Electronic Properties of Rare Earth Elements in Glass . 5
2.2 Optical properties of Ytterbium ions 8
2.2.1 Ytterbium Rate Equations 10
2.3 Optical properties of Erbium 11
2.3.1 Energy Transfer Processes 13
2.3.2 Rate Equations 16

3 Fabrication of Active Planar Waveguides **21**
3.1 Processing using PECVD and RIE 21
3.1.1 Plasma enhanced chemical vapor deposition . . 21
3.1.2 Reactive ion etching 27
3.1.3 Processing steps 30
3.2 Alternative fabrication techniques 31
3.3 Characterisation of waveguides and thin films 34
3.3.1 Setup for characterisation of planar waveguides 34
3.3.2 Setup for characterisation of thin films 35

4 Modelling of Lasers and Amplifiers **37**
4.1 Bragg Grating-Based Lasers 37
4.1.1 UV Induced Bragg Gratings 38
4.1.2 Coupled Mode Theory 39
4.2 Erbium/Ytterbium Doped Amplifiers 43

5 Ytterbium Doped Planar Waveguides **47**
5.1 Influence of Al on the Emission Properties of Yb 48
5.2 Planar Waveguide Amplifiers 53
5.3 Demonstration of an Yb Doped DBR Laser 55

5.4 Optimisation of Laser Design 61
5.4.1 Phaseshift dependence of a DBR laser 62
5.4.2 Asymmetric DBR lasers 69

6 Erbium-Ytterbium doped silica glass 73
6.1 Preliminary measurements 75
6.2 Optimal host glass 75
6.3 Simulations of Er/Yb doped planar waveguides 78
6.3.1 Planar waveguide amplifiers 78
6.3.2 Planar waveguide DBR lasers 84

7 Conclusion 89

Chapter 1

Introduction

The field of telecommunications have experienced a huge growth in the last decades leading to ever increasing demands on bandwidth. This has resulted in the developement of optical fiber technology, as an efficient alternative to the slower electrical based communication. Optical fibres are based on silica which has minimal loss in what is known as the 'third telecommunication window'. This is the main reason for the great success of the erbium doped fiber amplifier (EDFA) since it was first reported in 1987 [1]. EDFAs provide a cheap, efficient way of amplifying signals in long-haul transmission systems, and have also proven very useful in the wavelength division multiplexing (WDM) experiments of the recent years where it provides an efficient means of amplifying several signals at different wavelengths at once with low noise and cross-talk. In this way all-optical networks have become realisable, since there is no need for electrical amplification of each signal, which sets huge limitations on the capacity. With the introduction of WDM networks it has also become necessary to make integrated optical circuits to process the signals in order to avoid the transitions to the electrical domain alltogether. Presently, this type of components are mostly based on semiconductor technology, but due to the incompatibility of the semiconductor materials with the silica glass fibers, glass based integrated optical components have received great attention. This is reflected in the large number of start-up companies that have emerged over the past five years (see *e.g.* [2, 3, 4, 5, 6]).

An example of an integrated optical component that have become necessary with the use of WDM systems, is a lossless power splitter. This type of component is needed for splitting a signal from one input

port to many output ports, and therefore needs some sort of integration with an amplifier. For practical use, a short amplifier with high gain is preferable, and this can *e.g.* be envisioned by usion an erbium doped planar waveguide amplifier (EDWA). However in order to reach the high gain in a short amplifier it is necessary to codope with ytterbium in order to increase the pump efficiency. Furthermore, as an alternative to todays signal sources, the semiconductor lasers, an erbium doped planar waveguide glass laser could be envisioned, but again it is necessary to codope with ytterbium to reach the powerlevels needed for the transmission systems.

The goal of this project was to demonstrate ytterbium doped planar components, and investigate the possibilities of making erbium/ytterbium codoped planar waveguides in germano-silica glass. The choice of germanosilicate was based on the accumulated experience with fabrication of Ge-silicate waveguides, the useful UV sensitivity of this type of glass, and the recent successes with erbium doped planar waveguides [7, 8]. Furthermore, tools for modelling lasers and erbium/ytterbium doped amplifiers should be developed. The first part of the work have been to develop useful processes for incorporating ytterbium in the glass with the aim of maximising the fluorescense intensity and to optimise the etching processes in order to make waveguides of a high optical quality. Then, ytterbium amplifiers and lasers have been investigated, and finally the actual investigations of the Er/Yb codoped system have been done. The modelling have been done in parallel with this work.

In chapter 2 I give a brief description of the optical properties of ytterbium and erbium in glass. The influence of the host material on the energy level structure and the shape of the spectra will be discussed. Furthermore, energy transfer processes for erbium and erbium/ytterbium will be discussed, as will the importance of phonon energies in phonon assisted relaxations. Rate equation models for the ytterbium and erbium/ytterbium systems will also be presented here.

In chapter 3 the fabrication of the ytterbium and erbium doped planar waveguides and thin films is described. The glass thin films have been deposited using plasma enhanced chemical vapor deposition (PECVD) using a liquid delivery system to supply Er, Yb and Al. The principles involved in the deposition will be described, and control of film composition will be discussed. The waveguides are etched using reactive ion etching (RIE), and again the principles in the process will be

described. These technologies will then be compared with some of the other technologies used for fabrication of glass-based integrated optical components, and finally the measurement setups for characterisation of the waveguides and thin films will be descibed.

In chapter 4 I describe the numerical models that have been used for the simulations of Yb and Er/Yb doped components presented in chapter 5 and 6. The first model descibes a laser based on intra-core Bragg gratings such as a distributed feedback (DFB) or distributed bragg reflector (DBR) laser. The lasers presented here are based on UV-written Bragg gratings, and for this reason I will also describe the principle behind UV writing here. The second model describes an Er/Yb doped planar waveguide amplifier.

In chapter 5 the results for ytterbium doped thin films and waveguides are presented. First a study of the influence of aluminium on the emission properties of ytterbium is presented. Based on these results ytterbium doped planar waveguides with net gain in the 1000 - 1100 nm range are made, and these waveguides are then used for fabrication of a DBR laser by UV-writing of Bragg gratings in the photosensitive germanosilica core. Finally I discuss some means of optimising the design of DBR lasers with respect to maximum output power.

In chapter 6 the Er/Yb codoped system is investigated. First, measurements on Er/Yb doped planar waveguides in germanosilica and Er/Yb doped thin films in both germanosilica and phosphosilica are presented. Then, the amplifier and laser models are used to predict the performance of Er/Yb doped components.

Chapter 7 summarises the results presented in this thesis.

Chapter 2

Ytterbium and Erbium Doped Glass

Erbium doped fibers have had great influence on the development of optical communications, and in the recent years also planar components based on erbium doped glass have emerged. Often ytterbium is used as a sensitiser for erbium since it has an absorption band that overlaps with the erbium 980 nm pump band, and the ytterbium absorption cross section is much larger than the erbium absorption cross section at this wavelength. By means of an efficient energy transfer from ytterbium to erbium the pump efficiency can be greatly increased.

In this chapter I will begin by giving a brief introduction to some fundamental properties of rare earth earth elements in glass (section 2.1). Ytterbium has been used both as a single dopant and as a codopant with erbium. In section 2.2 I will talk about the optical properties of ytterbium doped glasses and in section 2.3 I will talk about the optical properties of erbium doped and erbium ytterbium codoped glasses.

2.1 Electronic Properties of Rare Earth Elements in Glass

The rare earths consist of the elements with atomic number $Z = 58$ (Ce) through $Z = 71$ (Lu) and $Z = 90$ (Th) through $Z = 103$ (Lr), constituting the lanthanide and actinide groups. The lanthanides are characterised by the filling of the $4f$-subshell, while the actinides are

characterised by the filling of the $5f$-subshell. Erbium and ytterbium (atomic number 68 and 70 respectively) belong to the lanthanide group, and therefore only the lanthanides are considered here.

Since the radius of the electron wavefunction increases with principal quantum number, n, the electrons in the $n = 4$ shell has a shorter radius than those in the $n = 5$ shell. The radius also increases with orbital angular momentum number, l, but not so strongly, so the $4f$ and $5d$ subshells have approximately the same orbital radius. Lanthanum has the electron configuration $[Xe]5d^16s^2$, where $[Xe]$ refers to the electron configuration of Xenon. However, the next element, cerium, has an electron configuration of $[Xe]4f^26s^2$, and of all the elements in the lanthanide series it is only Ce, Gd and Lu that has a $5d$ electron. For Gd and Lu which lies in the middle and end of the lanthanide series this irregularity occurs because the previous element, Eu and Yb, have a half-filled and full $4f$ subshell, respectively. The $4f$ electrons provides a partial shielding of the outer electrons from the core, and therefore the $4f$ electrons becomes increasingly more tightly confined with increasing Z. For Nd ($Z = 60$) the $4f$ electrons have contracted so much that the maximum of the wavefunctions are within the $5s^25p^6$ closed shells of the Xenon configuration. This is called the lanthanide contraction, and it has the effect that the $4f$ electrons are shielded against the surroundings, and hence, the Lanthanides have a relatively high insensitivity to the host material.

The lanthanides primarily occurs in the +3 oxidation state in chemical compounds, and it is also the trivalent ion that is observed when the lanthanides are used for doping of glasses. When the lanthanides are ionized it is the two $6s$ electrons and a $5d$ or $4f$ electron that is removed.

The available energy levels for a given electron configuration can be determined and labeled using the quantum numbers L, S and J, where L is the total orbital angular momentum, S is the total spin and J is the total angular momentum. The values of these quantum numbers are obtained using the Russell-Saunders (or LS) coupling scheme where the values of L and S are obtained by combining respectively the l, and s values of all electrons, and J is calculated as $J = L+S$. Filled subshells do not contribute in the calculations since the Pauli principle assures that L and S will be zero in this case. Thus the electrons that forms the basis for determining the available states of the lanthanides are the electrons in the $4f$ subshell. This also means that all optical transitions

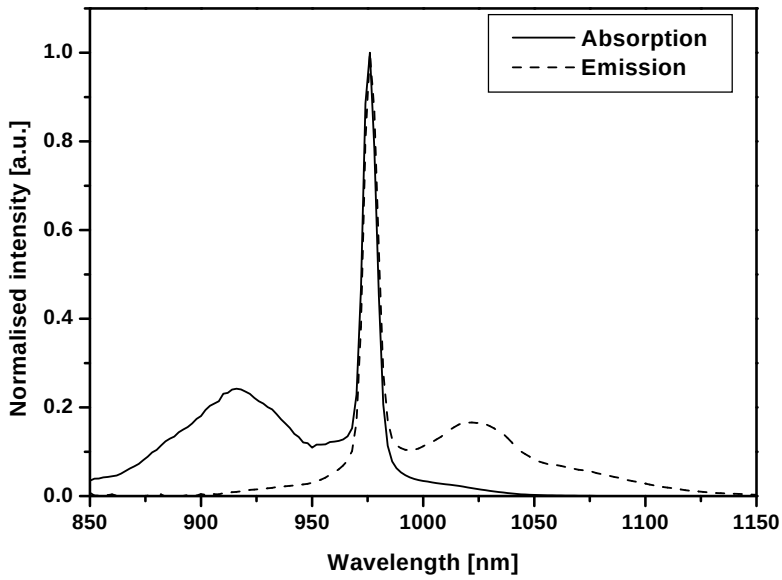

Figure 2.1: *Absorption (full line) and emission (dashed line) spectra of ytterbium in an Al/Ge-silica waveguide.*

take place within this subshell. However, since all the electrons have the same orbital angular momentum quantum number, $l = 3$, this transition is forbidden by the dipole selection rule which demands that $\Delta l = \pm 1$, and this results in long lifetimes for the excited states. When the ions are incorporated in a host material, *e.g.* glass, the local crystal field will cause a further splitting of the terms due to the Stark effect. The local crystal field will also allow mixing of higher order states with the $4f$ - based states and this may enhance the rate for electric dipole transitions between some of the states [9].

In glass, the term 'crystal field' is actually a misnomer, since the glass structure is not crystalline but rather amorphous. This means that there are small differences in the surroundings of each ion, and the emission spectrum becomes a broadened continuous spectrum that can span over as much as 200 nm as can be seen in figure 2.1. The oscillator strengths representing transitions between different components of the Stark-split levels are strongly dependent on the host material, and therefore large differences can be observed in spectra obtained for

different host glasses [10]. The crystal field is furthermore responsible for the observed differences in the lifetimes for rare earths in different host materials. This is due to the vibrational energy in the glass matrix in the vicinity of the rare earth ion which introduces an alternative relaxation path by phonon assisted relaxation. A nonradiative transition occur by the emission of a number of phonons corresponding to the released energy, thus increasing the vibrational energy of the glass (heating). If the energy gap, ΔE, separating the two levels is larger than the energy of the involved phonons, the nonradiative decay rate, W_{nr}, is inversely proportional to the exponential of the energy gap [9, 11]

$$W_{nr} = C[n(T) + 1]^p \mathrm{e}^{(-\alpha \Delta E)}. \tag{2.1}$$

Here, C and α are host-dependent parameters, p is the number of phonons needed to bridge the energy gap, and $n(T)$ is the Bose-Einstein occupation number for the effective phonon mode at temperature T

$$n(T) = \frac{1}{\exp(h\tilde{\nu}c/kT) - 1}. \tag{2.2}$$

h is Planck's constant, c the speed of light and k Boltzmann's constant. The phonon energy (or frequency), described by the wavenumber, $\tilde{\nu}$, is $1100\mathrm{cm}^{-1}$ in silica glass, while it is $1200\mathrm{cm}^{-1}$ for phosphate glass and $900\mathrm{cm}^{-1}$ for germanate glass [9]. This can *e.g.* be observed as a shorter lifetime of the 980 nm erbium pump level in phosphate than in germanate.

2.2 Optical properties of Ytterbium ions

Considering the electronic structure, the trivalent ytterbium ion is a very simple element. The electron configuration is $[Xe]4f^{13}$, and can be considered as a 'one-hole' configuration (similar to a 'one-electron' configuration), which results in a two-level system with the upper energy level manifold labeled $^2F_{5/2}$, and the lower energy level manifold labeled $^2F_{7/2}$, see figure 2.2. Since there are only two energy levels there are no upconversion or excited-state absorption (ESA) processes to care about.

Figure 2.1 shows absorption and emission spectra of the Yb^{3+} ion in a silica waveguide. The very broad absorption spectrum ranges from 850 nm to 1050 nm with a broad peak at 920 nm and a very strong,

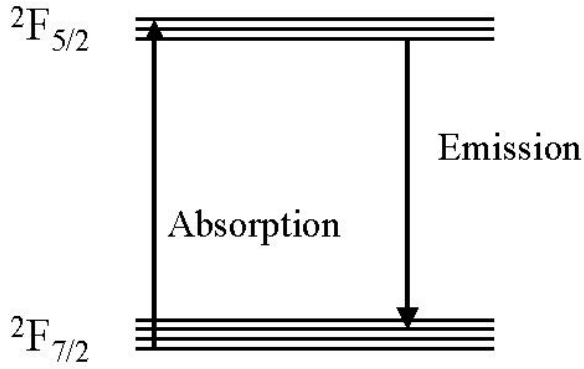

Figure 2.2: *Ytterbium energy levels with an indication of the Stark splitting.*

narrow peak at 976 nm. This broad absorption range means that there is a wide choice of pump sources to choose from. The emission ranges from 900 nm to 1200 nm, and gain is available from approximately 976 nm to 1200 nm making it possible to make amplifiers or lasers in this region using ytterbium [12]. The Stark splitting of the the two energy level manifolds is of the order of 10^2cm^{-1}, and the energy gap is approximately 10^4cm^{-1}. In *e.g.* germanate, with a phonon energy of approximately 900cm^{-1}, 11 phonons are thus required to span the gap. Using equation (2.1) and the values $T = 300K$, $C = 3.4 \times 10^{10}$ s^{-1} and $\alpha = 4.9 \times 10^{-3}$ cm [9], this results in a nonradiative decay rate of 2×10^{-11} s^{-1} which is so slow that multiphonon assisted nonradiative decay from the excited state can be neglected. A typical value of the lifetime of the excited state is approximately $0.7 - 0.9$ ms in germanosilicate glass [13].

The strong Stark splitting is the reason why it is possible to invert the ytterbium system, and thus obtain the gain that is necessary for amplification and laser action. Ytterbium can be described as a quasi three or four level system, as illustrated in figure 2.2. The Yb-ion can be pumped to a high-energy part of the $^2F_{5/2}$ manifold, where it will undergo fast thermal relaxation to a lower Stark level in the same manifold. From here it can then decay to the ground state manifold by emitting a photon.

For an ytterbium laser, the pump and laser wavelengths are very close, and thus the energy defect that would otherwise lead to heating of the host is very small. For instance, the defect in Yb:YAG is ap-

proximately three times smaller than for Nd:YAG (pumped at 800 nm and lasing at 1064nm) [12], and so, the ytterbium doped laser can be an attractive alternative to neodymium doped lasers.

Even though there are only two energy levels which should eliminate loss processes such as concentration quenching, there has been evidence of such processes in ytterbium, possibly associated with clustering of ytterbium ions and energy migration to a defect which can de-excite the ions [13]. I will return to this problem in chapter 5.

2.2.1 Ytterbium Rate Equations

The population of the energy level manifolds in ytterbium can be described by a standard rate equation model, assuming that the transitions between the upper and lower levels are primarily homogeneously broadened. For this purpose ytterbium is treated as a two level system with a ground state population n_a, an excited state population n_b and a total concentration of

$$N_{Yb} = n_a + n_b. \tag{2.3}$$

The thermal redistribution of the population of the sublevels in each manifold is so fast that it can be considered instantaneous. Therefore it is only necessary to know the fractional populations of each manifold, and the rate equation describing the populations can be written as

$$\frac{\mathrm{d}n_b}{\mathrm{d}t} = (W_{ab}^p + W_{ab}^s)n_a - (W_{ba}^p + W_{ba}^s)n_b - A_{ba}n_b \tag{2.4}$$

where

$$W_{ba}^{s,p} = \frac{\sigma_e(\nu_{s,p})P_{s,p}(z)}{h\nu_{s,p}}|\psi_{s,p}(x,y)|^2 \tag{2.5}$$

$$W_{ab}^{s,p} = \frac{\sigma_a(\nu_{s,p})P_{s,p}(z)}{h\nu_{s,p}}|\psi_{s,p}(x,y)|^2 \tag{2.6}$$

are the emission and absorption rates at the signal (s) and pump (p) frequencies, $P_{s,p}(z)$ the sum of forward and backward propagating power at position z, $|\psi_{s,p}(x,y)|^2$ the signal and pump field distributions, and $\sigma_e(\nu_{s,p})$ and $\sigma_a(\nu_{s,p})$ the emission and absorption cross sections. The rate of spontaneous emission is given by

$$A_{ba} = \frac{1}{\tau_{Yb}} \tag{2.7}$$

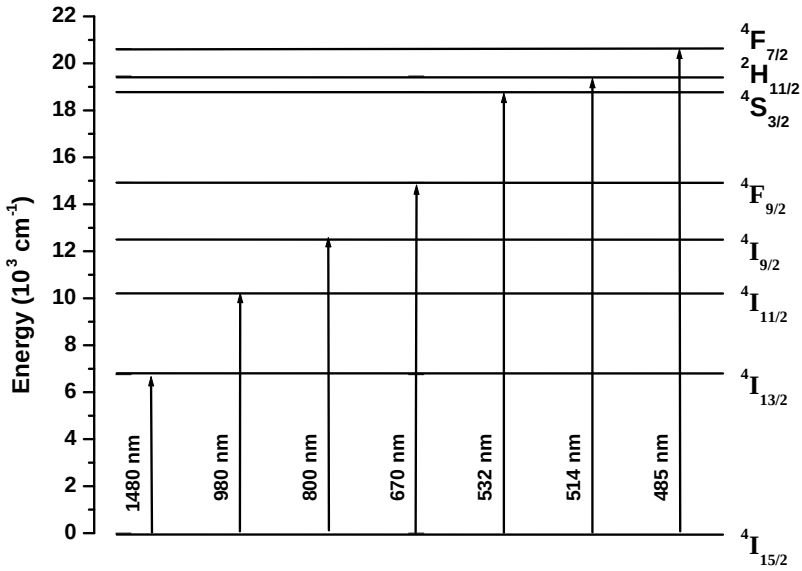

Figure 2.3: *The lowest energy levels of the Er^{3+} ion labeled according to the Russell-Saunders coupling scheme. The wavelengths needed to excite the various energy levels are indicated at the arrows. Reproduced from [11]*

with τ_{Yb} being the fluorescence lifetime of the $F_{5/2}$ manifold. Solving these equations in steady state ($dn_b/dt = 0$), we obtain the inversion

$$X_{Yb}(x,y,z) = \frac{n_b}{N_{Yb}} = \frac{W_{ab}^p + W_{ab}^s}{W_{ab}^p + W_{ab}^s + W_{ba}^p + W_{ba}^s + A_{ba}} \tag{2.8}$$

which will be used in the laser simulations in chapter 5

2.3 Optical properties of Erbium

The trivalent Erbium ion is a much more complicated system than ytterbium. The reason is, that the electron configuration $[Xe]4f^{11}$ gives rise to a large number of states which introduces the possibility of ESA and upconversion. Figure 2.3 shows the lowest energy level manifolds for an erbium ion along with the associated pump wavelength.

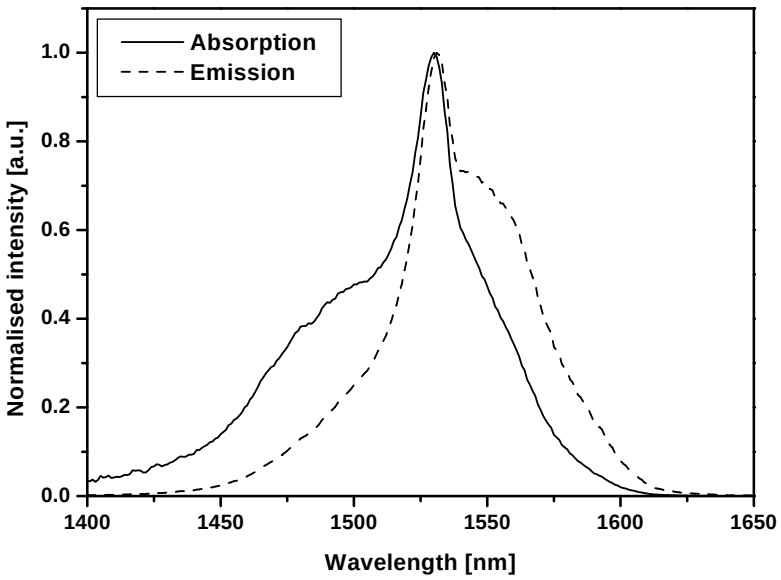

Figure 2.4: *Absorption (full line) and emission (dashed line) spectra of erbium in an Al/Ge-silica waveguide*

The Er^{3+} ion has the very fortunate property that it will emit light in the 1550 nm region when relaxing from the first excited state to the ground state as can be seen from figure 2.4. This coincides with the third telecommunications window, where the transmission loss of the standard silica fibers used for optical communications is at a minimum. For this reason the erbium doped fibers have had great success, and applications have been both as erbium doped fiber amplifiers (EDFAs) and fiber lasers.

The metastable $^4I_{13/2}$ level has a lifetime of approximately 10 ms, but most of the high-energy levels in erbium have nonradiative relaxation rates of $10^{-5}s^{-1}$ or faster [11]. Thus, pumping one of the high-energy levels, may yield a fast nonradiative relaxation to the metastable level which has an energy gap that is too large to allow fast nonradiative relaxation. Often 980 nm pumping is used, giving a very efficient indirect pumping of the $^4I_{13/2}$ level by using a three-level pumping scheme. In this way it is possible to obtain a high inversion of the erbium ions.

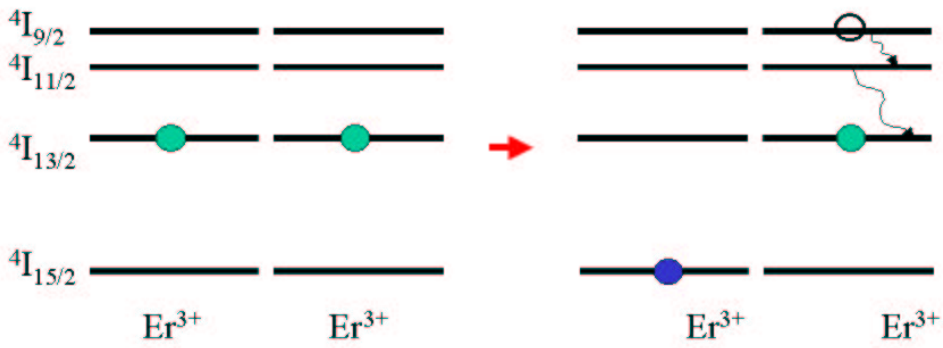

Figure 2.5: *Cooperative upconversion in erbium. The two ions are initially in the first excited state. One ion then transfers all its energy to the other. The resulting highly excited ion undergoes fast nonradiative relaxation back to the metastable state. The end result is one ion in the ground state and one in the first excited state.*

2.3.1 Energy Transfer Processes

Due to the limited length of erbium doped planar waveguides as compared to fibers, a high concentration is desired in order to obtain a high gain. However, as the erbium concentration increases the lifetime of the first excited state decreases [14]. This has been ascribed to a cooperative upconversion process that can occur when two excited erbium ions are close to each other.

The cooperative upconversion process is shown schematically in figure 2.5. Two erbium ions in the first excited state can interact in a way that all the excitation energy is transferred from one ion to the other. The donor ion thus returns to the ground state while the acceptor ion is further excited to the $^4I_{9/2}$ level from where it can undergo fast phonon-assisted relaxation back to the metastable state. The problem here is that the two ions are initially both in the metastable state, but after the upconversion process only one ion is in the metastable state while the other is in the ground state. Thus a pump photon has been lost.

The energy transfer process is believed to occur mainly through a dipole-dipole interaction and is thus proportional to R^{-6} [15, 16]. It has been shown that the energy transfer probability in the electronic dipole-dipole approximation can be expressed as the overlap of the

donor emission spectrum, $\sigma_e^A(\lambda)$, with the acceptor absorption spectrum, $\sigma_a^B(\lambda)$, of the corresponding optical transitions [17], and this can be written as [18]

$$P_{A\to B} = \frac{6c}{(2\pi)^4 R^6 n^2} \int_0^\infty \sigma_e^A(\lambda)\sigma_a^B(\lambda)\mathrm{d}\lambda. \tag{2.9}$$

Here c is the speed of light, n, the refractive index and R is the distance between donor and acceptor nucleus. Since the average separation between the erbium ions decrease when the concentration increases, the probability for upconversion increases with concentration. Furthermore, since the erbium ions are not soluble in the silica glass structure, they will tend to form clusters when the concentration increases, thus bringing them even closer to each other. In the kinetic limit, such a cluster acts as an unsaturable absorber since the erbium ions will de-excite each other before any fluorescence can be emitted [19]. For homogeneous upconversion, *i.e.* when there are no clusters, the upconversion is related to the fluorescence lifetime by [11]

$$\frac{1}{\tau_{fl}} = \frac{1}{\tau_{rad}} + \frac{1}{\tau_{up}}. \tag{2.10}$$

This lifetime quenching sets in when the concentrations are above $10^{25}\mathrm{m}^{-3}$ [20], and it sets some severe limitations on the performance of an erbium doped planar waveguide amplifier or laser.

The erbium solubility can be increased by using multicomponent glasses such as aluminosilicate glass. Here Al_2O_3 is dissolved in the silica glass structure and creates dangling bonds that can form a complex with the erbium ions, surrounding the ions and shielding them from each other [21]. Also phosphate glass have been shown to have a low degree of clustering [22]. The structure of phosphate glass is more open than that of silica, since in phosphate the tetrahedral structure of the oxide contains one non-bridging oxygen (NBO) atom that is double-bonded to phosphor. As network modifiers are added to the glass, the phosphate network depolymerises and creates even more NBOs [23]. It has been shown, that a high number of NBOs is required to shield the electric charge of the rare earth ions [24, 25], thus allowing a higher concentration of rare earths in phosphate glass before clustering effects sets in. However, while Al codoping tends to make the erbium emission broader and more flat [26], codoping with phosphorous has the opposite effect, and results in a limited bandwidth [27].

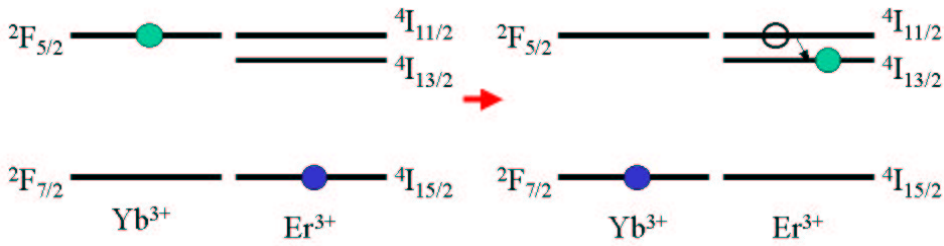

Figure 2.6: *Energy transfer from ytterbium to erbium. An ytterbium ion in the $^2F_{5/2}$ state transfers its excitation energy to an erbium ion in the ground state. The erbium ion is thus excited to the $^4I_{11/2}$ level from where it relaxes to the upper laser level.*

Codoping with ytterbium

A way of increasing the pump efficiency is by codoping with ytterbium. Since the excited level in ytterbium has a large spectral overlap with the $^4I_{11/2}$ level in erbium, energy can be transfered between the two species in a dipole-dipole interaction with a transfer probability given by equation (2.9). This is shown schematically in figure 2.6 Ytterbium has an absorption cross section that is an order of magnitude larger than the erbium absorption cross section at 980 nm (see *e.g.* [28, 29]), so the ytterbium ions will efficiently absorb the pump. The absorbed energy can then be transfered to an erbium ion in the ground state, and thus the ytterbium ions can be used to indirectly pump the erbium ions. However, this process can of course occur in both directions, so in order to obtain efficient energy transfer *from* ytterbium *to* erbium a suitable glass host must be chosen. To assure that the back-transfer to ytterbium is negligible, the lifetime of the $^4I_{11/2}$ level should be as short as possible. This can be obtained by using a glass host with a high phonon energy since few phonons will be required to bridge the $^4I_{11/2}$ - $^4I_{13/2}$ energy gap, and the nonradiative decay from $^4I_{11/2}$ to $^4I_{13/2}$ will be faster according to equation (2.1). Table 2.1 shows the nonradiative decay rates for the $^4I_{11/2}$- $^4I_{13/2}$ transmision of erbium in phosphate, silicate and germanate calculated using equation (2.1). We see, that the nonradiative decay rate is much lower in germanate than in the other glass hosts. The nonradiative decay rate corresponds to a lifetime of

$$\frac{1}{655\mathrm{s}^{-1}} = 1.5\mathrm{ms} \tag{2.11}$$

Host	C [s^{-1}]	α [cm]	$\tilde{\nu}$ [cm^{-1}]	W_{nr} [s^{-1}]
Phosphate	5.4×10^{12}	4.7×10^{-3}	1200	206353
Silicate	1.4×10^{12}	4.7×10^{-3}	1100	53804
Germanate	3.4×10^{10}	4.9×10^{-3}	900	655

Table 2.1: *Nonradiative decay rates for the* $^4I_{11/2}$- $^4I_{13/2}$ *transmission of erbium. Data from [9].* $\Delta E = 3636\ cm^{-1}$.

which is more than the lifetime of the excited state in ytterbium. Hence, a high degree of back-transfer from erbium to ytterbium must be expected, in aggreement with the observations of Gapontsev [30]. For this reason, the preferred glass host for Er/Yb systems is phosphatete. I will return to this in chapter 6.

2.3.2 Rate Equations

A standard rate equation model has been used to evaluate the inversion in the erbium system for use in amplifier and laser calculations assuming homogeneously broadened transitions. Figure 2.7 shows the erbium and ytterbium transitions included in the calculations.

Many models have been suggested for modeling the erbium system. In a planar waveguide, the concentration levels are so high that it is necessary to take account of upconversion processes, and therefore a widely used four-level model has been proposed [31] which includes 'low' upconversion from the $^4I_{13/2}$ metastable state and 'high' upconversion from the $^4I_{11/2}$ pump level as well as a cross relaxation process that is the inverse of the 'low' upconversion. However, due to the large uncertainty on the upconversion parameters, and since it is possible to obtain a simple analytical solution for a more simple system, but not for the four-level system, I have chosen to use a simplified two-level system to model the population in erbium. Asuming a random distribution of erbium ions, the probability per unit volume that the neigbor is an excited erbium ion is n_2. This means that the rate of upconversion will be proportional to n_2, and therefore homogeneous upconversion has been included in the model as a quadratic term with an upconversion coefficient C_{up}, and $C_{up}n_2$ being the rate of upconversion.

Because of the fast nonradiative relaxations of levels 3 and 4, these

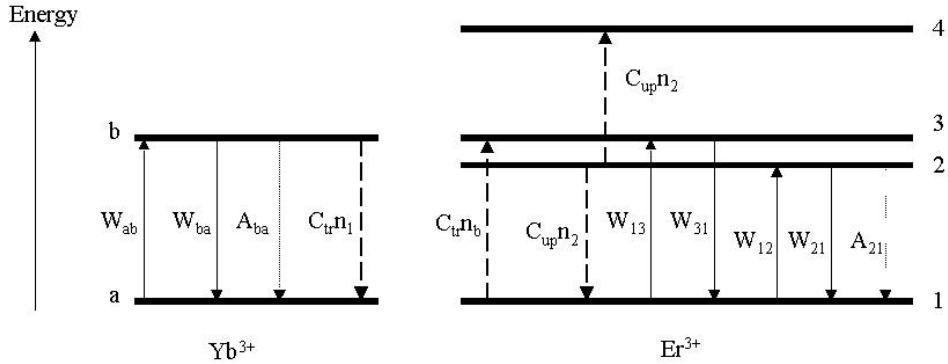

Figure 2.7: *Energy level diagram for the erbium/ytterbium system.*

levels are assumed to be empty in the rate equations. This means that only pump absorption is considered for erbium at this wavelength range, and that backtransfer to ytterbium is neglected. This assumption is not valid for germanium-doped glasses due to the low phonon energy, and hence the model will be used to simulate Er/Yb doped amplifiers in phosphosilicate in chapter 6. For the codoped erbium/ytterbium system with erbium level populations n_1, n_2 and total erbium concentration N_{er}, and ytterbium level populations n_a, n_b and total concentration N_{Yb}, the rate equations are

$$\frac{\mathrm{d}n_1}{\mathrm{d}t} = -W_{12}n_1 - W_{13}n_1 + A_{21}n_2 + W_{21}n_2 + C_{up}n_2^2 - C_{tr}n_1n_b \quad (2.12)$$

$$n_1 + n_2 = N_{Er} \quad (2.13)$$

$$\frac{\mathrm{d}n_a}{\mathrm{d}t} = -W_{ab}n_a + W_{ba}n_b + A_{ba}n_b + C_{tr}n_1n_b \quad (2.14)$$

$$n_a + n_b = N_{Yb}, \quad (2.15)$$

where

$$W_{ij}(x,y,z) = \frac{\sigma_{ij}(\nu_{s,p})}{h\nu_{s,p}} P_{s,p}(z)|\psi_{s,p}(x,y)|^2, \quad (2.16)$$

are the stimulated emission and absorption rates for transitions between level i and j at signal (s) and pump (p) frequencies, σ_{ij} are the corresponding transition cross sections, and $P_{s,p}(z)$ the sum of forward and backward propagating power at position z. The spontaneous

emission rates of erbium and ytterbium are given by the respective fluorescence lifetimes as

$$A_{21} = 1/\tau_{Er} \tag{2.17}$$

and

$$A_{ba} = 1/\tau_{Yb}, \tag{2.18}$$

and C_{tr} is the energy transfer coefficient, with $C_{tr}n_1$ being the rate of transfer from ytterbium to erbium. At steady state, the ytterbium inversion, defined as

$$X_{Yb} = \frac{n_b}{N_{Yb}}, \tag{2.19}$$

becomes

$$X_{Yb} = \frac{W_{ab}}{W_{ba} + W_{ab} + A_{ba} + (1 - X_{Er})C_{tr}N_{Er}}. \tag{2.20}$$

where

$$X_{Er} = \frac{n_2}{N_{Er}} \tag{2.21}$$

is the erbium inversion. If we define the effective absorption and emission rates of erbium as

$$W_a = W_{12} + W_{13} + C_{tr}N_{Yb}X_{Yb} \tag{2.22}$$

$$W_e = W_{21} + A_{21} \tag{2.23}$$

then the erbium rate equation (2.12) becomes

$$\frac{\mathrm{d}n_1}{\mathrm{d}t} = -W_a(1 - X_{Er})N_{Er} + W_eX_{Er}N_{Er} + C_{up}(X_{Er}N_{Er})^2 = 0. \tag{2.24}$$

Solving for X_{Er} yields

$$X_{Er} = \frac{-(W_a + W_e) \pm \sqrt{4C_{up}N_{Er}W_a + (W_a + W_e)^2}}{2C_{up}N_{Er}}. \tag{2.25}$$

Since the erbium inversion has to be a positive number, the positive solution must be the correct one. This can be verified by examining this expression in the limit where the upconversion coefficient goes to zero. We should then get the erbium inversion for a system without upconversion. By making a Taylor expansion of the inversion in equation (2.25), we see that the positive solution is the correct one

$$\begin{aligned} X_{Er} &= \frac{-(W_a + W_e) + \sqrt{4C_{up}N_{Er}W_a + (W_a + W_e)^2}}{2C_{up}N_{Er}} \\ &\rightarrow \frac{W_a}{W_a + W_e}\ ,\ C_{up} \rightarrow 0. \end{aligned} \tag{2.26}$$

We thus have an analytical expression for the erbium inversion including homogeneous upconversion (equation (2.26)), and for the erbium/ytterbium codoped system, the erbium inversion may be found in an iterative procedure, alternating between equation (2.26) and (2.20).

Chapter 3

Fabrication of Active Planar Waveguides

In this chapter I will discuss how the ytterbium and erbium doped planar waveguides have been fabricated and characterised in this project. In section 3.1 I will discuss the methods that have been used in this work, and in section 3.2 I will review some of the alternative techniques that are being employed to fabricate active waveguides by other groups. The experimental setups for characterisation of the waveguides and thin films will be described in section 3.3.

3.1 Processing using PECVD and RIE

The core and cladding layers for the planar waveguides and thin films have all been deposited with Plasma Enhanced Chemical Vapor Deposition (PECVD), and the waveguides were defined by Reactive Ion Etching (RIE).

3.1.1 Plasma enhanced chemical vapor deposition

Chemical vapor deposition (CVD) is a process where chemical species in the gas phase react to form a solid product at a surface. The chemical reaction is thermally activated, and the processing temperatures can thus be quite high in order to obtain adequate deposition rates. The deposition rate can be greatly increased at the same substrate temperature by using PECVD [32]. In the PECVD process, the feed-stock gases are fed into the reactor where a plasma is formed and reactive

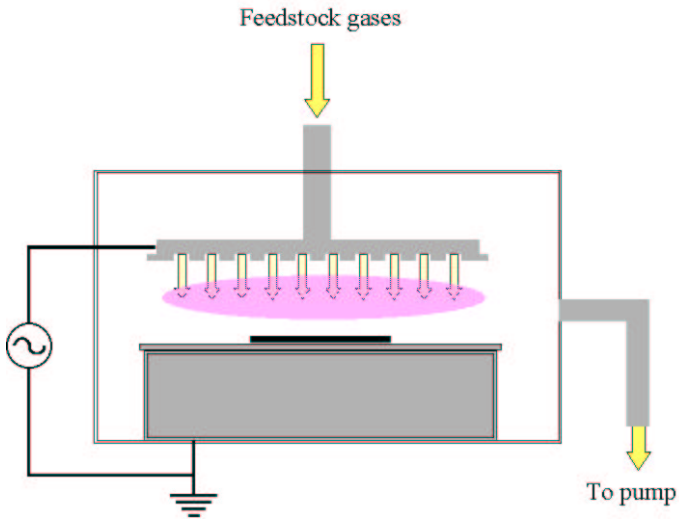

Figure 3.1: *Schematic view of the PECVD chamber.*

radicals are created by electron impact. This process enhances the chemical reactions, and results in the deposition of material on the surface of the substrate.

A schematic illustration of a PECVD chamber is shown in figure 3.1. The reaction chamber consists of two parallel electrodes connected to an RF generator. The process gases are introduced through the top electrode which is shaped like a shower head to ensure uniform gas distribution. The substrate is placed on the bottom electrode which is in electrical contact with the grounded chamber walls. The electrodes are heated to 250-300 °C for the deposition of the Yb/Er/Al doped films and the pressure in the chamber is controlled by constant pumping through a hole in the sidewall.

By applying an RF field to the electrodes, a plasma is formed by dissociative collisions of free electrons with the feed-stock gases. In steady state the plasma consists of a glow region where free radicals are formed, surrounded by thin plasma sheaths where the electrons are accelerated to the electrodes. The radicals diffuse to the substrate where they react at the surface.

Silica (SiO_2) can be deposited using silane (SiH_4) and Nitrous oxide (N_2O) as feed-stock gases. The overall chemical reaction from start to

end is

$$SiH_4(g) + 2N_2O(g) \rightarrow SiO_2(s) + 2N_2(g) + 2H_2(g), \qquad (3.1)$$

but, as is usual for plasma reactions, the total set of reactions leading from the initial reactants to the final products is very complex and not known in detail. However, the deposition precursors are believed to be SiH_3, SiH_2 and O radicals created from electron impact dissociation of SiH_4 and N_2O. The sticking probabilities of the precursors SiH_3 and SiH_2 in silane discharges are high, and the surface diffusion is not significant [32]. This means that it can be a problem to cover structures on a small scale such as the splitting region of a y-splitter. Another problem is that some 'intermediate' reaction products involving nitrogen and hydrogen, such as OH and NH, may be incorporated in the glass during deposition. This can give rise to large optical losses due to second harmonics of the vibration frequencies of OH (at 1400 nm) and NH (at 1500 nm) and is therefore very harmful for optical components operating in this wavelength range. OH bonds are broken at temperatures of 850–900 °C, and NH bonds around 1050 °C, so in order to drive out impurities and to stabilise the glass, annealing at high temperatures (1000–1200 °C) for several hours is required. The thickness reduction due to the annealing step is approximately 10 %, and the thickness variations across the wafer are less than 5 %.

Since the planar waveguides guide the light by the principle of total internal reflection [33], the refractive index of the core has to be higher than that of the cladding. An increase in refractive index can be obtained by including *e.g.* germane (GeH_4) in the feed-stock gases. In this way GeO_2-sites are incorporated in the glass giving rise to an increase in the refractive index. It is also possible to include phosphine (PH_3) in the feed-stock gases, giving P_2O_5-sites in the glass, however, the resulting phosphosilica glass has a low melting point, and will diffuse into the cladding during annealing. This results in a linewidth reduction that can be quite severe. For this reason, the waveguides presented in his work are all based on germanosilica glass. I will discuss the influence of this in chapter 6.

Figure 3.2 shows the refractive index of Yb-doped germanosilicate films as a function of germane flow for a deposition rate of 800 Å/min. The refractive index was measured with a prism coupler after annealing, and shows a linear dependence on the germane flow. This kind of measurement was made prior to all core layer depositions in order to

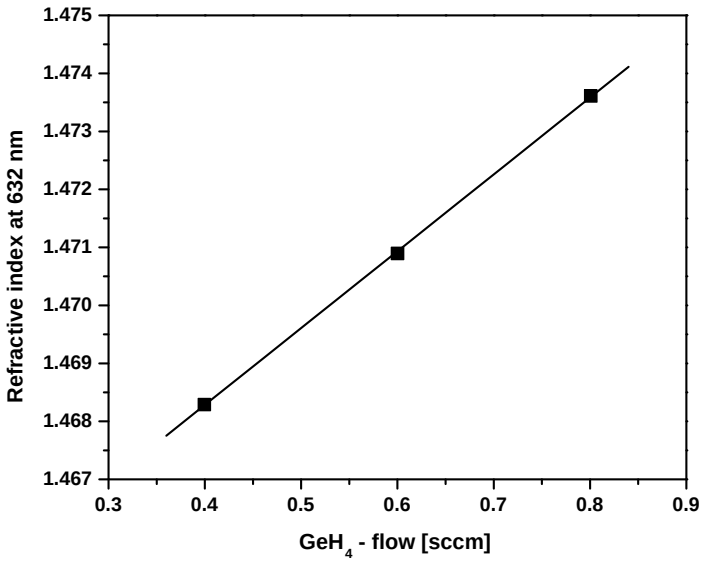

Figure 3.2: *Refractive index as a function of germanium flow. The line represents a linear fit to the data.*

calibrate the refractive index.

Liquid delivery system

There are no convenient erbium, ytterbium and aluminium precursors in gaseous form at room temperature, and therefore special techniques have to be used to feed Er and Yb to the PECVD plasma. For the work in this thesis, a liquid delivery system (LDS) have been used. The rare earths are supplied as a chelate in an organic solvent. The liquid is driven by pressurised N_2 from three different containers to a mixing manifold. There is one container for each of the dopants Er, Yb and Al. Each container is connected to the manifold by a valve which is opened for a fraction of a second corresponding to the amount of liquid that is needed from the specific valve.

From the mixing manifold the mixed liquids are pumped to the vaporiser shown schematically in figure 3.3. The liquid is led through a capillary tube, and falls onto a porous metal disk (frit). The frit and

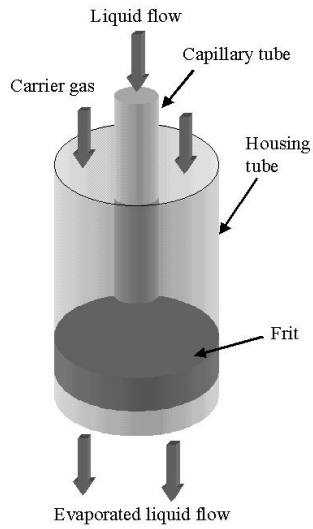

Figure 3.3: *Schematic view of the LDS vaporiser.*

the housing tube can be heated to 150–250 °C, and the liquid is flash evaporated when it falls on the frit, and the gas is subsequently mixed with the other PECVD feed-stock gases before entering the plasma chamber. All of the pipeline following the vaporiser is also heated in order to prevent condensation.

Film composition

The composition of the deposited films were examined by Rutherford back-scattering spectrometry (RBS) and secondary ion mass spectrometry (SIMS). In the RBS experiments the sample is exposed to a flux of highly energetic (2 MeV) alpha particles. The incident alpha particles are scattered on the atoms in the sample, and by measuring the energy of the back-scattered particles the mass of the scattering atom can be determined through conservation of energy and momentum. This provides a very accurate measurement of the absolute content of atomic species in a solid [34].

Because of the small mass difference between Si (atomic weight 28) and Al (atomic weight 27), as well as the low Al concentration, it is not possible to measure the aluminium concentration by RBS. Instead the aluminum concentration was determined indirectly using SIMS and a calibrated Al-doped sample as a reference.

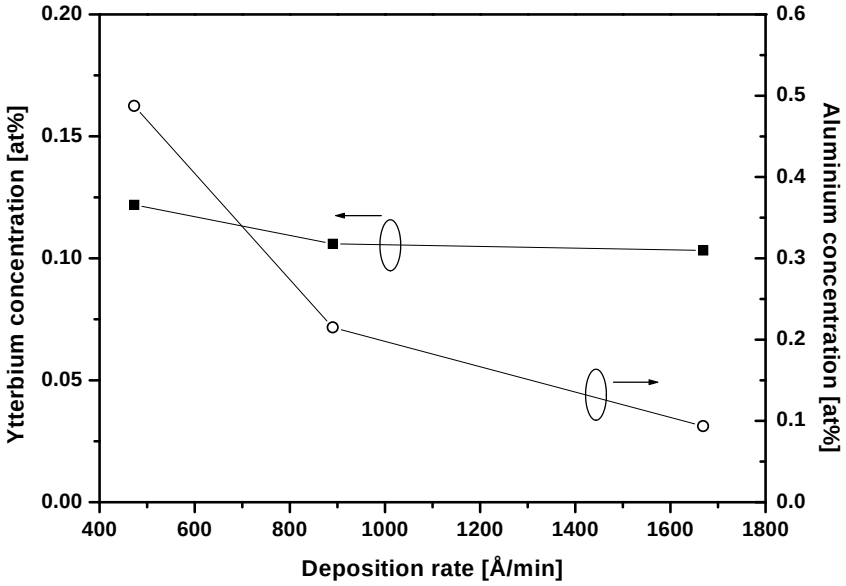

Figure 3.4: *Ytterbium and aluminium concentrations as a function of deposition rate. Yb/Al ratios were 13/87, 25/75 and 50/50 respectively.*

In the SIMS measurements the sample is placed in an ultra-high vacuum chamber, where a focused beam of energetic oxygen-ions is scanned across a small area of the sample. The beam is angled with respect to the sample, and as the ions hit the sample, material is sputtered off. Some of this material is ionic, and can be detected with a quadrupole mass spectrometer above the sample. Since the ionisation cross section is strongly dependent on the chemical environment of the species, SIMS does not give an absolute information about the concentrations of different species in the sample.

The SIMS can be used in two ways: First, it can be used to record mass spectra of the sputtered ions. This allows for identification of the species in the sample. Second, it can be used to count the number of ions of a specific mass as a function of time. In this way the ion beam digs into the sample as the ions are sputtered off, and a depth profile is obtained. From this depth profile it is possible to study concentration variations in the glass as a function of depth.

Figure 3.4 shows the concentration of Yb and Al as a function of deposition rate. In this experiment it has been attempted to keep the ytterbium concentration constant while varying the aluminium concentration. The dopant concentrations depend both on the LDS flow and the deposition rate, since for a given LDS flow the concentrations will increase if the deopsition time increases. The ytterbium concentration has been kept constant in the three samples by doubling the deposition rate when the ytterbium content of the LDS flow was doubled. The deposition rate is primarily controlled by the SiH_4-flow. The first point corresponds to an LDS Yb/Al mixing ratio of 13/87, and was deposited with a deposition rate of approximately 470 Å/min. Next, the Yb/Al ratio was approximately doubled to 25/75, and the deposition rate was doubled to approximately 890 Å/min. Finally the Yb/Al ratio was doubled to 50/50, and the deposition rate was again doubled to approximately 1660 Å/min. The figure shows that the ytterbium concentration is indeed almost constant at approximately 11 at%, with the main deviation at the first point where the Yb/Al ratio is not exactly half that of the next point. With the chosen process paramteters is is possible to span an aluminium concentration from 0.09 to 0.49 at%.

3.1.2 Reactive ion etching

In order to define the waveguide core structure, reactive ion etching (RIE) is commonly used to remove the excess material from the surface. RIE is a dry etching process, that takes place in a plasma chamber, in principle similar to the one used for PECVD. As opposed to a wet etch, which is usually isotropic, the RIE process, can be made highly anisotropic, and is therefore very useful for *e.g.* creating waveguide cores with vertical sidewalls. In the RIE process the plasma supplies both the reacting free radicals and ions, and uses the combined effect of chemical etching and sputtering to reach etch rates that are higher than those produced by either pure chemical etching or by sputtering alone [32]. The chemical etch, is a process where gas-phase atoms or molecules diffuse to the surface where they react to give gas-phase products. This is an isotropic etch process *i.e.* the horisontal and vertical etch rates are equal. In order to obtain an anisotropic chemical etch, the material to be etched must have a crystal structure where etching along certain crystal axes is preferred, and this is not the case

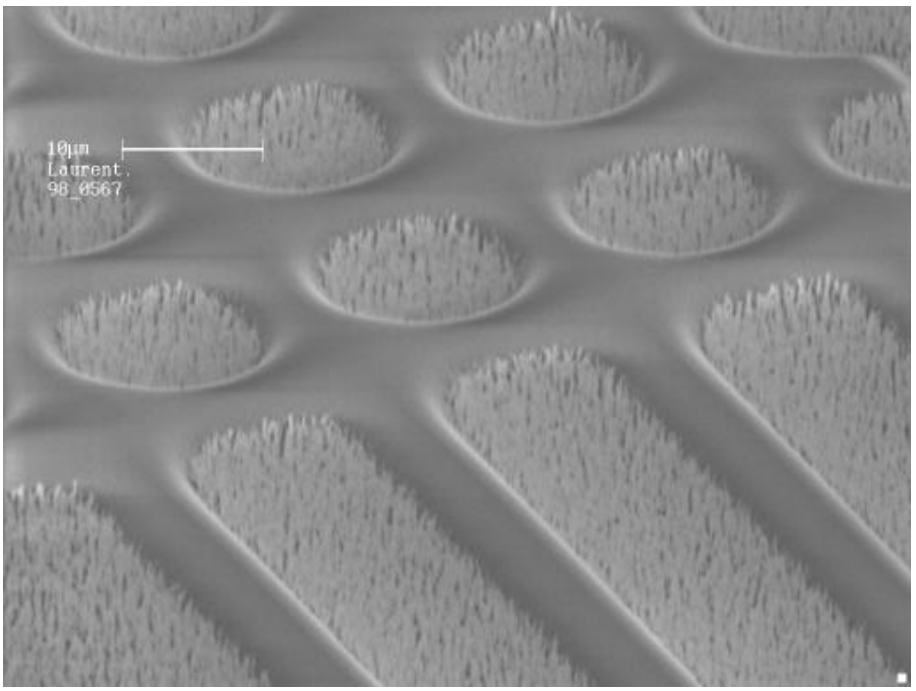

Figure 3.5: *SEM micrograph of test structures for planar waveguides. The etched spacings in the structure are filled with a grass-like structure originating from non-volatile reaction products that acts as a micro mask.*

for an amorphous material like glass. Sputtering is a physical effect where high-energy ions impact on the surface causing atoms to be ejected. The process is unselective since the sputtering yield roughly depends on the surface binding energy and the masses of the involved particles, and these do not vary by more than a factor of 2-3 for different materials [32]. Since the sputtering yield strongly depends on the incident angle of the ions, it is an anisotropic process. Therefore there is essentially no removal of material from vertical surfaces. The combination of the two - ion enhanced etching - uses sputtering to remove material on the surface and to provide the necessary activation energy for chemical reactions at the surface. The balance between chemical etching and sputtering can be adjusted by carefully controlling the RF power, flow of feed-stock gases and background pressure.

For etching of silica, fluor is very suitable and yield volatile reaction products that can be pumped out of the chamber. However, rare earths

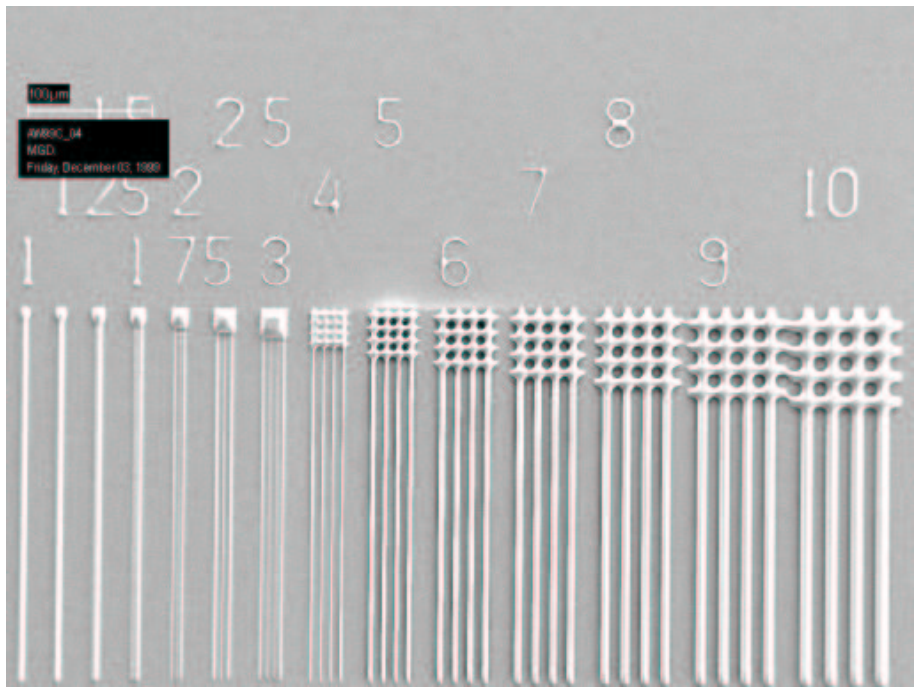

Figure 3.6: *SEM micrograph of test structures for planar waveguides. The etch has been optimised to avoid the creation of RIE-grass, but the waveguides have a triangular shape, indicating heavy mask erosion due to the Ar-ion sputtering.*

and aluminium does not react with fluor to give volatile products, but acts as a 'micro mask'. This problem causes 'RIE-grass' as shown in figure 3.5, because the micro mask shield the underlying glass from the etch. The presence of RIE-grass makes it impossible to obtain useful waveguides because of the very high propagation losses. In order to overcome the problem of RIE-grass, the etch was further combined with sputtering by argon ions to remove non-volatile material. Since RIE-grass next to the waveguides can be difficult to avoid, the waveguides were given a slightly trapezoidal shape by carefully controlling the mask erosion due to the sputtering.

Figure 3.6 shows a SEM micrograph of a test structure for planar waveguides where the etch has been optimised to avoid formation of RIE-grass. The lines in the structure have an almost triangular shape indicating that the mask has not survived the Ar-ion erosion throughout the etch. The numbers in the top part of the figure indicate the

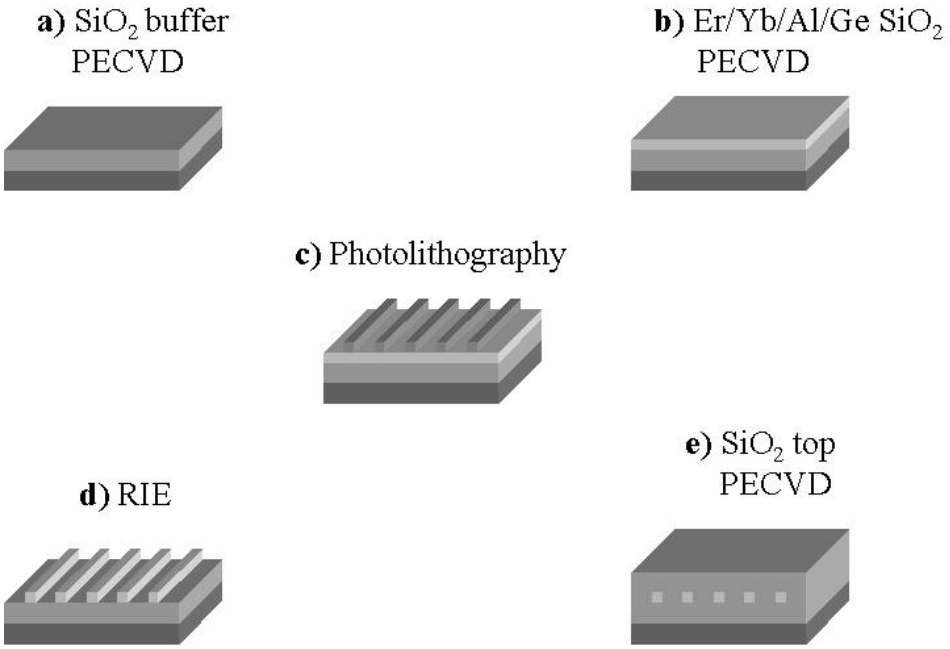

Figure 3.7: *Fabrication of planar waveguides. a) Deposition of a buffer layer using PECVD. b) Deposition of the core layer using PECVD. c) Photolithographic step where the mask pattern is transferred to the core layer. d) Etching of core layer using RIE. e) Deposition of top cladding using PECVD.*

width of the respective lines as defined on the mask, and the separation of the lines should be the same as the width of the lines. We see that it is possible to fabricate structures of dimensions down to approximately 5 μm, but the lines are no longer as wide as the spacings between them indicating a linewidth reduction from the etch process. In the following chapters the reported waveguide widths correspond to the widths defined on the mask.

3.1.3 Processing steps

The rare earth doped planar waveguides were produced on 4 inch, 0.5 mm thick silicon wafers using PECVD and RIE, as illustrated in figure 3.7. Each deposition was followed by an annealing step (1100 °C), which is not shown in the figure.

First a lower cladding layer ('buffer') was deposited using PECVD

(a). This layer consists of pure silica, and is 12-15 μm thick in order to ensure isolation of the optical field in the final waveguide from the high-index substrate. Later in the project the buffer layers were made by thermal oxidation of silicon wafers in an oxygen rich atmosphere (H_2O). Because high quality mono-crystalline wafers are used, and since the process only involves water, the quality of the glass obtained in this way is far superior to what is obtainable with PECVD. On top of the buffer layer the core layer was deposited using PECVD with the LDS (b). The core layer had a thickness of approximately 4.7 μm and the refractive index was controlled by codoping with Ge. A photoresist layer was then spun on the core layer and a mask pattern transferred to the photoresist by exposure to UV light (c). After exposure the pattern was developed by dipping the wafer into a developing solution where the areas of the photoresist which was illuminated were removed. The waveguides were etched using RIE (d), and finally a top cladding was deposited using PECVD (e).

3.2 Alternative fabrication techniques

Many techniques have been used to fabricate active planar waveguides. I will here briefly review some of these techniques. Often the waveguides are made by using some sort of deposition technology such as flame hydrolysis deposition, sputter deposition or sol-gel, but also planar waveguides based on ion exchange have been made with great success.

Flame hydrolysis deposition (FHD) is a process in which a gas such as $SiCl_4$ is exposed to an oxy-hydrogen flame whereby small silica particles (soot) are formed on the substrate. The resulting films are porous, and needs annealing at high temperatures to consolidate the glass [35]. Rare earth doping can be done by adding rare earth compounds to the process gas [35], or by soaking the porous film in a rare earth solution [36]. Waveguides can then be formed using RIE.

In sputter deposition atoms from a solid target in a vacuum chamber are sputtered onto a silicon substrate, *e.g.* by ions from an RF plasma. In this way films of high optical quality can be obtained. Since the glasses used for this technique are not always silica, but instead *e.g.* sodalime [37] which do not yield volatile products in a conventional RIE process, argon ion beam etching is usually used instead to

Technology	Host	Gain [dB/cm]	Loss [dB/cm]	Yb-codoped	Ref.
Ion-exchange	Phosphate	2.9	0.1	Yes	[38]
Sputtering	Soda-lime	4.2	1	No	[37]
	Al-silica	1.1	0.2	No	[39]
FHD	P-silica	0.6	0.1	No	[35]
PECVD	P-silica	0.67	0.17	No	[40]
	Al/Ge-silica	0.33	0.1	No	[41]

Table 3.1: *Examples of planar waveguide amplifiers.*

define the waveguides.

The sol-gel process is a process where the precursors react with water, and are then condensated to form a solution, or a *sol*. The sol is spun or dip-coated on a silicon substrate, and after evaporation of the solvent a *gel* is obtained. The film is then annealed to form the glass. The process is very attractive due to the high degree of flexibility concerning the material composition and the potential for mass production. However, the technique suffers from problems with clustering of the rare earth ions and fluorescence quenching by remaining OH groups [42, 43]. Erbium doped strip-loaded waveguides were presented in 1999 with a propagation loss of approximately 0.7 dB/cm, and a relative gain of 1 dB [44], but there have still not been reports of amplifiers with net gain based on this technology.

A method that have proven very efficient is ion exchange. Here, a glass sample with the desired composition is placed in a bath of melted salt containing ions that can diffuse into the glass sample and take the place of other types of ions thereby increasing the refractive index. A metal mask (usually Al) is deposited on the surface of the glass to define the areas where ion exchange, and thus waveguide creation, will take place. The waveguides can then be buried in a second step where an electric field is applied to pull the exchanged ions further into the glass [18]. A problem with this type of waveguides is, that the rare earths are not confined to the core so that the tails of the signal field experience low inversion.

Tables 3.1 - 3.3 shows some examples of what have been accomplished for erbium doped waveguides fabricated using ion-exchange, sputtering, FHD and PECVD technologies. The ion-exchange tech-

Technology	Host	Slope eff [%]	Thresh. [mW]	Reflectors	Yb-cod.	Ref.
Ion-exch.	Phosphate	26	50	DM/EG	Yes	[50]
	Silicate	5.5	14.8	DM	Yes	[51]
	B-silica	2	5	DM	Yes	[52]
FHD	P-silica	0.14	60	UV	No	[53]
PECVD	Al/Ge-silica	0.15	21	UV	No	[7]

Table 3.2: *Examples of planar waveguide lasers. DM: Dielectric mirrors, EG: Etched gratings, UV: UV-written gratings*

Technology	Splitting ratio	Noise figure [dB]	Yb-codoping	Ref.
Ion-exchange	1×8	4.5	Yes	[47]
	1×2	8	Yes	[45]
PECVD	1×4	4.5	No	[8]

Table 3.3: *Examples ofloss-less planar waveguide splitters.*

nology seems very useful, and has a strong advantage in the choice of glass composition. However, these glasses needs a high pump power, and are not well suited for integration with passive components. The lossless 1×2 splitter reported in [45] was made in one Er/Yb doped glass sample. This can be a problem if higher splitting ratios are desired since it may not be possible to obtain complete inverison in the spillter arms leading to absorption of the signal. By seperating the amplifier and splitter regions splitting ratios of 1×8 were obtained in [46] and [47]. The two parts were assembled in an cative alignment process followed by bonding with UV curing glue. Recently an EDWA integrated with a passive pump/signal multiplexer have been made by the same technique as the 1×8 lossless splitter [48]. However, a major problem with this design is the alignment between the active and passive waveguides. This problem can be solved if both types of waveguides are ono the same substrate, and have been demonstrated for PECVD grown planar waveguides [49].

3.3 Characterisation of waveguides and thin films

I will here describe the measurement setups used for characterisation of planar waveguides and thin films.

3.3.1 Setup for characterisation of planar waveguides

The waveguides were characterised using a setup as illustrated in figure 3.8. The sample is mounted on a translation stage and the input and output fibers (singlemode at 980 nm) are aligned to a waveguide using a piezo-controlled x-y-z translation stage. CW light from a white light or ASE source is launched into the input fiber, coupled into the waveguide, and collected by the output fiber. Finally the signal is detected by an optical spectrum analyser. In order to extract the effect of the waveguide from the data, a fiber-to-fiber measurement is made before the actual measurements are made. A fiber-to-fiber spectrum is a transmission spectrum obtained by coupling the light directly from the input fiber to the output fiber. The measured signal is then normalised to the fiber-to-fiber spectrum, and the effect of inserting the waveguide between the fibers is obtained. After the measurements another fiber-to-fiber spectrum is made to make sure that the reference spectrum have not changed during measurements. This control should always be made since the reference spectrum can change because of temperature fluctuations, and, most severely, if the facet of the fiber becomes damaged. As indicated, polarisation controllers, polarisers and U-brackets with filters can be inserted between the signal source and the wafer as needed. When pumping is required, the output from

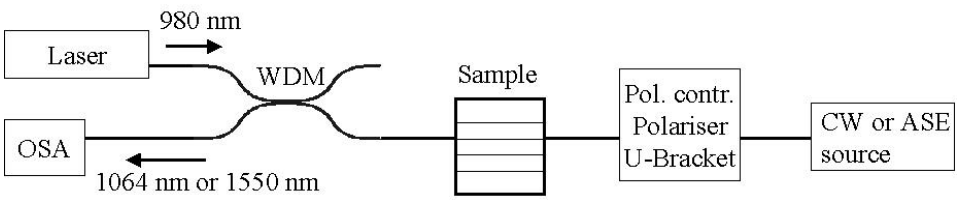

Figure 3.8: *Schematic illustration of the characterisation setup.*

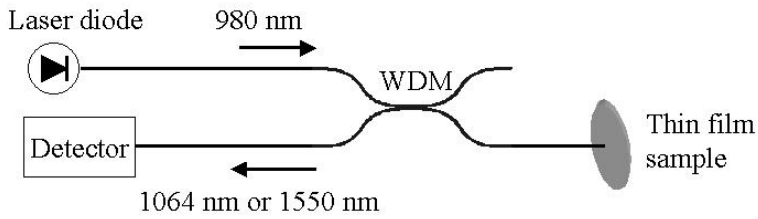

Figure 3.9: *Schematic illustration of the characterisation setup.*

a Ar-ion pumped Ti:sapphire laser is sent through a WDM (980/1064 nm or 980/1550 nm as needed) in order to separate the backward propagating signal from the pump when measurements on ytterbium doped waveguides are made. Since index matching oil had a tendency to burn when the waveguides were pumped, an index matching gel was used for optimisation of the fiber-to-waveguide coupling. In this way an improvement of the insertion loss of approximately 0.2 dB could be obtained.

3.3.2 Setup for characterisation of thin films

For these measurements a setup as illustrated in figure 3.9 was used. The wafer with the thin film is mounted vertically, and a fiber with an angled connector was placed against the film. A 980 nm diode laser is coupled into an optical fiber (singlemode at 980 nm), and sent through a WDM (980/1064 nm or 980/1550 nm as needed) to the angled connector. The fluorescence generated in the film in this way is collected by the same fiber, and separated from the pump in the WDM. Finally the signal is detected by a photodiode using a lock-in technique.

Chapter 4

Modelling of Lasers and Amplifiers

I will here present two models that have been used to simulate lasers and amplifiers. The first model describes a laser based on UV-written Bragg gratings in the core of an ytterbium doped planar waveguide (or fiber). The model is based on coupled-wave theory [54], and uses a transfer matrix method to propagate the fields in the laser [55]. The laser model will be described in section 4.1. The second model describes a planar waveguide amplifier, and is based on a model presented by Lester *et al.* [56] using an optimised effective index method for determination of the pump and signal modes [57]. The amplifier model will be described in section 4.2

4.1 Bragg Grating-Based Lasers

UV sensitivity of glass was discovered in 1978 by Hill *et al.* [58]. By launching an Ar-ion beam into an optical fiber, they observed the formation of a permanent change of the refractive index in the fiber core, and explained it by the interference of the forward propagating field with a backward propagating field originating from a reflection at the cleaved facet. Two-photon absorption at points of constructive interference induced a refractive index modulation, a Bragg grating, with a period of half the wavelength of the Ar-ion laser light, reflecting light at the same wavelength as the launched laser. The discovery was not utilized until Melz *et al.* made a Bragg grating in 1989 by holographic exposure with UV-light from the side of the fiber [59]. Since then there

has been a huge growth of Bragg grating based fiber- and integrated optical components, and also planar waveguide DBR lasers [36, 7] with UV-written gratings have been demonstrated. Although the process involved in the UV induced refractive index change has not yet been completely understood, the technology is widely used in both research laboratories and for commercial applications.

4.1.1 UV Induced Bragg Gratings

In this work UV writing of Bragg gratings has been facilitated by illuminating a waveguide by UV light through a phase mask placed directly on top of the wafer holding the waveguide as illustrated in figure 4.1(a). The phase mask consists of a grating with period Λ_{mask} etched into silica glass. The corrugation depth of the grating is made such that the zeroth order diffracted light will be minimized due to destructive interference, while the first order diffracted light will be maximized. This type of phase masks is therefore called zeroth-order nulled phasemasks. The resulting interference pattern in the waveguide will have a period of $\Lambda = \Lambda_{mask}/2$. If the glass is photosensitive this process will increase the refractive index at the points in the interference pattern where there is constructive interference (light). The resulting refractive index modulation will thus have a period that is equal to the period of the interference pattern. Light that propagates along a waveguide with a Bragg grating will be reflected each time the refractive index changes. This results in forward- and backward-propagating waves which will be in phase for specific values of the propagation constant, β, and thus interfere constructively, see figure 4.1(b). β varies with the signal wavelength, λ, as $\beta = \frac{2\pi}{\lambda} n_{eff}$, where n_{eff} is the effective refractive index of the propagating mode. The condition for constructive interference for the first order Bragg reflection (*i.e.* between light reflected from two neighboring refractive index 'peaks') is that the optical path difference must equal 2π. Hence

$$2\Lambda\beta_B = 2\pi \Rightarrow \beta_B = \frac{\pi}{\Lambda}. \tag{4.1}$$

This will result in a sharp reflection centered at the Bragg-wavelength

$$\lambda_B = 2n_{eff}\Lambda. \tag{4.2}$$

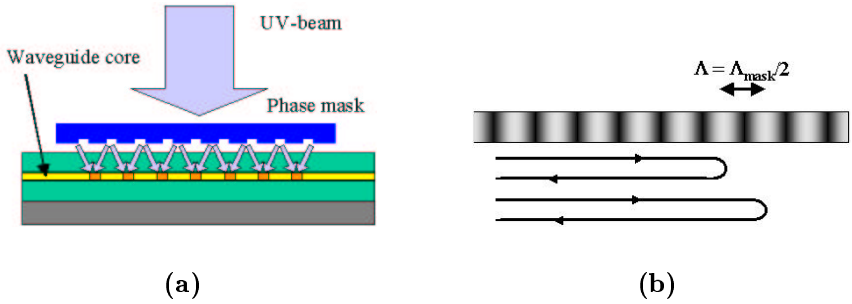

Figure 4.1: *(a) Principle of UV writing. A waveguide is illuminated by UV light sent through a zero'th-order nulled phase mask. The resulting interference of the first order diffracted light generates an interference pattern on the waveguides that translates into a modulation of the refractive index in the Ge-doped core. (b) Period in the Bragg grating.*

4.1.2 Coupled Mode Theory

In order to study lasers based on Bragg gratings I have used a transfer matrix model [55] based on coupled mode theory [54]. This model is very flexible, and allows for easy integration with a gain medium making it a very efficient tool for distributed feedback laser modelling. The model assumes that the waveguide is sufficiently small that the field has negligible dependence on the x and y coordinates. The total field can then be described by a forward and a backward propagating wave

$$E(z) = E_+(z) + E_-(z) = A^-(z)\mathrm{e}^{-i\beta z} + A^+(z)\mathrm{e}^{i\beta z}, \tag{4.3}$$

which is required to be a solution to the scalar wave equation

$$\frac{\partial^2 E(z)}{\partial z^2} + \beta^2(z)E(z) = 0. \tag{4.4}$$

Since β is dependent on the refractive index, the refractive index variations caused by the Bragg grating causes the propagation constant to vary as:

$$\beta(z) = \beta + \Delta\beta(z). \tag{4.5}$$

For laser modelling, the gain, g, is included by writing β as a complex propagation constant

$$\beta = n_{eff}k + i\frac{g}{2}, \tag{4.6}$$

where $k = 2\pi/\lambda$ is the free-space propagation constant. $\Delta\beta(z)$ is the small perturbation caused by the grating. If we assume that the refractive index modulation can be described by a cosine function, $\Delta\beta(z)$ becomes

$$\Delta\beta(z) = \Delta n k \cos(2\beta_B z + \phi). \tag{4.7}$$

Here ϕ is the phase and Δn the amplitude of the refractive index modulation. The gain and the refractive index modulation are treated as small perturbations to the field propagation. Furthermore we assume that the real part of the propagation constant of the fundamental mode is close to β_B (*i.e.* the field propagates at a wavelength close to the Bragg wavelength), and we write the difference as

$$\delta = n_{eff}k - \beta_B = 2\pi n_{eff}\left(\frac{1}{\lambda} - \frac{1}{\lambda_B}\right), \tag{4.8}$$

which is called the detuning. These assumptions assure that A^+ and A^- are slowly varying, and thus their second derivatives can be neglected when solving equation (4.4).

Based on these assumptions it is now possible to write a matrix equation relating the forward and backward propagating waves

$$\begin{pmatrix} E_+(L) \\ E_-(L) \end{pmatrix} = \begin{bmatrix} F_{11} & F_{12} \\ F_{21} & F_{22} \end{bmatrix} \begin{pmatrix} E_+(0) \\ E_-(0) \end{pmatrix}, \tag{4.9}$$

where the elements of the transfer matrix are given by [60]

$$\begin{aligned} F_{11} &= (\cosh(\gamma\Delta z) - i\frac{\Delta\beta'}{\gamma}\sinh(\gamma\Delta z))e^{-i\beta_B\Delta z} \\ F_{12} &= -i\frac{\kappa}{\gamma}\sinh(\gamma\Delta z)e^{i\beta_B\Delta z - i\phi} \\ F_{21} &= i\frac{\kappa}{\gamma}\sinh(\gamma\Delta z)e^{-i\beta_B\Delta z + i\phi} \\ F_{22} &= (\cosh(\gamma\Delta z) + i\frac{\Delta\beta'}{\gamma}\sinh(\gamma\Delta z))e^{i\beta_B\Delta z}. \end{aligned} \tag{4.10}$$

Here, $\Delta\beta' = \delta + ig/2$ and γ is defined by

$$\gamma^2 = \kappa^2 - (\Delta\beta')^2 \tag{4.11}$$

where the coupling coefficient, κ is

$$\kappa = \pi\Delta n/\lambda. \tag{4.12}$$

The transfer matrix is reciprocal (*i.e.* the determinant is one). Using this it is easy to show that the transmission and reflection coefficients of a uniform grating can be obtained directly from the transfer matrix as $t = 1/F_{22}$ and $r = -F_{21}/F_{22}$. Thus the peak reflectivity, R, and transmission, T, is found to be

$$R = \left|\frac{F_{21}}{F_{22}}\right|^2 = \tanh^2(\kappa L) \tag{4.13}$$

$$T = \left|\frac{1}{F_{22}}\right|^2 = (\cosh^2(\kappa L))^{-1}. \tag{4.14}$$

There are two types of lasers that rely on Bragg gratings; The distributed feedback (DFB) laser and the distributed Bragg reflector (DBR) laser. The DFB laser has a long grating with a phaseshift in the middle, and the DBR laser typically uses two Bragg gratings in a Fabry-Perot configuration. Hence, the gratings in these lasers are not always uniform. Non-uniform gratings can be modelled by the transfer matrix method by splitting the gratings into m elements, each with constant grating period, Λ, average effective refractive index, n, amplitude of the refractive-index modulation, Δn, and gain, g, as shown in figure 4.2. Now the total transfer matrix is obtained by calculating the transfer matrix of each element and multiplying the matrices:

$$\mathbf{F} = \prod_{n=1}^{m} \mathbf{F}^n. \tag{4.15}$$

The model is therefore very flexible, and allow for simulations on many different laser structures. In order to satisfy the approximation that the amplitudes of the fields are slowly varying, the condition

$$\Lambda^n \ll L^n \tag{4.16}$$

must be fulfilled. Here Λ^n and L^n are the grating period and section length of the nth section. Typical values of m in this thesis are 100-1000. We have demonstrated erbium [7] and ytterbium (see chapter 5) doped DBR lasers in our group, and I therefore focus on this type of lasers in this work.

A laser has no in-going signal field, so $E_+(0) = E_-(L) = 0$. This boundary condition can now be used to find the physical solution to the equations. The method for doing this is straight forward: A value

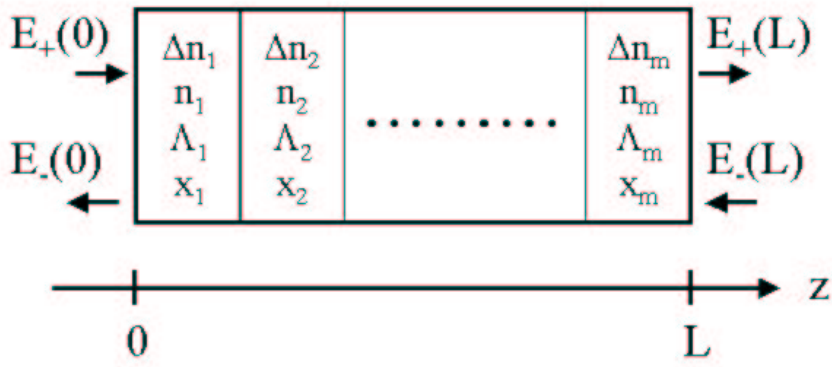

Figure 4.2: *Schematic diagram of a Bragg grating divided into m elements. The forward and backward propagating signals are indicated at each end.*

of β and $E_-(0)$ is assumed. Since $E_+(0) = 0$, both forward and backward propagating fields are thus known at $z = 0$. Now the inversion, gain and pump attenuation in the first section is calculated, and using the transfer matrix the signal and pump fields for the next section is determined. This continues until $z = L$, where the requirement is that $E_-(L) = 0$. The values of β and $E_-(0)$ are now adjusted using linear interpolation until the boundary condition is fulfilled.

Gain Model for the Laser

The assumption, that the waveguide is sufficiently small that the field has negligible dependence on the x and y coordinates, means that the variations of the rare earth inversion in the transverse direction are negligible. In this case the optical fields of the signal and pump can be described by confinement factors

$$\Gamma_{s,p} = \frac{\iint_{core} |\psi_{s,p}(x,y)|^2 \, \mathrm{d}x \, \mathrm{d}y}{\int_{-\infty}^{\infty}\int_{-\infty}^{\infty} |\psi_{s,p}(x,y)|^2 \, \mathrm{d}x \, \mathrm{d}y}, \tag{4.17}$$

and the waveguide is described by average values of the erbium and ytterbium concentration and inversion over a cross section of the waveguide. To include this in the rate equations, the stimulated transition rates are written as

$$W_{ij}^{s,p} = \frac{\sigma_{ij}(\nu_{s,p}) P_{s,p}(z)}{h\nu_{s,p}} \frac{\Gamma_{s,p}}{\text{core area}} \tag{4.18}$$

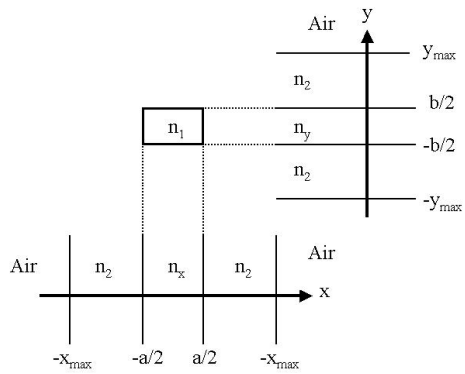

Figure 4.3: *Schematic diagram showing how the actual waveguide structure is divided into slab waveguides in the x and y directions.*

where the intensity term, $|\psi_{s,p}(x,y)|^2$ from equations (2.5) and (2.6) is replaced by the confinement factor divided by the core area. The inversion, X, is determined using equations (2.8) for Yb or (2.20) and (2.26) for Er/Yb doped systems respectively, and the gain coefficient can be calculated as

$$g(z,\nu_{s,p}) = N_{Er,Yb}\Gamma_{s,p}(X_{Er,Yb}(z)\sigma_e(\nu_{s,p}) - (1-X_{Er,Yb}(z))\sigma_a(\nu_{s,p})) - \alpha_{s,p} \tag{4.19}$$

where $\alpha_{s,p}$ is the propagation loss of the waveguide at pump and signal wavelengths. Since the ASE level is usually more than 60 dB below the laser signal level (see chapter 5), the effect of ASE is neglected in the model. Due to the z-dependence of the inversion, spatial holeburning is included in the model.

4.2 Erbium/Ytterbium Doped Amplifiers

To describe an erbium/ytterbium doped amplifier, the pump and signal modes are first determined using an accurate optimised effective index method [57]. The optimised effective index method works by separating the field into two orthonormal functions, $X(x,n_x)$ and $Y(y,n_y)$, which are solutions of the scalar wave equation for slab waveguides in the x and y direction, respectively (see figure 4.3). The trial function, $\psi(x,y)$, is then a product of X and Y, and the propagation constant is found by varying the refractive indices of the x and y solutions, n_x

and n_y, until the integral

$$\int_{-\infty}^{\infty}\int_{-\infty}^{\infty} XY\left(\frac{\partial^2}{\partial x^2}+\frac{\partial^2}{\partial y^2}+n^2(x,y)k^2\right)XY\,\mathrm{d}x\,\mathrm{d}y \tag{4.20}$$

is maximised. This method is very fast and accurate compared to results obtained from circular harmonic analysis [57], but has the disadvantage that it can only handle rectangular waveguides, and not *e.g.* waveguides of a trapezoid shape. This means, that the calculated modeprofiles can only be considered as an approximation of the actual waveguide cores, as defined by the parameters in the RIE process.

The erbium and ytterbium inversions are determined using equations (2.20) and (2.26) as described in chapter 2. However, the amplifier model includes both forward and backward propagating ASE for ytterbium in the pump band, and erbium in the signal band. Therefore the absorption and emission rates for ytterbium and erbium have to be defined as

$$W_{ij}=\left[\frac{\sigma_{ij}(\nu_{s,p})}{h\nu_{s,p}}P_{s,p}(z)+\int_0^{\infty}\frac{\sigma_{ij}(\nu)}{h\nu}P_{ASE}^{Er,Yb}(\nu,z)\,\mathrm{d}\nu\right]|\psi_{s,p}(x,y)|^2, \tag{4.21}$$

where $P_{ASE}^{Er,Yb}$ is the sum of forward and backward propagating erbium or ytterbium ASE power in the signal or pump band respectively

$$P_{ASE}^{Er,Yb}(\nu,z)=P_{ASE}^{+Er,Yb}(\nu,z)+P_{ASE}^{-Er,Yb}(\nu,z). \tag{4.22}$$

The absorption and emission coefficients describing the attenuation and gain along the waveguide are determined by

$$\gamma_a^{Er,Yb}(\nu,z)=\sigma_a^{Er,Yb}(\nu)\iint_{core}(1-X_{Er,Yb})N_{Er,Yb}|\psi(x,y)|^2\,\mathrm{d}x\,\mathrm{d}y \tag{4.23}$$

and

$$\gamma_e^{Er,Yb}(\nu,z)=\sigma_e^{Er,Yb}(\nu)\iint_{core}X_{Er,Yb}N_{Er,Yb}|\psi(x,y)|^2\,\mathrm{d}x\,\mathrm{d}y. \tag{4.24}$$

The propagation of pump and signal are then described by the differential equations

$$\begin{aligned}\frac{\mathrm{d}P_p(z)}{\mathrm{d}z} &= \pm[\gamma_e^{Yb}(\nu_p,z)-\gamma_a^{Yb}(\nu_p,z)]P_p(z)\\ &\quad \pm[\gamma_e^{Er}(\nu_p,z)-\gamma_a^{Er}(\nu_p,z)]P_p(z)\mp\alpha_pP_p(z)\end{aligned} \tag{4.25}$$

$$\frac{\mathrm{d}P_s(z)}{\mathrm{d}z} = [\gamma_e^{Er}(\nu_s, z) - \gamma_a^{Er}(\nu_s, z)]P_s(, z) - \alpha_s P_s(z), \tag{4.26}$$

and the propagation of erbium and ytterbium ASE at frequency ν_j by

$$\begin{aligned}\frac{\mathrm{d}P_{ASE}^{\pm Er,Yb}(\nu_j, z)}{\mathrm{d}z} &= \pm[\gamma_e^{Er,Yb}(\nu_j, z) - \gamma_a^{Er,Yb}(\nu_j, z)]P_{ASE}^{\pm Er,Yb}(\nu_j, z) \\ &\quad \pm 2h\nu_j\Delta\nu_j\gamma_e^{Er,Yb}(\nu_s, z) \mp \alpha_{s,p}P_{ASE}^{\pm Er,Yb}(\nu_j, z)\end{aligned} \tag{4.27}$$

where the $\pm$ signs indicates forward or backward propagating pump and ASE power. The factor of 2 accounts for the two perpendicular polarization modes, and the term $\Delta\nu_j$ is the width of the jth frequency interval. To obtain the total ASE power, equation (4.27) is integrated over the entire ASE spectrum.

The solution is found by an iterative procedure where equations (4.25), (4.26) and (4.27) are integrated numerically forward and backward through the waveguide using a fourth order Runge Kutta method. The input parameters for each iteration are the pump and signal input powers, $P_p^+(0)$ and $P_s(0)$, the forward propagating ASE, $P_{ASE}^+(\nu, 0)$, and the result of the previous backward integration as a guess value for the backward propagating ASE, $P_{ASE}^-(\nu, 0)$. In the first forward integration $P_{ASE}^-(\nu, z)$ is set to zero. If bidirectional pumping is desired, an additional pump, $P_p^-(z)$ is introduced, and handled in the same way as the backward propagating ASE.

Once the calculations have converged, the gain of the amplifier is determined as

$$G(dB) = 10\log_{10}\left[\frac{P_s(L)}{P_s(0)}\right], \tag{4.28}$$

and the noise figure can then be found from the gain and the spectral density of the forward propagating ASE at the signal frequency, $P_{ASE}^+(\nu_s, L)$, as

$$NF(dB) = 10\log_{10}\left[\frac{P_{ASE}^+(\nu_s, L)}{h\nu_s\Delta\nu_s G} + \frac{1}{G}\right]. \tag{4.29}$$

The noise figure is thus a measure of the spectral density of the ASE in a narrow frequency interval around the signal wavelength. If a strong gain increase is obtained at the input of the amplifier, the forward propagating ASE power, $P_{ASE}^+(\nu_s, L)$, decreases, and hence the noise figure decreases [61]. This means that a counter-propagating pumping

scheme (*i.e.* where the pump propagates in the opposite direction of the signal) is unsuitable, and therefore the model only allows for co-propagating pump (pump in the same direction as the signal), and bidirectional pumping (pumping from both directions).

Chapter 5

Ytterbium Doped Planar Waveguides

Components based on ytterbium doping of glass and crystals has been used for a number of different applications including 1083 nm amplifiers for spectroscopy of helium [62, 63], optical coherence tomography (OCT) [64], 1020 nm pump for 1300 nm Pr^{3+} doped fluoride amplifiers [65] and Pr^{3+} doped ZBLAN upconversion lasers [66], and 1140 nm pump for Tm^{3+} doped ZBLAN upconversion lasers [67]. Ytterbium is also often used as a sensitiser for Er^{3+} ions as will be discussed in the next chapter, and has furthermore been used as a sensitiser for many other rare earths including Tm, Ln, Nd and Tb (see *e.g.* [68]. Ytterbium lasing was reported the first time in an oxide glass rod in 1962 [69], and has since then been reported in Yb doped glass and crystal hosts [70, 71]. In 1988 the first Yb doped fiber laser was made [72], and in 1993 an Yb doped fiber DBR laser was reported [73]. Recently planar waveguide lasers in ion-exchanged glass have been reported [74, 75].

Two types of loss mechanisms that could affect an ytterbium doped (or codoped) component are lifetime quenching [13] and cooperative upconversion [76, 77]. Cooperative upconversion is a process where two excited ytterbium ions close to each other decay simultaneously by emitting a single green photon. Although the process has been shown not to have a serious effect on the gain in even strongly doped fibers [78], it can be a quite strong effect in crystals such as $LiNbO_3$ where the upconversion is enhanced by interaction with the crystal lattice [77]. For this kind of crystals green upconversion laser action with a

maximum output power of 10.5 mW at 531 nm has been demonstrated [79].

We have also observed green fluorescence from our ytterbium doped waveguides. The waveguides furthermore had trace doping levels of erbium resulting from small amounts of erbium left in the frit after a previous deposition. This could be seen be monitoring the fluorescence of a pumped waveguide at 1550 nm. By recording the green fluorescence spectra and scanning the pump over the erbium 980 nm absorption peak, it could be seen that the green ytterbium upconversion fluorescence intensity was comparable to the green fluorescence intensity from the trace doping with erbium. Hence, it could be concluded that ytterbium upconversion is too weak to influence the gain of our waveguides in accordance with [78].

In this chapter I will start by discussing how to make ytterbium optically active by codoping with aluminium (section 5.1), then I will discuss the results obtained for ytterbium doped amplifiers and lasers (section 5.2 and 5.3), and finally I will apply the numerical model described in chapter 4 to discuss the design of ytterbium doped planar waveguide lasers, section 5.4.

5.1 Influence of Al on the Emission Properties of Yb

Due to the very simple energy level structure it should be relatively simple to fabricate an ytterbium doped laser or amplifier, however, it has been reported that high ytterbium concentrations can lead to a lifetime quenching process, that is believed to be due to energy migration in clusters [13]. If a defect capable of de-exciting the ytterbium ions is near an ytterbium cluster it will act as an energy drain, and all the pump power will be lost in this process. This observation was confirmed by measurements on the first ytterbium doped planar waveguides made in this project. The waveguides had an ytterbium concentration of approximately 0.28 at%, and showed no gain.

In view of the possible concentration dependent lifetime quenching, the concentration was reduced in the next waveguides. Two methods were used to reduce the ytterbium concentration; dilution by aluminium and increased deposition rate combined with a reduced ytterbium flow. In this way waveguides with and without Al codoping, but

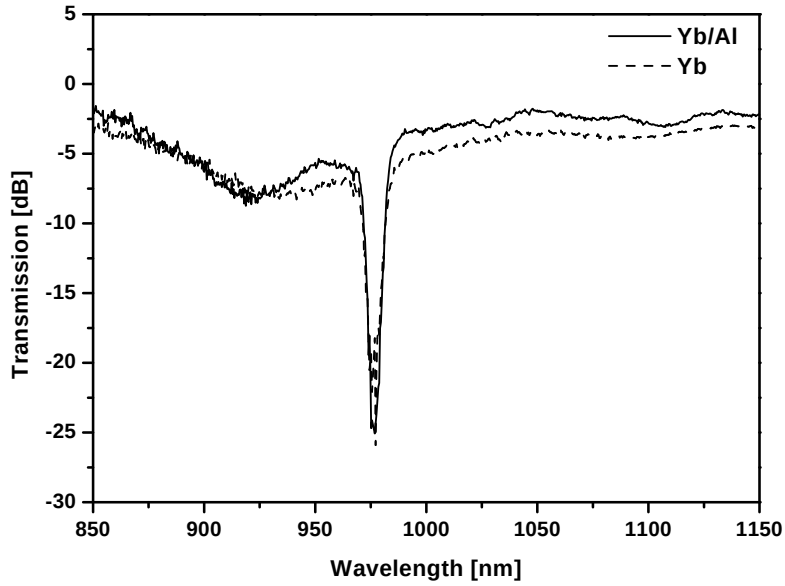

Figure 5.1: *Ytterbium absorption for waveguides with and without Al codoping.*

with comparable ytterbium concentrations were obtained. Figure 5.1 shows absorption spectra of waveguides with and without Al codoping. The spectra are very similar, but the absorption in the waveguide without aluminium has a broad background of increasing absorption towards shorter wavelengths. This is similar to the observations of Pashotta *et al.* [13] who observed this phenomenon as a quenching effect. Figure 5.2 shows a spectrum of the forward propagating ASE for the two waveguides. The waveguides both had a width of 10 μm (as defined on the mask), and the insertion loss was approximately 2 and 3 dB for the waveguide with and without aluminium, respectively. The waveguides were pumped with 976 nm laser light, and the pump power was 7.7 mW for the waveguide with auminium, while 28 mW was used for the one without aluminium. The main difference here is the ASE power level which is significantly lower for Ge-silica than for Al/Ge-silica, even though much higher pump power was used for the Ge-silica waveguide.

As would be expected from this observation, only the waveguides

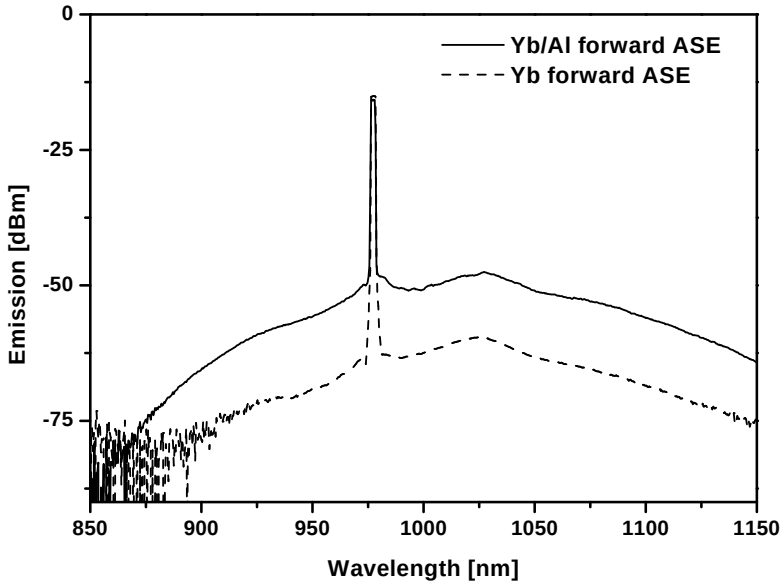

Figure 5.2: *Ytterbium forward propagating ASE for waveguides with and without Al codoping. The sharp peak at 976 nm is the pump laser.*

with Al codoping showed gain when pumped. To investigate this further, and remove the effect of the length and insertion loss of the waveguides, a series of thin films were made. The ytterbium concentration in the thin films were kept constant at 0.11 at% while the aluminium concentration increased from 0.09 to 0.49 at% as shown in figure 3.4 on page 26. Gain measurements on Al codoped waveguides will be discussed in the next section.

The influence of aluminium on the optical emission properties of ytterbium were now investigated by measuring the ytterbium fluorescence as a function of pump power when pumped at 980 nm for the different thin films. For this measurement a setup as described in section 3.3.2 was used.

Unfortunately, the laser diode used in this experiment had side-modes that overlapped with the ytterbium emission and pump power reflected from the thin film was thus detected also. The fluorescence dependence on pump power was therefore calibrated by subtracting a

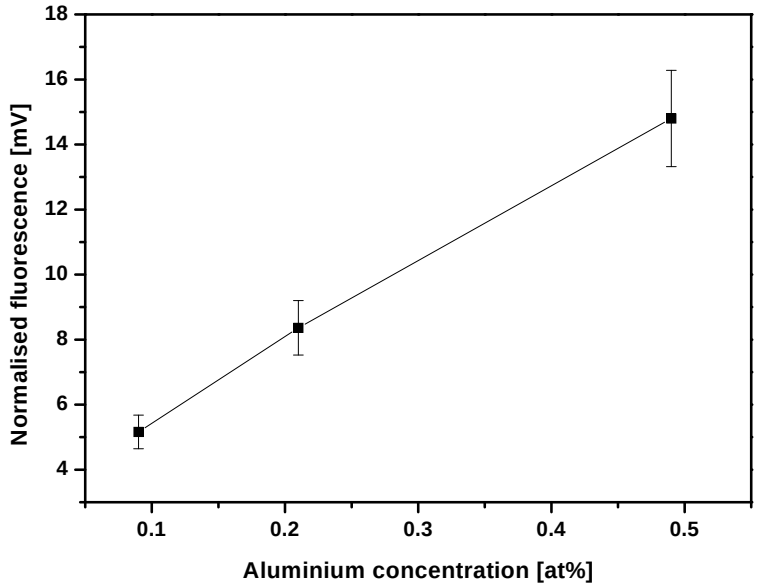

Figure 5.3: *Ytterbium fluorescence as a function of aluminium concentration.*

measurement made on a similar wafer with an undoped silica thin film. The measurements were made several times, repeatedly measuring first the fluorescence and then the reference, and in this way it was determined that the calibration was accurate within approximately 10%. To take the varying ytterbium concentration and film thickness into account, the data have been normalised by dividing with these parameters. Figure 5.3 shows the result of this measurement. A dramatic increase in the maximum obtainable fluorescence is observed with increased aluminium concentration, in accordance with the observation in figure 5.2.

Lifetime measurements could not be made on the thin films because of the quality of the laser diode, but were instead made on the ytterbium doped waveguides by measuring the fluorescense emitted perpendicular to the waveguide. In this way the lifetimes of the Yb and Yb/Al doped waveguides were determined to be approximately 750 and 790 μs respectively as is normal for this type of glass [13]. No short lifetime component could be observed, so the lifetime quenching

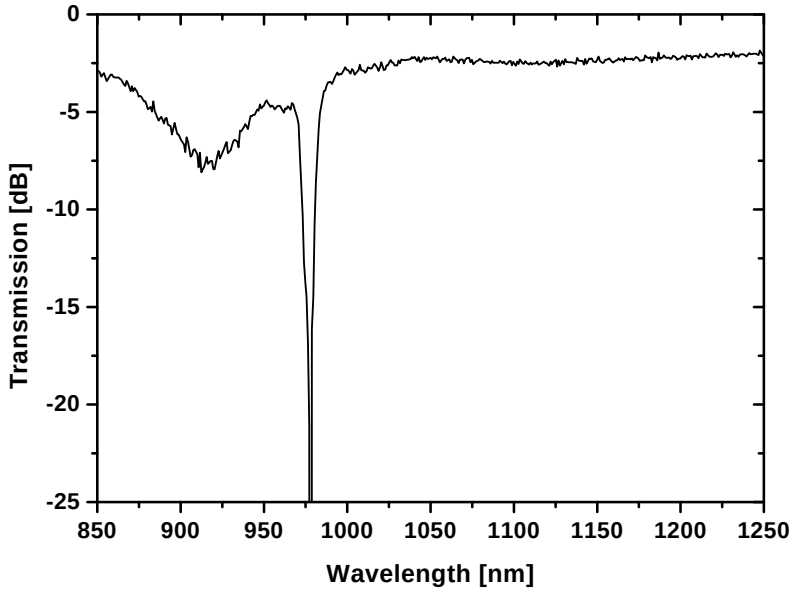

Figure 5.4: *Absorption spectrum for an ytterbium/aluminium-doped planar waveguide. The insertion loss of the waveguide is measured at 1250 nm where the ytterbium absorption is negligible. In this way the insertion loss is determined to be 2 dB*

must be faster than the risetime of 2 μs of the photodiode used in the measurements.

This explains why it was not possible to obtain a net gain in the pure ytterbium doped waveguides, and stresses how important codoping with Al is in order to make useful components based on ytterbium codoping.

The observation that aluminium is needed to obtain a strong fluorescence intensity is in good agreement with the explanation of the ytterbium lifetime quenching. By codoping with aluminium clustering of the ytterbium ions should be reduced, and hence the effect of cluster induced lifetime quenching should also be reduced.

5.2 Planar Waveguide Amplifiers in the 1000 – 1100nm range

As shown in the previous section, codoping with aluminium improves the emission properties of ytterbium. Therefore ytterbium/aluminium codoped planar waveguides were made as described in chapter 3. Waveguides with a height of approximately 4.5 μm and widths of 8 and 10 μm were made. The refractive index of the core measured at 632 nm was 1.4621. The dopant concentrations of ytterbium and aluminium were approximately 0.07 at% and 0.3 at% respectively, and after cleaving of the facettes the waveguides were 5.5 cm long.

Figure 5.4 shows an absorption spectrum of an Yb/Al doped planar waveguide. The insertion loss of the waveguide may be estimated by measuring the transmission loss at 1250 nm where where the ytterbium absorption is negligible, and we see that it is approximately 2 dB. The insertion loss is obtained as a sum of the propagation loss of the waveguide and the fiber-to-waveguide coupling loss. The propagation loss originates from sidewall roughness, impurities in the glass etc. while the coupling loss stems from a mode mis-match between the fiber and waveguide modes. The coupling loss can thus also be estimated by measuring fiber and waveguide mode profiles, and calculating the overlap integral for the fiber and waveguide modes. Based on measured modeprofiles, the propagation loss has been estimated to be approximately 0.1 dB/cm, corrresponding to the value of our best erbium doped waveguides.

The small-signal gain of the waveguides was measured as

$$G(dB) = 10 \log \frac{P_{out} - P_{ASE}}{P_{in}} \tag{5.1}$$

using the ASE spectrum from an Yb-doped fiber as signal source. For this experiment the signal power was approximately 10 % of the ASE level, and the gain spectrum was measured using a lock-in technique. Figure 5.5 shows a gain spectrum of a waveguide with a nominal width of 8 μm when pumped with 150 mW at 976 nm. The waveguide showed gain in the range from approximately 1000 nm to 1150 nm, with a maximum of 0.3 dB/cm at 1020 nm. Figure 5.6 shows the gain of the amplifier at 1020 nm as a function of pump wavelength when pumped with 100 mW. Due to the optics involved in coupling the Ti:sapphire output into the fiber, the available pump wavelengths were reduced

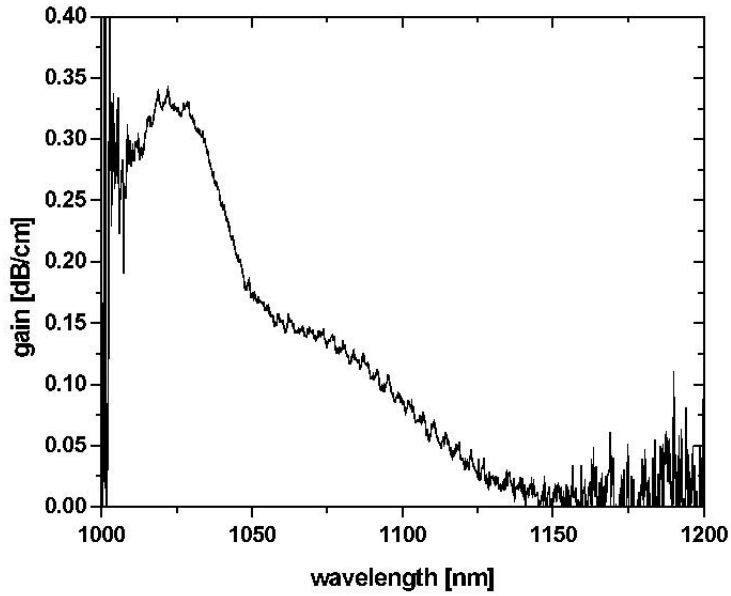

Figure 5.5: *Gain spectrum for an ytterbium/aluminium doped planar waveguide pumped with 149 mW at 976 nm.*

to the interval in the figure rather than covering the entire ytterbium absorption spectrum. From the figure we see, that the gain drops gradually with increasing pump power until $\lambda \sim 976$ nm where it falls abruptly. This happens because the rate of stimulated emission at the pump wavelength becomes comparable to the rate of absorption. For short pump wavelengths, a high inversion can be obtained since the emission cross section is low, however, if pumped at 976 nm, the maximum obtainable inversion is 50% since the emission and absorption cross sections are comparable. Figure 5.7 shows the gain as a function of pump power, when the amplifier is pumped at 957 and 976 nm respectively. We see, that when pumped at 976 nm the gain saturates at a maximum value of approximately 1.75 dB, while the gain is not saturated with the available pump power when pumped at 957 nm, but instead increases above 2.25 dB. We have thus demonstrated active 5.5 cm long ytterbium doped planar waveguides with a gain of more than 0.4 dB/cm at 1020 nm.

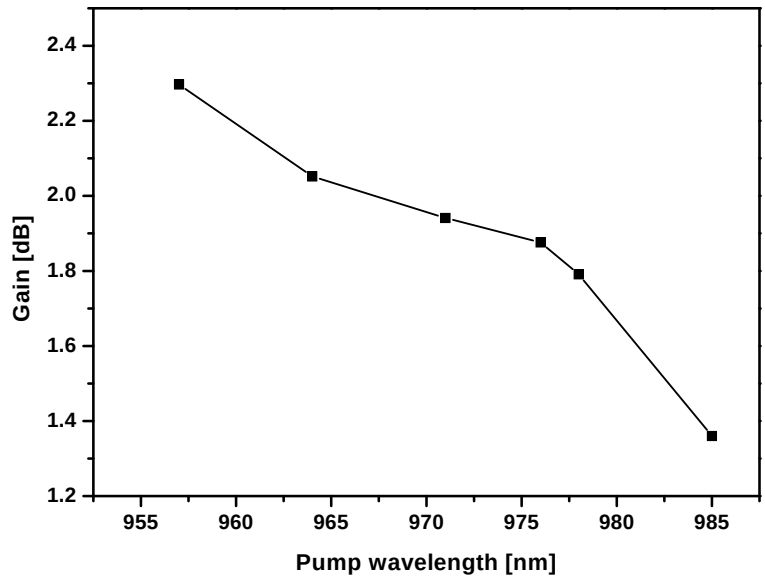

Figure 5.6: *Gain at 1020 nm as a function of pump wavelength when pumped with 100 mW.*

5.3 Demonstration of an Yb Doped DBR Laser

Ytterbium doped fiber lasers and lasers made in bulk crystals, have been available for some time, however, ytterbium doped planar waveguide lasers have only recently been presented by other groups. Florea *et al.* presented the first laser of this kind in 1999 [74]. Their laser was made by ion-exchange, and the cavity was formed by gluing broadband reflecting mirrors to the end facets, and consequently the laser operated in the entire band between 1020 and 1030 nm. Veasey *et al.* reported a more sophisticated laser in 2000 [75]. This laser was also made by ion exchange, but used a DBR surface-relief grating in one end of the cavity to provide a more narrow emission range, however, the laser was still multimoded. Table 5.1 shows some characteristic values of these lasers. To the best of my knowledge, these are the only other groups that have presented ytterbium doped planar waveguide lasers,

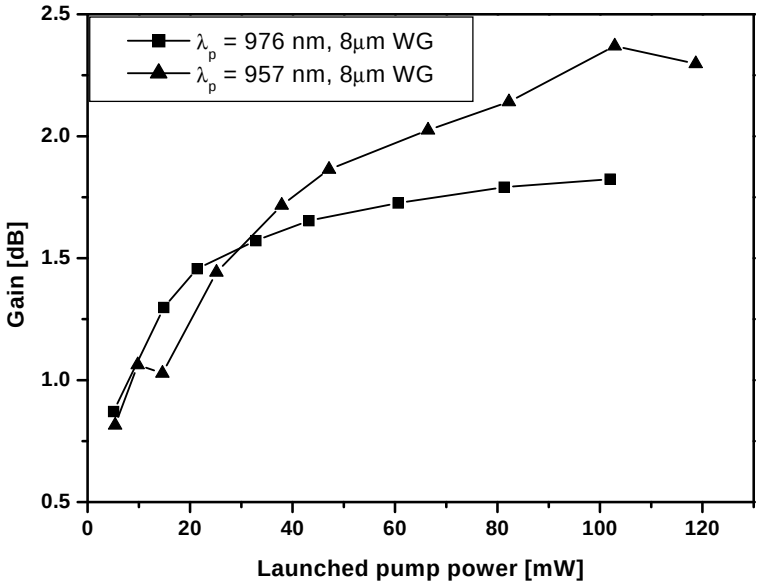

Figure 5.7: *Gain at 1020 nm as a function of pump power.*

and they both used ion exchange to make the channel waveguides.

Having verified that there was optical gain in the ytterbium doped waveguides, it was attempted to use the waveguides for lasers.

The measured results will here be compared to those predicted by the model presented in chapter 4. I have modelled the actual DBR laser using the parameters given in table 5.2, and the absorption and emission cross sections shown in figure 5.8. The absorption cross section spectrum has been calculated from measured absorption spectra using the formula [61]

$$\sigma_a(\nu) = \frac{att(\nu)}{10\log_{10}(e)N_{yb}\iint_{core}|\psi(x,y)|^2 \mathrm{d}x\mathrm{d}y}, \tag{5.2}$$

where $att(\nu)$ is the attenuation in dB, and the emission cross section calculated from this using the McCumber relation [80]

$$\sigma_e(\nu) = \sigma_a(\nu)\exp\left(\frac{hc}{kT}\left(\frac{1}{\lambda} - \frac{1}{\lambda_0}\right)\right). \tag{5.3}$$

The scaling of the emission spectrum have been done by assuming that the absorption and emission spectra are equal at the main peak at $\lambda_0 =$ 976 nm, which should be correct within a few percent [78]. It was not possible to accurately resolve the peak of the strong absorption at 976 nm, and therefore, the values of the cross sections may not be correct at this wavelength. The confinement factors have been calculated using the improved effective index method described in chapter 4. The values of τ_{Yb}, κ, $\alpha_{p,s}$ and N_{Yb} correspond to the measured values.

The lasers were made in a DBR configuration using Bragg gratings that were UV-written into the Ge-doped waveguide core. Figure 5.9 shows a schematic illustration of the laser design. To improve the photosensitivity of the glass, the waveguides were deuterium loaded for 60 hours at 120 bar and room temperature. The gratings were made by exposing the waveguides to 248 nm light through a zero-order nulled phase mask with a period of 716 nm. The fluence was 200 mJ/cm^2 per pulse for a total of 100 J/cm^2. Two 5 mm long beam apodised Bragg gratings [81] were written in the waveguides with a center-to-center spacing of 3.5 cm, and subsequently annealed at 200°C to ensure long-term stability of the gratings. The phasemask used for the UV writing was only 1 cm long so the two gratings were written separately. In this way the gratings are not guaranteed to be exactly the same, and small differences in the gratings coupling strength and Bragg wavelength should be expected. A more optimal way of writing the gratings would be to use a long phasemask, and mask the cavity region from the UV light during exposure. In this way it is ensured that the phasemask is aligned to the waveguides in the same way for both gratings, and that each grating receive the same total UV fluence.

Figure 5.10 shows a transmission spectrum of a planar waveguide

Ref.	Technology	Reflectors	Host	Conc. [at.%]	Thresh. [mW]	Slope
[74]	Ion exch.	DM	Ba-SiO_2	1.02	45	5%
[75]	Ion exch.	DM/EG	P_2O_5	0.38	25	67%
This work	PECVD	UV-grat.	Al/Ge-SiO_2	0.07	12	14%

Table 5.1: *Parameters for reported ytterbium planar waveguide lasers. DM: Dielectric mirror, EG: Etched grating.*

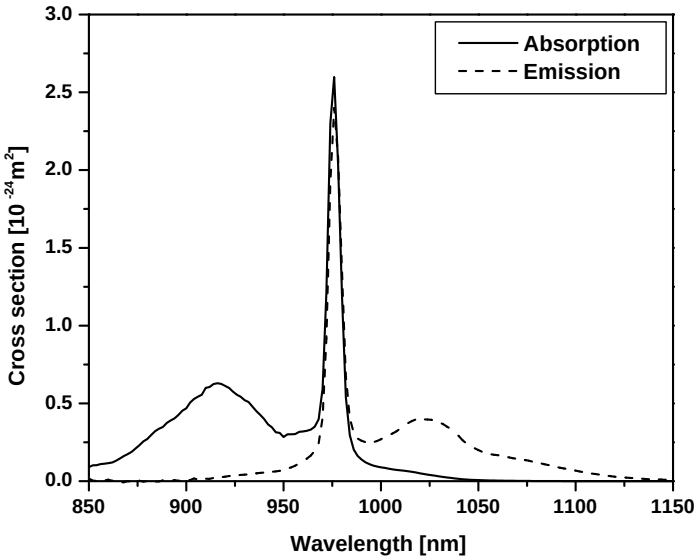

Figure 5.8: *Ytterbium cross section used for calculations.*

laser cavity with a nominal width of 10 μm. The spectrum shows two broad transmission dips, corresponding to the two polarisation modes of the waveguide. The two polarisations have arbitrarily been labeled TE and TM in the figure. From this we see that there is a strong birefringence causing a splitting of approximately 0.6 nm of the two polarisation modes. This large splitting of the otherwise degenerate polarisation modes is mainly due to stress in the glass and substrate. In the fabrication a total of 25 - 30 μm of silica is deposited on *one* side of the silicon substrate. This induces stress in the wafer that can be clearly seen as a bending of the wafer. To give a feeling for the amount of stress in the waveguide, a cleaved wafer placed on a flat table has a gap between table and wafer of approximately 1 mm at the center. The two broad transmission dips each have two minima close to each other. This shows that the two Bragg gratings are indeed not completely identical.

The waveguides were pumped by a Ti:sapphire laser operating at 976 nm coupled into a 980 nm singlemode fiber. The DBR laser signal was sent through a fiber U-bracket with a filter that suppressed

Parameter	Value	Parameter	Value
Height	4.5 μm	Cavity length	30 mm
Width	8 μm	Grating lengths	5 mm
Core Index	1.455	α_p, α_s	0.1 dB/cm
Cladding index	1.445	N_{Yb}	6×10^{25}ions/m^3
λ_p	976 nm	σ_a^p (976 nm)	2.5989×10^{-24} m^2
λ_s	1042 nm	σ_e^p (976 nm)	2.3998×10^{-24} m^2
Γ_p	0.95	σ_a^s (1042 nm)	1.2349×10^{-26} m^2
Γ_s	0.93	σ_e^s (1042 nm)	2.6204×10^{-25} m^2
Λ	358 nm	τ_{Yb}	0.75 ms
κ	447 m -1		

Table 5.2: *Parameter values for simulation of actual laser.*

light with a wavelength below 990 nm more than 20 dB in order to reduce any residual pump power. The 1042 nm laser light was spectrally resolved using a double-monochromator optical spectrum analyser (OSA) with a spectral resolution of 0.02 nm. Additionally the lasing emission was investigated using a scanning Fabry-Perot interferometer with a free spectral range of 10 GHz.

Figure 5.11 shows the laser output spectrum of a planar waveguide laser with a nominal width of 10 μm measured with the OSA at a spectral resolution of 0.02 nm using 147 mW of 976 nm pump power. At this pump power the output power of the laser was 19 mW at 1042 nm. Above 50 mW pump power the laser had a signal-to-ASE ratio of more than 60 dB, comparable to that of DFB fiber lasers. Compared to semiconductor lasers which normally have a signal-to-ASE ratio of approximately 35 dB (see *e.g.* [82]) this is a very impressive noise suppression.

The laser presented here only showed lasing operation in one of the two polarisation modes, but many of the other lasers on the wafer operated in two polarisation modes. Often, one polarisation mode could be suppressed by careful optimisation of the coupling and use of index matching gel which suggests a polarisation-dependent reflection from the waveguide facet. Furthermore, the long-wavelength polarisation mode experiences a weaker reflection by the gratings, and is thus expected to have a higher pump threshold. The spectral properties of the laser were investigated further using a scanning Fabry-Perot in-

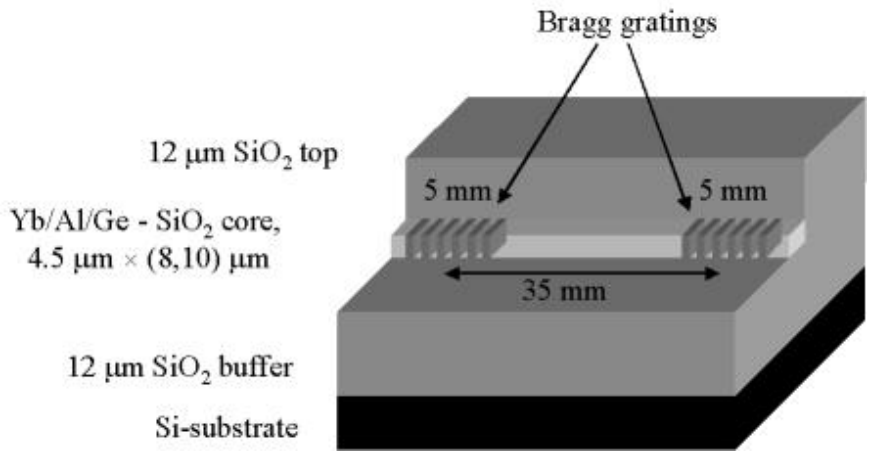

Figure 5.9: *Schematic drawing of the laser structure.*

terferometer which showed that the laser operated in two longitudinal modes with a measured spectral separation of approximately 3 GHz. This corresponds to the modespacing between the two lowest-threshold modes as calculated with the laser model.

To investigate the response of the laser to the pump wavelength, the laser output power at 1042 nm was measured as a function of pump wavelength when pumped with 115 mW as shown in figure 5.12. The squares are the measured data, and the dashed line is calculated with the laser model. Besides the differences in power the figure shows good agreement between theory and experiment. As expected, the output power peaks strongly at a pump wavelength of 976 nm where the absorption cross section has the maximum value. The differences between the calculated and measured values are not surprising, since the simluation only considers one mode, does not include waveguide-to-fiber coupling, and is for a 4 cm long ytterbium doped waveguide laser. The actual laser is also 4 cm long, but since the total length of the waveguide is 5.6 cm, some loss of pump and signal due to absorption must be expected.

The laser output power versus pump power is shown in figure 5.13 along with calculations for one of the lowest-threshold modes. The measured lasing threshold and slope efficiency was approximately 12 mW and 14%, respectively, while the calculations predict a threshold of 9 mW, and a slope of 17% for one mode. The higher pump threshold for the actual laser is expected since two modes are competing for the gain

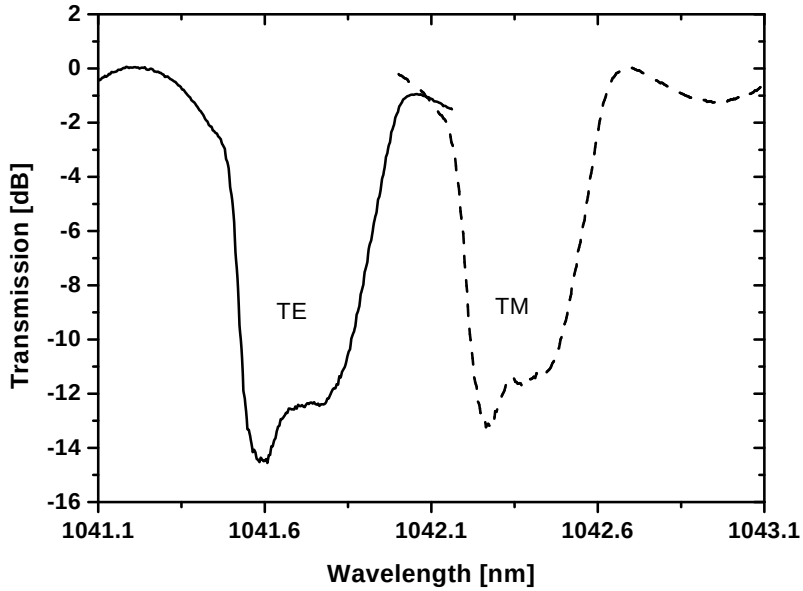

Figure 5.10: *Transmission spectrum of a laser cavity within a planar waveguide with a nominal width of 10 μm. The transmission dip is split by 0.6 nm due to birefringence.*

in the laser cavity. The backward propagating laser emission differed from the forward propagating emission by approximately 10%. This is not taken into account in the calculations here, but will be considered in the next section.

5.4 Optimisation of Laser Design

There are several points where the DBR laser design can be improved. For example the demonstrated laser emits in both ends. Since this is rarely, if ever, needed, it would be more optimal to have the laser emitting all the laser power in one end. This could be done by using an asymmetric laser design. Another point is the optimal cavity length. In order to reduce the number of lasing modes, the cavity length should be short, but this means low output power, and it may be necessary to fine-tune the phaseshift. These points will be discussed here. As will

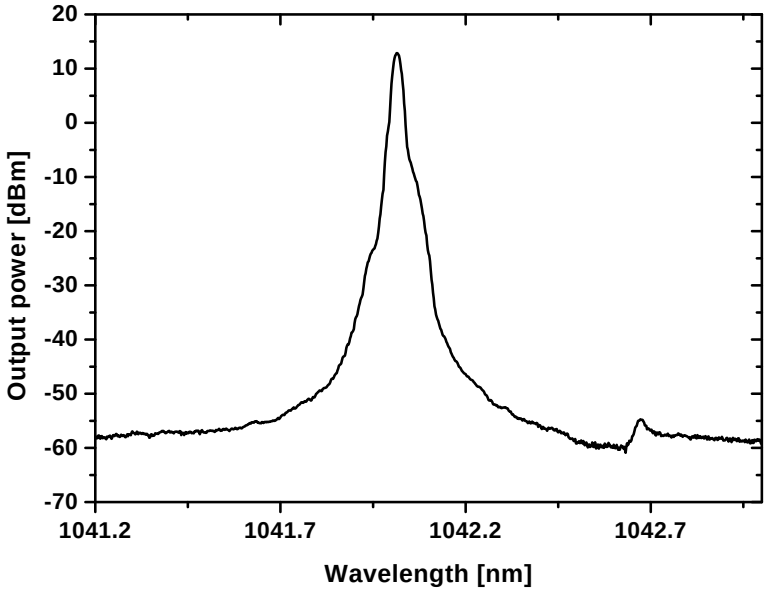

Figure 5.11: *Spectrum of a planar waveguide laser with a nominal width of 10 μm pumped with 147 mW at 976 nm. The limited spectral resolution of the OSA is insufficient to reveal that the laser oscillates in two longitudinal modes.*

be shown, a DBR laser without phaseshift is expected to operate in at least two longitudinal modes. Therefore the simulations presented here focus on optimising the laser design with respect to maximum output power. The parameters used for the simulations are given in table 5.3.

5.4.1 Phaseshift dependence of a DBR laser

In a DFB laser a central phaseshift of π is required to obtain single mode operation, but usually the phaseshift dependence of a DBR laser is neglected, since it has no influence in a Fabry-Perot like cavity. To investigate when this assumption is valid I have studied the transition from a DFB to a DBR laser by introducing a cavity in a 5 cm long DFB laser with a discrete central π phaseshift as illustrated in figure 5.14. The DBR lasers created in this way will thus also have the discrete π

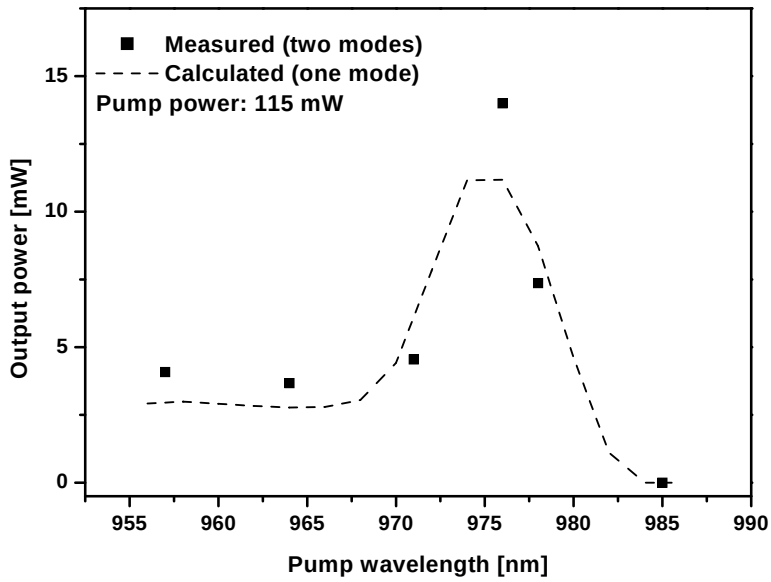

Figure 5.12: *Laser output power as a function of pump wavelength when pumped with 100 mW.*

phase shift of the DFB laser, and the effect of this will be investigated. I consider the entire laser to be ytterbium doped, *i.e.* there is gain in the DBR gratings.

Figure 5.15 shows the output power as a function of the grating coupling strength, κ, for lasers pumped with 100 mW. The lower limit of the coupling coefficient occurs because the reflectivity of the gratings in this case is too low to provide the feedback to the cavity required for laser oscillation. The effect of the loss is to set an upper limit for the coupling coefficient since more power will be lost due to the background losses compared to what is coupled out of the gratings. This means that the laser will operate optimally for values of κL in a narrow interval determined by the effective gain in the laser. A similar effect is seen if the coupling coefficient is held constant, and the grating length is increased [83].

As the grating length decreases, the optimal κ - value increases since the grating has to be stronger in order to provide the same reflectivity as a long grating. Furthermore we see that the maximum available

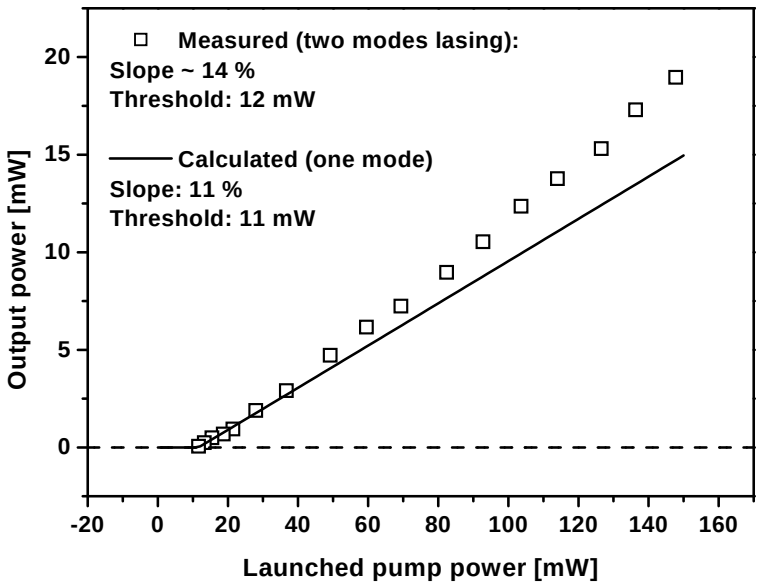

Figure 5.13: *Laser output power at 1042 nm as a function of launched pump power at 976 nm.*

power increases with the cavity length. Looking at figure 5.16, we see that even though the DFB laser has the highest signal power in the center of the cavity, it is only a small fraction of the power that is actually coupled out through the long gratings.

Figure 5.17(a) shows the output power as a function of phaseshift for lasers with increasing cavity lengths. For these calculations the optimum value of κL as determined from figure 5.15 has been used, and the pump power is set to 100 mW. For short cavity lengths we see a strong phaseshift dependence of the output power, as the short cavity can be interpreted as a long distributed phaseshift of a DFB laser. As the laser approaches a Fabry-Perot configuration with short gratings and a long cavity, the phaseshift dependence decreases as expected. From this we see, that a minimum cavity length of 20 mm is needed if the fluctuations in output power due to the phaseshift should be kept below 3%. It is not reasonable to impose more strict requirements on the design since the experimental uncertainty on the actual grating strength and phaseshift will give fluctuations of this order of

Parameter	Value	Parameter	Value
Height	4.5 μm	Λ	358 nm
Width	8 μm	α_p, α_s	0.1 dB/cm
Core Index	1.455	N_{Yb}	4×10^{25}ions/m^3
Cladding index	1.445	σ_a^p (976 nm)	2.5989×10^{-24} m^2
λ_p	976 nm	σ_e^p (976 nm)	2.3998×10^{-24} m^2
λ_s	1042 nm	σ_a^s (1042 nm)	1.2349×10^{-26} m^2
Γ_p	0.95	σ_e^s (1042 nm)	2.6204×10^{-25} m^2
Γ_s	0.93	τ_{Yb}	0.7 ms

Table 5.3: *Parameter values for optimisation of DBR laser design.*

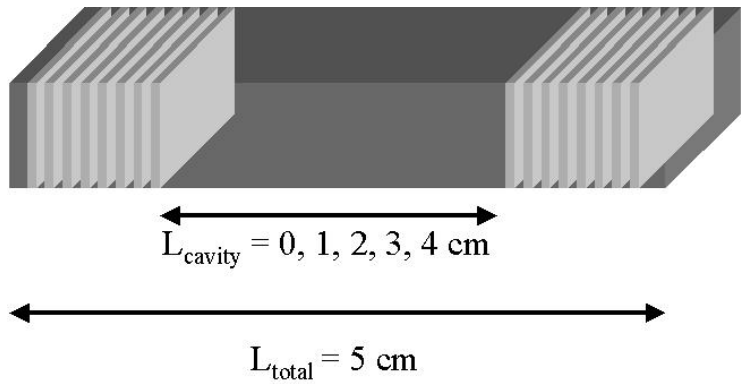

Figure 5.14: *Laser structure used for simulations*

magnitude. Figure 5.17(b) shows the output power as a function of phaseshift for a laser with a 10 mm cavity. The three curves correspond to a low κ-value, the optimum κ-value for a π phaseshift, and the optimum κ-value for no phaseshift, respectively. If the coupling strength is higher than the optimum for a π phaseshift, then the output power reaches a minimum if the phaseshift becomes equal to π. The dip causes a variation of 5-10 % in the output power, and is due to the shape of the reflectance spectrum. In the center of the bandgap the reflectivity is highest, so for a weak grating it is most optimal to have the lasing mode exactly in the center of the bandgap, *i.e.* have a π phaseshift. However, if the grating becomes too strong, the grating reflectivity combined with the propagation loss will be too large if the mode is in the center, and therefore more output power can be

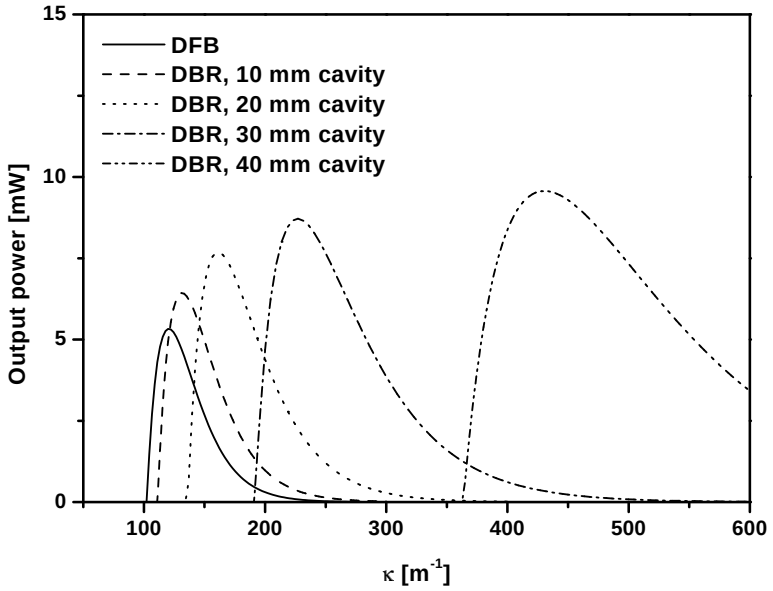

Figure 5.15: *Output power as a function of k for increasing cavity length. All curves are for a laser with a central π-phaseshift.*

obtained if the mode is moved away from the center, *i.e.* if there is no phaseshift.

This effect can also be seen from figure 5.18 (a) and (b) where the output power is plotted as a function of pump power for the laser with a 10 mm and a 20 mm cavity respectively. Each graph shows four curves, two for a π phaseshift, and two for no phaseshift. In each case the curves correspond to the optimum value of the coupling coefficient for no phaseshift, and a phaseshift of π, respectively. For the 10 mm cavity we see, that for a phaseshift of π, and a value of κ that is higher than the optimum value ($\kappa = 150$ m^{-1}), the slope efficiency is lower than for the optimum value of κ ($\kappa = 131$ m^{-1}), but so is the pump threshold. The reduced slope is due to losses in the cavity, as we already saw for the κ-dependence. The reduced threshold occurs because the higher reflectivity provides a stronger feedback to the cavity, and thus a better use of the available gain in the cavity. For the case of no phaseshift we see that the curve for the optimal value of κ ($\kappa = 150$ m^{-1}) is almost identical to the corresponding one for

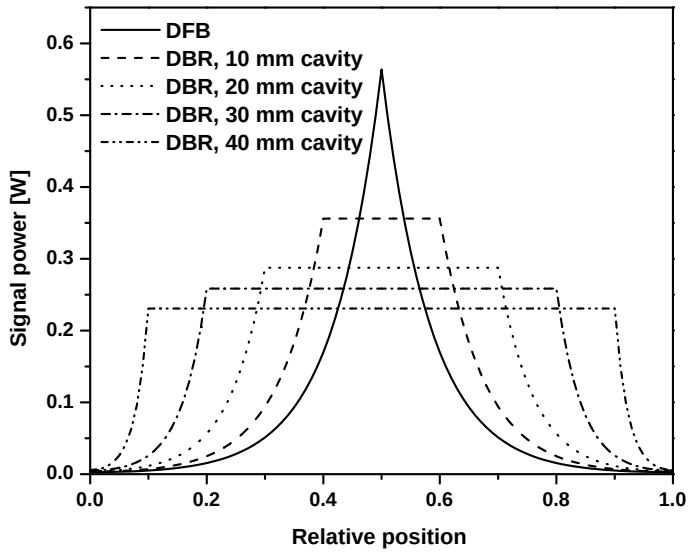

Figure 5.16: *Signal intensity along the laser.*

a π phaseshift as expected. However, the curve for a low value of κ ($\kappa = 131$ m^{-1}) has a much lower slope and much higher threshold. This is because the reflectivity of the grating is not strong enough to provide efficient feedback to the cavity. For comparison, the right graph shows the same case for a laser with a 20 mm cavity. Here the phaseshift dependence should be almost negligible, and we also see that all the curves are almost identical.

This can be understood by looking at figure 5.19 which shows the transmission spectra of laser cavities with varying length. As the cavity length increases, the modespacing decreases, and the modes experinece an almost equal threshold gain. The number of modes supported by the cavity increases as the laser approaches a Fabry-Perot configuration which has a free spectral range (FSR) of

$$\Delta\nu = \frac{c}{2nd} \tag{5.4}$$

where c, is the speed of light, n, the refractive index and d, the distance between the mirrors in the Fabry-Perot cavity. For comparison I also

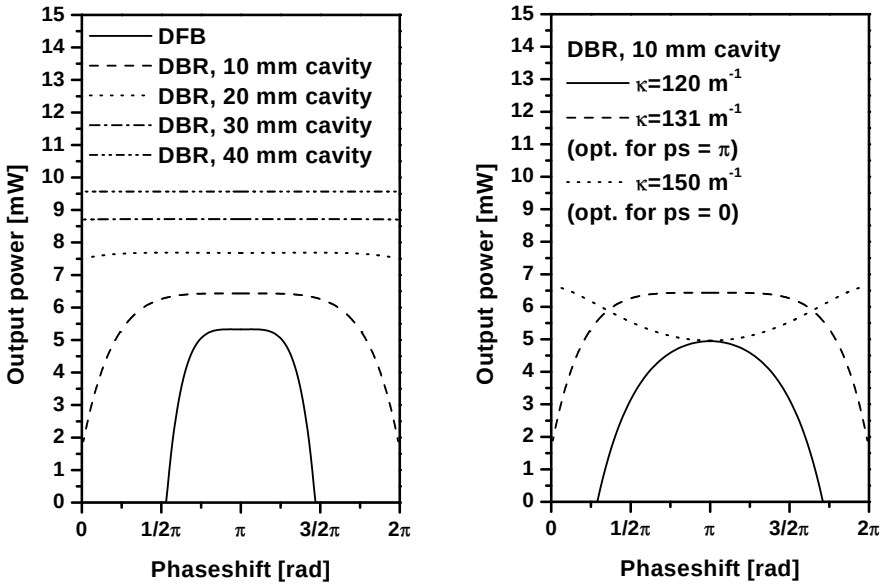

Figure 5.17: *Output power as a function of phaseshift. (a) Effect of introducing a cavity. (b) Effect of non-optimal coupling strength on the phaseshift dependence for a laser with a 10 mm cavity.*

show a similar spectrum for a DFB laser with a central discrete π phaseshift. It is clearly seen that the DFB laser can be brought to oscillate in a single mode while the DBR lasers are expected to be multimode in all cases.

From this, we can conclude, that in order to avoid problems with phaseshift dependency for DBR lasers, the cavity in a 5 cm long laser should be at least 2 cm long. However, by choosing a DBR design, we must expect that the laser will operate in at least two longitudinal modes unless there are external features that suppress one of the modes (*e.g.* an external narrow grating to provide feedback in only one laser mode, reduced overlap between the gratings or wavelength dependent losses in the waveguide). In the following I will consider only DBR lasers without a phaseshift.

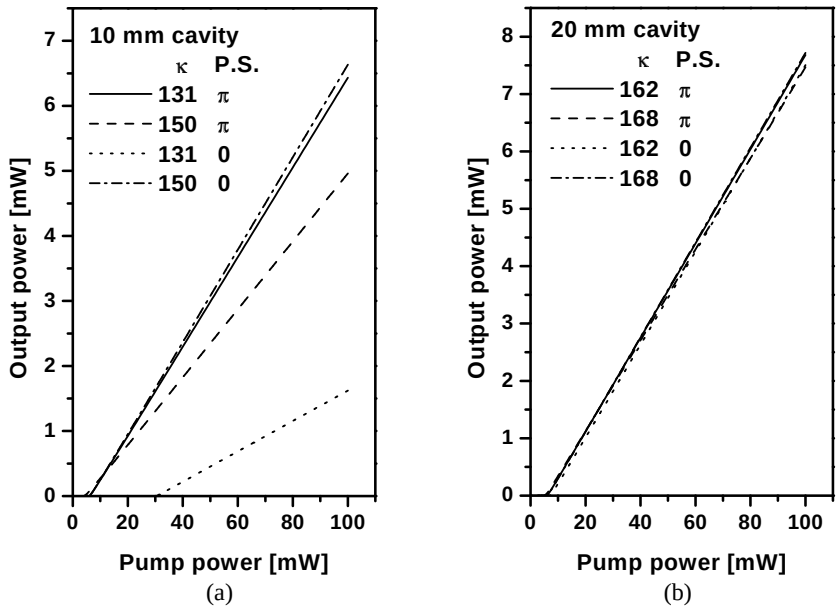

Figure 5.18: *Output power as a function of pump power.*

5.4.2 Asymmetric DBR lasers

The symmetric DBR laser design studied so far emits the same amount of power in both ends. This is usually not desirable, and can be avoided if an asymmetric design is used. As discussed earlier in this chapter, a good way of making DBR lasers with a well defined relation between the gratings is to use a single long phasemask which is blocked in the region of the cavity. An easy way of making asymmetric DBR lasers is then to displace the cavity from the center of the laser making the grating have unequal lengths. An alternative way could be to write the gratings separately, and with different modulation strength, but in this way there is a risk that the spectral overlap of the gratings will not be sufficient to allow laser oscillation since the Bragg wavelength is dependent on the UV induced refractive index change. Both of these methods result in gratings that have equal modulation strength and are asymmetric only in the respective lengths of the gratings.

Figure 5.20 (a) shows the output power in the right end as a function of κ, for a DBR laser with a cavity length of 20 mm. The pump

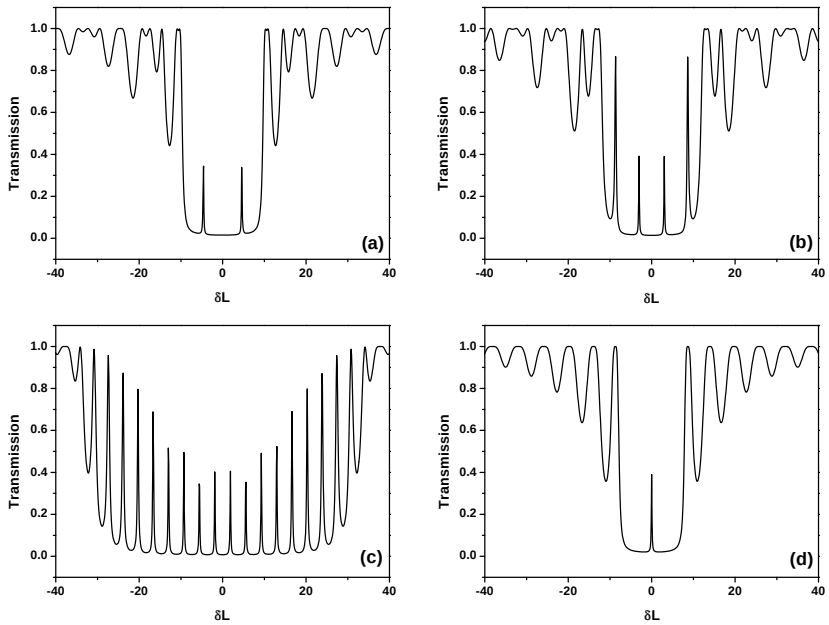

Figure 5.19: *Calculated transmission spectra. (a) DBR laser with a 10 mm cavity. (b) DBR laser with a 20 mm cavity. (c) DBR laser with a 40 mm cavity. (d) DFB laser with central discrete π phaseshift.*

power is 100 mW. The different curves correspond to a gradual displacement of the cavity towards the right of the laser. As the cavity is moved to the right, the output power from the right end increases. Part (b) of the figure shows the suppression of emission from the left end, and the corresponding maximum output power, as a function of asymmetry in the laser. The maximum output power of 13.5 mW is reached for an asymmetry of 1.7, and then decreases slightly since the right grating becomes too short to provide sufficient feedback to the cavity. At this asymmetry the suppression of emission from the left end is almost 15 dB corresponding to an output power of 0.4 mW.

Figure 5.21 shows a similar plot when the cavity is expanded to the right while keeping the length of the left grating constant. Again, the pump power is 100 mW. In this case the optimum is reached for an asymmetry of approximately 2, but since the cavity length increases, the maximum obtainable output does not decrease as strongly as in

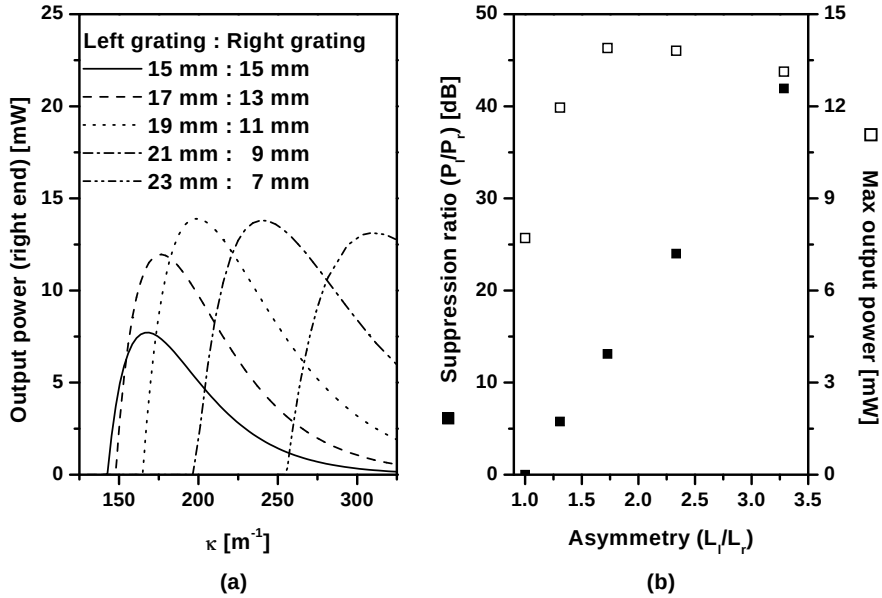

Figure 5.20: *(a) Output power as a function of κ for asymmetric DBR lasers. Displacing the cavity to the right.(b) Suppression ratio (left axis) and maximum obtainable output power (right axis) as a function of the asymmetry in the laser.*

figure 5.20 since the expansion of the cavity compensates for the decrease in output power. Since the length of the left grating is kept constant, the suppression of emission from the left end is not quite as strong as when the cavity length is kept constant and the length of the left grating increases.

Thus a DBR laser can be made to emit almost entirely from one end only, by making one grating approximately twice as long as the other. However, if the asymmetry becomes too large the maximum obtainable output power deceases, as the grating in the output end becomes too short.

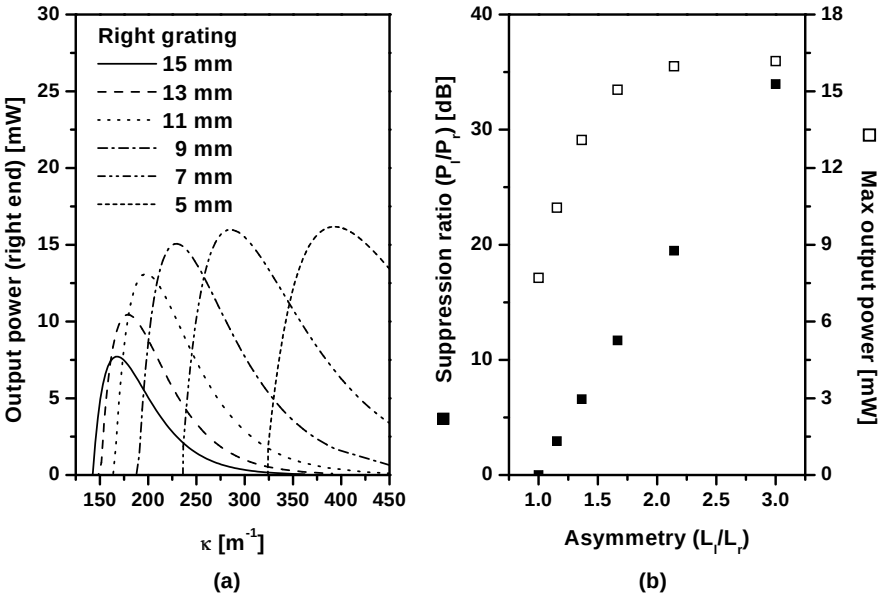

Figure 5.21: *(a) Output power as a function of κ for asymmetric DBR lasers. Expanding the cavity to the right. (b) Suppression ratio (left axis) and maximum obtainable output power (right axis) as a function of the asymmetry in the laser.*

Chapter 6

Erbium-Ytterbium doped silica glass

As discussed in chapter 2, the energy transfer process from ytterbium to erbium is more efficient in phosphate glass than in germanate glass due to the higher phonon energies. Although UV writing is possible in P-doped glass [84, 85, 86], there is currently no setup for doing this at COM. On the other hand we have very good facilities for UV writing in Ge-doped glasses using 248 nm light [87], and for laser applications it would therefore be convenient if it was possible to make Er/Yb codoped components in this type of glass. Pure silicate seems to be useful, and Er/Yb doped lasers have also been demonstrated in this host material [51]. Therefore it should be possible that doping with a small amount of germanium to increase the refractive index would not completely ruin the good qualities of silica glass.

To investigate this, point of reference was taken in a recipe for erbium/aluminium doped planar waveguides, that has been used for fabrication of lasers and amplifiers using Ge-doped glass. First, the influence of a small amount of ytterbium on the gain was investigated by substituting a small amount of aluminium with ytterbium in the recipe. The results of this are discussed in section 6.1. Then, thin films were made by substituting aluminium for ytterbium in order to reach high Er/Yb ratios. The thin film experiments were made for both P- and Ge- doped glass and are discussed in section 6.2. In section 6.3 I will use the models described in chapter 4 to simulate Er/Yb codoped amplifiers and lasers.

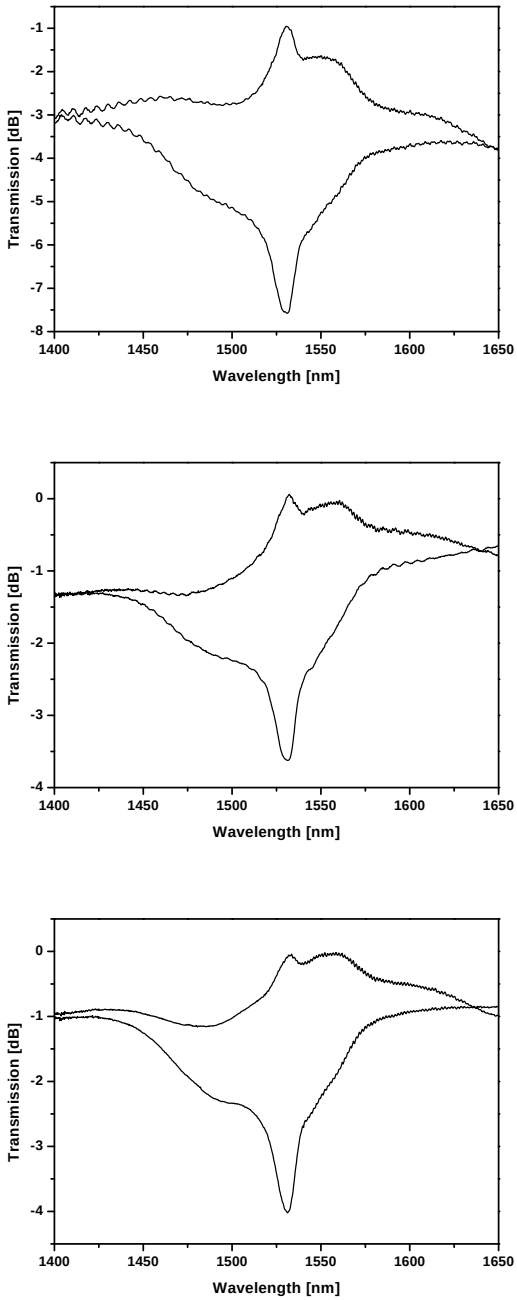

Figure 6.1: *(Top) Transmission spectrum of an Er/Al doped waveguide. (Middle) Transmission spectrum of an Er/Yb/Al doped waveguide (LDS mixing ratio: 10/4/86). (Bottom) Transmission spectrum of an Er/Yb/Al doped waveguide (LDS mixing ratio: 10/6/84).*

6.1 Preliminary measurements

Erbium-ytterbium doped waveguides were made, where the ytterbium concentration was kept lower than the erbium concentration in order to see how small amounts of ytterbium affects the erbium fluorescence. Four waveguides were made with increasing ytterbium concentration so that the Er:Yb LDS mixing ratio increased from 10:2 to 10:8. Aluminium was used to dilute the rare earths, and the waveguides were made as described in section 3.

Gain and absorption spectra were measured for each of the samples, and spectra for three of the waveguides can be seen in figure 6.1. As proposed by Armitage [88], the degree of inversion can be estimated by looking at a gain spectrum and comparing the main peak at 1530 nm with the broad peak at higher wavelengths. If there is a high inversion, the gain spectrum has the shape of the emission spectrum, *i.e.* the main peak is much stronger than the broad peak. Figure 6.1 shows the gain spectra from the waveguide without ytterbium ans two waveguides with increasing ytterbium concentration when pumped with 200 mW at 980 nm. The waveguide without ytterbium reaches almost full inversion, while the inversion decreases for increasing ytterbium concentration. The figure also includes absorption spectra, and we see that the insertion loss is bigger for the Er/Al waveguide than for the others, illustrating how the waveguide quality have been improved. We can thus see that even a small amount of ytterbium can be very harmful for a component based on erbium - doped germanosilicate.

6.2 Optimal host glass

In order to gain further insight into the role of the host glass, Er/Yb doped thin films were made, again with a fixed erbium concentration comparable to the pure erbium reference, and with increasing ytterbium concentration, but now with Yb concentrations that were higher than the Er concentrations, and both Ge- and P-doped films were made.

Table 6.1 shows the dopant concentrations in the two thin films. The two sets of thin films are based on a process optimised for doping Ge-silica with erbium, and the only difference between the two sets is the Ge or P doping. Comparing the concentrations of the two films, we see that the Er and Yb concentrations are higher in Ge-silica than

Ge-silica				
LDS mixing ratio	Er [at%]	Yb [at%]	Al [at%]	Ge [at%]
10/10/80	0.06	0.10	0.40	1.59
10/30/60	0.05	0.27	0.28	1.66
10/50/40	0.04	0.43	0.17	1.70
P-silica				
LDS mixing ratio	Er [at%]	Yb [at%]	Al [at%]	P [at%]
10/10/80	0.04	0.07	0.36	2.34
10/30/60	0.04	0.20	0.27	2.16
10/50/40	0.03	0.30	0.17	1.98

Table 6.1: *Dopant concentrations in the thin films.*

P-silica. Furthermore, the erbium concentration, which is fixed in the LDS mixing ratio decreases for both sets of thin films. Since some of the lauminium is replaced by ytterbium the aluminium content decreases with increasing ytterbium concentration.

The thin films were characterised by measuring the emitted erbium fluorescence, and lifetime in a setup as described in section 3.3.2, and the results are shown in figure 6.2. As the erbium concentrations and thicknesses of the films varied slightly from sample to sample, the measured fluorescense intensities have been normalised by dividing with the erbium concentration and film thickness corresponding to the measured thin film. For comparison, a measurement of a purely erbium/aluminium doped film with Ge-silica was included in the fluorescense measurements shown in part (a) of the figure. This sample had an erbium concentration of approximately 0.06 at%. For the Ge-silica films we see clearly that the sample without ytterbium has the highest fluorescence intensity, and that the fluorescence intensity decreases with increased ytterbium concentration in accordance with the measurements presented in the previous section. However, the aluminium concentration also decreases with increasing ytterbium concentration, and this will also lead to a reduction in fluorescence since there will be an increased degree of clustered erbium ions. It is therefore not possible to say if the decrease in fluorescence happens only because of the increased ytterbium concentration, or because of the decreased aluminium concentration. Comparing with the measurements in the

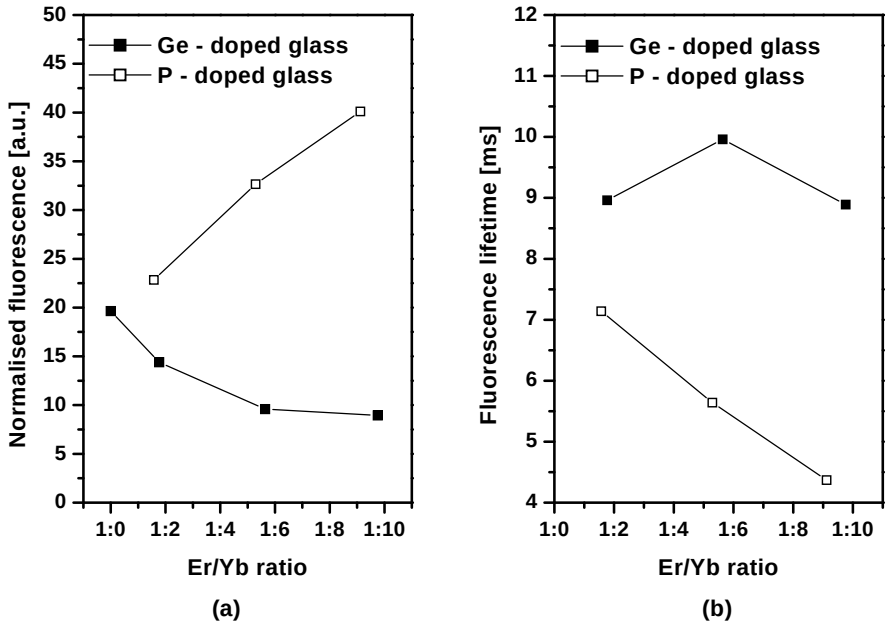

Figure 6.2: *(a) Er fluorescence as a function of Er/Yb ratio in the thin film. (b) Erbium fluorescence lifetime as a function of Er/Yb ratio in the thin film.*

previous section, however, it does seem to indicate a negative effect of the ytterbium codoping, presumably due to backtransfer from the excited erbium ions to ytterbium. For the P-silica films the opposite is true. The fluorescence intensity increases with ytterbium concentration. This indicates an efficient energy transfer in the P-doped glass.

Part (b) of the figure shows the fluorescence lifetime of the metastable erbium level as a function of Er/Yb ratio measured by modulating the laser diode externally. For the Ge-silicate films the lifetime is approximately 9 ms, independent of the ytterbium concentration. For the P-silicate films, however, the lifetime decreases with ytterbium concentration.

Based on these results it must be concluded that components based on Er/Yb in Ge-silicate glass are ineffective if the inclusion of ytterbium happens on the expense of the aluminium concentration. With the current deposition system, where the Er, Yb and Al flows are given as fractions of the total LDS flow, Ge-silicate therefore not a good host

for the Er/Yb system. P-silicate, however, have shown superior performance, as expected, and would be a good choice as host material.

6.3 Simulations of Er/Yb doped planar waveguides

The previous two sections have shown that Yb codoping of waveguides is only beneficial in P-silicate glass. To estimate the performance of Er/Yb doped components in P-silicate glass, I have made simulations on Er/Yb doped planar waveguide amplifiers and planar waveguide DBR lasers using the models presented in chapter 4.

6.3.1 Planar waveguide amplifiers

Previously, a loss-less Er/Al - doped planar waveguide 1×4 power splitter has been presented by the group [8]. The design consists of a 63 cm long folded amplifier integrated with the splitter that provides the sufficient gain to compensate for the coupling, propagation and splitting loss of 16 dB.

In order to determine the expected improvements on the long amplifier by codoping with ytterbium, I will here present simulations of a similar amplifier made in P-silicate glass. The erbium emission and absorption spectra, shown in figure 6.3, have been measured on a phosphosilicate fiber by Lumholt *et al.* [89], and the ytterbium spectra are the same as those shown in figure 5.8 on page 58 for an Al/Ge-silicate planar waveguide. According to Nilsson *et al.* [90], the gain is relatively insensitive to the Yb cross sections. In the simulations only a single pump wavelength of 980 nm is used, and therefore I don't expect a big influence of using ytterbium cross sections for a slightly different host glass. The ASE spectra used in the calculations are divided into 151 frequency slots for the ytterbium ASE, and 139 for erbium ASE. The upconversion and energy transfer coefficients have been assumed to be linearly dependent on the erbium and ytterbium concentrations

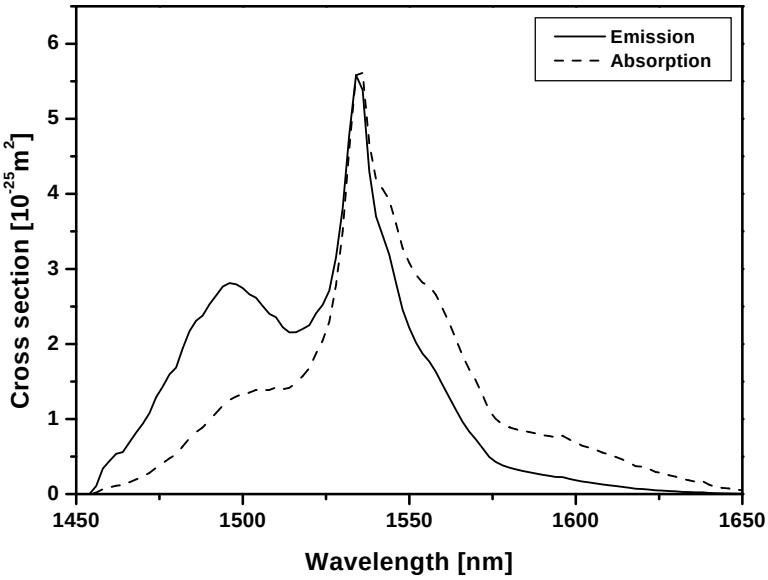

Figure 6.3: *Emission and absorption cross section spectra for erbium in P-doped silica. From [89]*

respectively, and values from [91, 56] have been used:

$$C_{up} = 3.5 \times 10^{-24}\mathrm{m}^3/\mathrm{s} + 2.4 \times 10^{-49}\mathrm{m}^6/\mathrm{s}(N_{Er} - 4.4 \times 10^{25}\mathrm{m}^{-3}) \quad (6.1)$$

$$C_{tr} = 1.0 \times 10^{-22}\mathrm{m}^3/\mathrm{s} + 4.0 \times 10^{-49}\mathrm{m}^6/\mathrm{s}(N_{Yb} - 1.0 \times 10^{25}\mathrm{m}^{-3}). \quad (6.2)$$

For erbium concentrations below 4.4×10^{25} ions/m^3 the upconversion coefficient have been set to 3.5×10^{-24} m^3/s. The erbium lifetime has been set to 7 ms, based on the measurements in section 6.2, while the ytterbium lifetime has been set to 1.3 ms which is common for phosphosilicate glasses [13]. Corresponding to the amplifier design, the waveguide dimensions are: length 63 cm, height: 4.5 μm and width: 8.0 μm, with a core-cladding index difference of 0.01. The propagation loss is 0.1 dB/cm for pump and signal. Recently, a model for simulating spiral and folded planar waveguide amplifiers was presented [92]. The model relies on a method of lines to resolve the effects of

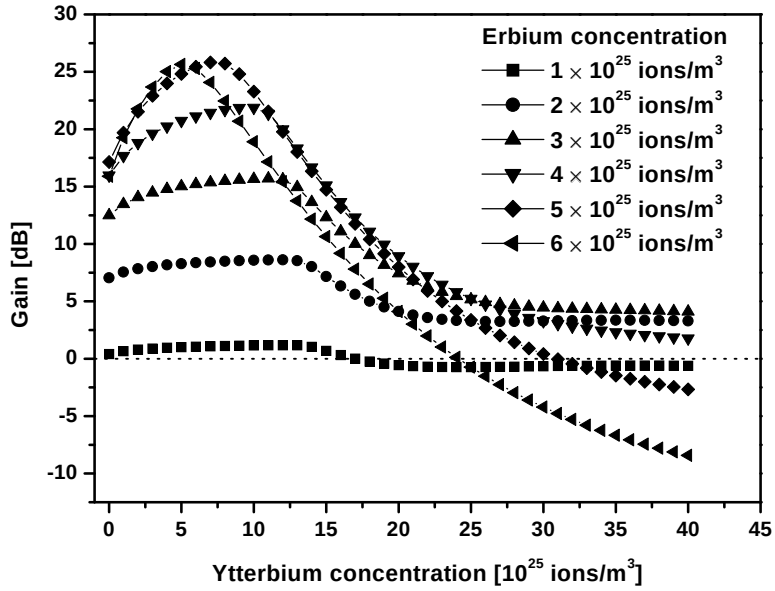

Figure 6.4: *Gain at 1535 nm as a function of ytterbium concentration. Codirectional pumping with 200 mW.*

the curved waveguides. However, in the design of the amplifier that I consider here, the bending radii was chosen large enough that bending loss could be neglected, and I will therefore consider the amplifier as being straight. I will consider two pumping schemes, codirectional and bidirectional pumping, to see if an improvement can be obtained by using bidirectional pumping. The model does not take coupling to the fibers into account, and the calculated gain is therefore the internal gain of the waveguide.

Figure 6.4 shows the gain at 1535 nm as a function of ytterbium concentration for increasing erbium concentration. The input signal power is 1 μW, and the waveguide is codirectionally pumped with 200 mW. An optimal ytterbium concentration, corresponding to maximum gain, can easily be identified for each value of the erbium concentration. The strong decrease of the gain if the ytterbium concentration is increased further, occurs because the pump is completely absorbed before it reaches the end of the waveguide leading to absorption of the signal.

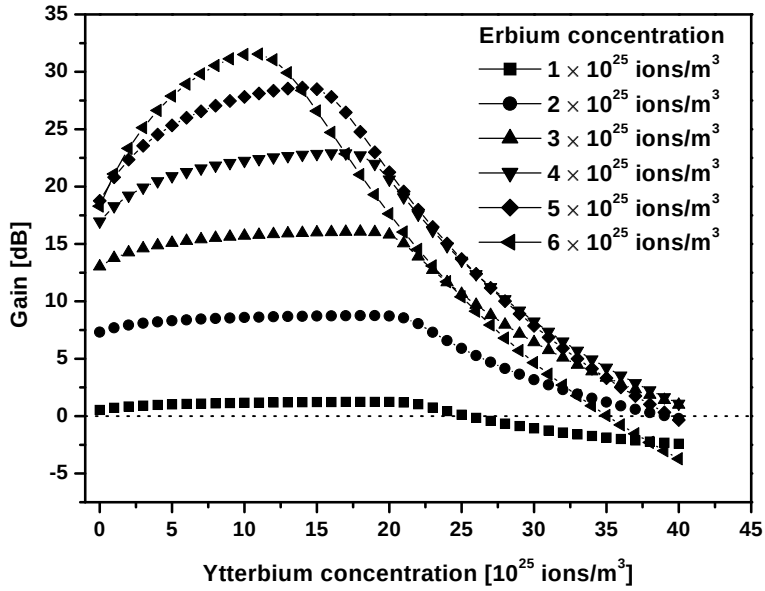

Figure 6.5: *Gain at 1535 nm as a function of ytterbium concentration. Bidirectional pumping with 100 mW in each direction.*

Figure 6.5 is similar to figure 6.4, except that bidirectional pumping is used. The total pump power is kept at 200 mW by launching 100 mW in each direction. Since the waveguide is pumped from both directions a situation with very little, or no, pump power can only be reached in the center of the waveguide at high ytterbium concentrations. In this way a higher ytterbium concentration can be used. However, the curves saturate above a certain ytterbium concentration, and *e.g.* for an erbium concentration of 4×10^{25} ions/m^3 nothing much is gained by increasing the ytterbium concentration above 10×10^{25} ions/m^3. If we compare with the results for codirectional pumping we see that the maximum obtainable gain is increased from approximately 25 to 30 dB with an erbium concentration of 6×10^{25} ions/m^3, but if the erbium concentration is 4×10^{25} ions/m^3, the maximum obtainable increase is less than one dB.

Figure 6.6(a) shows the gain as a function of the total pump power for the two pumping schemes and Yb/Er ratios of 0 and 2.5. The erbium concentration is 4×10^{25} ions/m^3 corresponding to the concen-

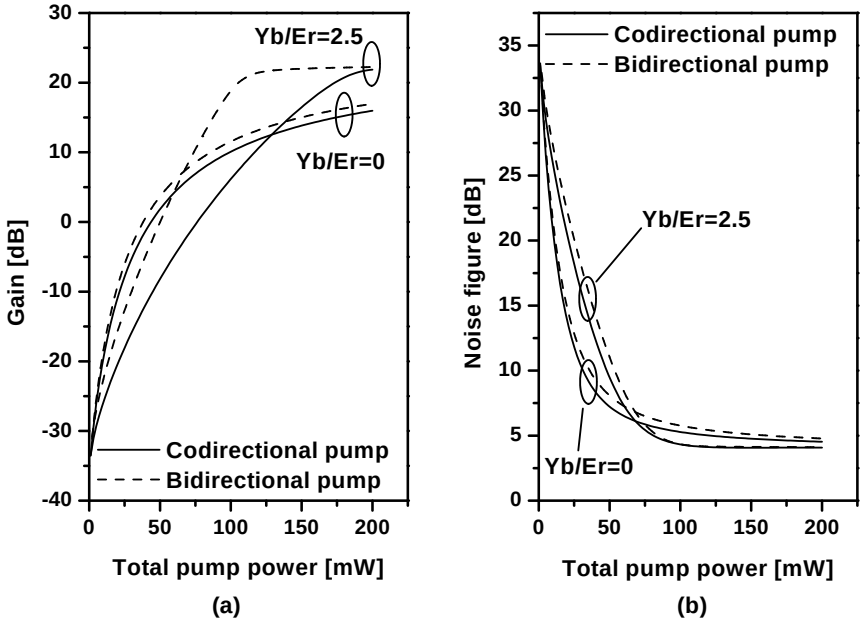

Figure 6.6: *(a) Gain as a function of pump power. (b) Noise as a function of pump power.*

tration of the folded amplifier. We see, that without ytterbium codoping the gain is not fully saturated at 200 mW, while the gain is fully saturated at 60 mW pump from both directions if ytterbium codoping and bidirectional pumping is used. This shows that the pump power can be used much more efficiently in an ytterbium codoped amplifier than an amplifier without ytterbium if bidirectional pumping is used. A higher gain can be obtained if ytterbium codoping is used since a higher inversion can be obtained with the more efficient pumping provided by the ytterbium codoping. However, at low pump powers (less than 50 mW) the gain of the ytterbium codoped amplifier is less than the gain of the amplifier without codoping for both pump schemes. This is because the pump power is insufficient to assure erbium inversion throughout the amplifier due to the strong ytterbium absorption. The effect of this can also be seen in part (b) of the figure as a higher noise figure for low pump powers. It is also seen that the noise figure decreases faster as a function of pump power for codirectional pumping than for bidirectional pumping when the total pump power is the same.

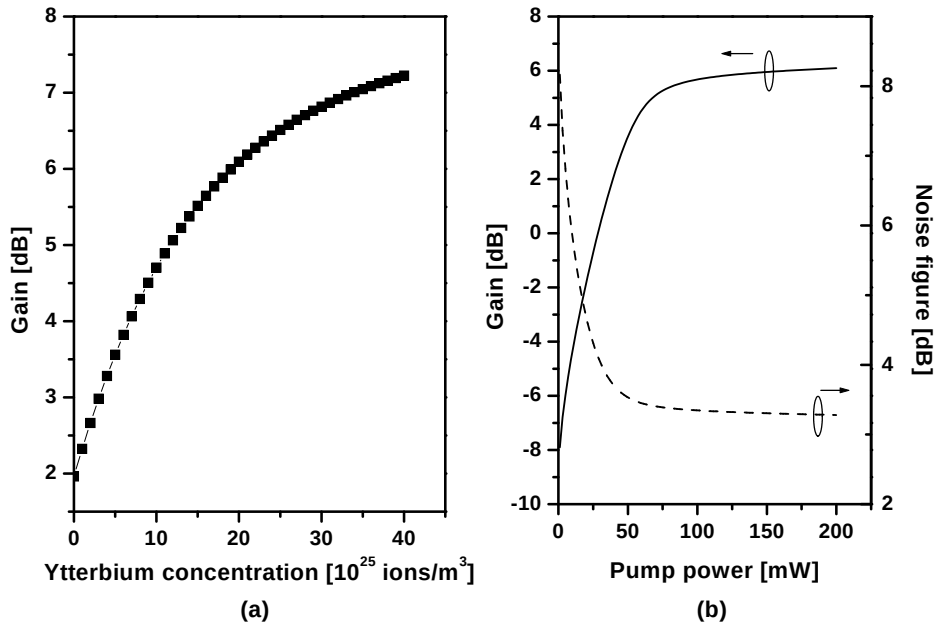

Figure 6.7: *Amplifier with an erbium concentration of* 12×10^{25} *ions/m*^{3} *pumped with 200 mW at 980 nm. (a) Gain as a function of ytterbium concentration. (b) Gain and noise figure as a function of pump power.*

This is in agreement with the observation that the initial inversion is, the lower the noise figure becomes [61]. For total pump powers higher than 100 mW the increase in noise figure for the codoped amplifier by using bidirectional pumping is negligible, and a noise figure of 4.1 dB is reached in both cases.

To summarise, a gain increase from 16 to 22 dB can be obtained by codoping with ytterbium to an Yb/Er ratio of 5/1 using the erbium concentration of the present components. If bidirectional pumping is used, the increased pump efficiency allows to reduce the total pump power to approximately 120 mW compared to the more than 200 mW needed to saturate the amplifier with codirectional pumping. There should be almost no penalty in the noise figure by using bidirectional pumping with the codoped amplifier.

A more elegant solution than a 63 cm long amplifier integrated with a 1×4 would be a short straight amplifier. The maximum length of

the waveguides on the 4 inch wafers is 6 cm, and to compensate for the splitting loss in a 1×4 splitter, a gain of 6 dB corresponding to 1 dB/cm would be required. Figure 6.7 (a) shows the gain as a function of ytterbium concentration for a 6 cm long amplifier with an erbium concentration of 12×10^{25} ions/m^3 pumped with 200 mW at 980 nm. We see, that a gain of 6 dB is reached for an ytterbium concentration of 20×10^{25} ions/m^3. Part (b) of the figure shows the gain (left axis) and noise figure (right axis) as a function of pump power. It requires approximately 150 mW of pump power to saturate the amplifier, and the noise figure will then be approximately 3.3 dB, 0.8 dB less than for the long amplifier. Very high concentrations are thus needed in order to make efficient short waveguides. Since phosphosilicate have to be used, the high concentrations are not unrealistic, as phosphate glass have been shown to hold very high concentrations while still maintaining a low degree of clustering [22].

6.3.2 Planar waveguide DBR lasers

In order to make lasers with UV written Bragg gratings using P-silicate glass as the core material, the UV sensitive section has to be moved away from the active section. This can be done by *e.g.* using a UV sensitive cladding, as in Er/Yb doped DFB fiber lasers [93], or a UV sensitive passive (or erbium doped) waveguide section should be made before and after the active Er/Yb-doped section on the wafer. The last solution is easy to implement in the laser model for a DBR laser. I will here consider the extreme case where passive gratings are used, use the optimised design from chapter 5, and consider a 50 mm long laser with a 20 mm cavity length, and gratings of length 10 and 20 mm respectively. The waveguide dimensions, index step and propagation loss are the same as for the amplifier simulations in the previous section. Using passive gratings instead of active gratings, means a dramatically reduced length of the amplifying part of the laser from 5 cm to 2 cm. The effect of this can be seen from figure 6.8 where the output power is shown as a function of grating coupling strength for a laser with active and passive gratings, respectively. The reduced length of the amplifier results in a much reduced output power, and stronger gratings are required to compensate for the reduced gain by providing stronger feedback to the cavity.

Figure 6.9 shows the output power as a function of pump power for a

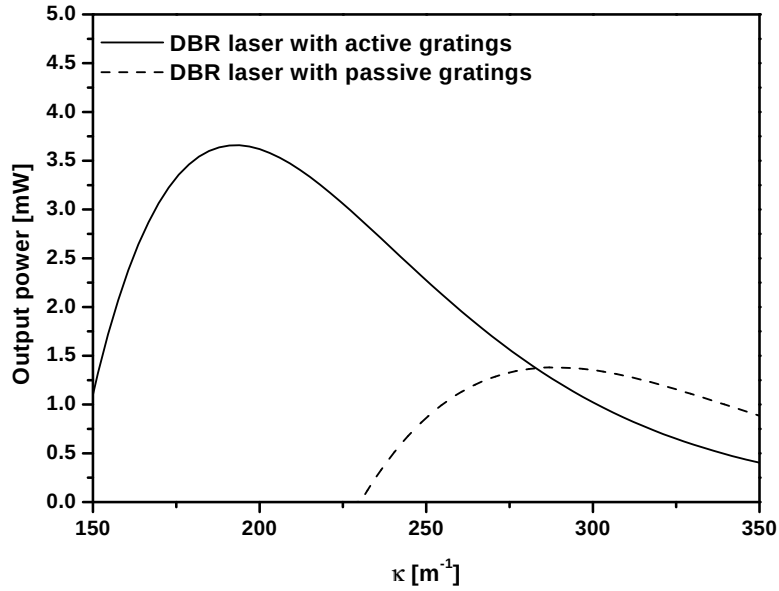

Figure 6.8: *Output power as a function of coupling strength. The dopant concentrations are Er:* 4×10^{25} *ions/m*^{3}*, Yb:* 8×10^{25} *ions/m*^{3}.

laser doped only with erbium. We see, that output powers of the order of 1 mW is achieved along with a very high pump threshold due to the limited gain in the short cavity. For a codoped laser, figure 6.10 shows the calculated output power as a function of pump power for increasing ytterbium concentration when the erbium concentration is fixed at 4×10^{25} ions/m^3. We see, that for an Er/Yb ratio of 1:10, an output power of approximately 11 mW is possible. The decrease in pump efficiency as the pump power increases corresponds to a bottleneck effect due to the finite energy transfer time from erbium to ytterbium (related to C_{tr} through $C_{tr} = 1/(t_{tr}N_{Er})$), and has also been observed experimentally [94].

If a photosensitive cladding is used, the maximum obtainable output power should be close to what can be obtained if the grating is written directly in the core. The main difference is that the grating have to be stronger to compensate for the fact that it will only be the evanescent field outside the core that will experience the refractive

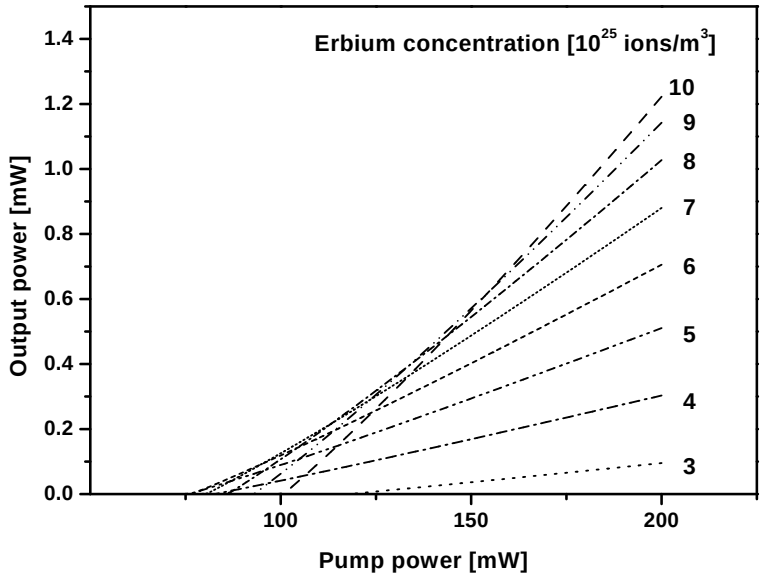

Figure 6.9: *Output as a function of pump power for a DBR laser with passive gratings. Pure erbium doping.*

index modulation. Thus an Er/Yb doped planar waveguide DFB laser should be realizable, and with erbium and ytterbium concentrations of 4×10^{25} ions/m^3 and 40×10^{25} ions/m^3 respectively an output power of 13 mW will be possible.

It is thus clear, that a huge increase in laser output power could be obtained by codoping with ytterbium, even with the alternative laser designs as proposed above.

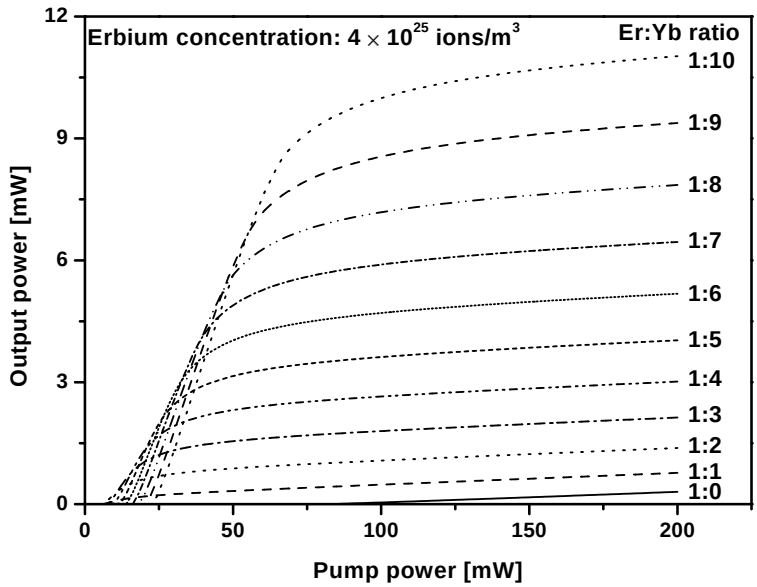

Figure 6.10: *Output as a function of pump power for a DBR laser with passive gratings. The erbium concentration is fixed at* 4×10^{25} *ions/m*^{3} *while the ytterbium concentration is varied.*

Chapter 7

Conclusion

This project have covered two areas: experimental work and numerical modelling. In the experimental part it has been investigated how to incorporate ytterbium in glass, both alone and as a sensitiser for erbium. Numerical modelling have then been applied to describe ytterbium and erbium/ytterbium doped lasers and amplifiers.

Ytterbium, erbium and aluminium doped films have been deposited using plasma enhanced chemical vapor deposition (PECVD) and a liquid delivery system (LDS), and waveguide structures have then been defined using reactive ion etching (RIE). The depostition and etching processes have been optimised to give planar waveguides of good optical quality with a propagation loss of approximately 0.1 dB/cm, and it has been demonstrated that there is good control of the dopant concentrations if only two of the dopants from the LDS system is used, while there is an overall decrease of dopant concentration if all three (Yb, Er, Al) are used.

Ytterbium doped waveguides have been made and optimised to show net gain in the 1000-1100 nm range. The optical properties of ytterbium were investigated, and it was shown that the emission properties of the ytterbium ions could be improved significantly by codoping with aluminium, which suggests a cluster-induced quenching of the excited ytterbium ions. Based on these results ytterbium doped waveguides with a net gain of more than 2 dB (0.36 dB/cm) at 1020 nm were made. The amplifying waveguides were then used to make DBR lasers by photoimprinting 5 mm long gratings in the waveguides. The lasers had a threshold of 12 mW and a slope efficiency of 14% yielding a total output power of 19 mW when pumped with 150 mW

at 976 nm. As expected for a DBR laser, the laser operated in two longitudinal modes. The measurements on the laser were compared to the theroretical model, and good agreement was observed. The model was then used to investigate how to optimise the design of DBR lasers with respect to maximum output power. For a 5 cm long laser it was shown that the caity length should be at least 2 cm if fine tuning of the phaseshift should be avoided. Furthermore, an asymmetric configuration where one grating is approximately twice as long as the other, will give a laser that emits from one end only, with a suppression of emission from the other end of more than 20 dB.

The erbium/ytterbium system was studied in germano-silicate and phospho-silicate glass. First, the influence of small amounts of ytterbium in erbium/aluminium doped germano-silica waveguides were investigated, and It was shown that even small amounts of ytterbium can reduce the erbium inversion. In a thin film experiment including both germano-silicate and phospho-silicate glass, it was shown that the erbium fluorescense decreases in germano-silicate when codoping with ytterbium. The inclusion of ytterbium is at the expense of aluminium, and hence this could explain the reduced fluorescense. However, in combination with the result of the germano-silica waveguide measurements, it seems that there is a high amount of backtransfer from erbium to ytterbium, and that germano-silica is a bad choice for a codoped erbium/ytterbium waveguide. Phospho-silicate, however, showed the expected good performance, and must be concluded to be superior for erbium/ytterbium codoping.

Based on this result the numerical models were used to estimate the effect of codoping with ytterbium if the components were made in phpspho-silicate glass. For a 63 cm long amplifier, it was shown that an increase in the internal gain of approximately 6 dB could be obtained by codoping with ytterbium to an Er/Yb ratio of 1:10 using bidirectional pumping. A short (6 cm) long amplifier was also investigated, and it was shown that a gain of 6 dB could be obtained using an erbium concentration of 12×10^{25} ions/m^3 and an ytterbium concentration of 20×10^{25} ions/m^3. This gain would be sufficient to compensate for the splitting loss in a 1×4 splitter. Er/Yb doped planar lasers were also modelled. If phospho-silica is used, it is not possible to make UV-written gratings using the present setup, and hence, the active region and the UV sensitive resion must be separated if lasers with UV written gratnigs are to be made. For a DBR laser with passive gratings

it was shown that an output power of 11 mW for an Er/Yb ratio of 1:10 should be possible when pumped with 200 mW at 976 nm. If a photosensitive cladding is used, a DFB laser should be possible with an output power of 13 mW with the same pump power and Er/Yb ratio as for the DBR laser.

Bibliography

[1] R. Mears, L. Reekie, I. Jauncey, and D. Payne, "Low-noise erbium-doped fibre amplifier operating at 1.54 μm," *Electronics Letters*, vol. 23, no. 9, pp. 1026–1028, 1987.

[2] www.ionas.dk.

[3] www.cisilias.dk.

[4] www.teemphotonics.com.

[5] www.kymata.com.

[6] www.symmorphix.com.

[7] S. Guldberg-Kjær, J. Hübner, M. Kristensen, C. Laurent-Lund, M. R. Poulsen, and M. Sckerl, "Planar waveguide laser in Er/Al-doped germanosilicate," *Electronics Letters*, vol. 35, no. 4, pp. 302–303, 1999.

[8] M. W. Sckerl, S. Guldberg-Kjær, C. L. Lund, and M. R. Poulsen, "Loss-less planar waveguide 1:4 power splitter at 1550 nm," in *ECOC'99 Nice*, 1999. Paper MoD1.

[9] W. J. Miniscalco, "Optical and electronic properties of rare earth ions in glasses," in *Rare Earth Doped Fiber Lasers and Amplifiers* (M. J. F. Digonnet, ed.), Marcel Dekker INC., 1993.

[10] S.Zemon, G. Lambert, L. Andrews, W. M. B. Hall, T. Wei, and R. Folweiler, "Characterization of Er^{3+}-doped glasses by fluorescense line narrowing," *Journal of Applied Physics*, vol. 69, no. 10, pp. 6799–6811, 1991.

[11] E. Desurvire, *Erbium doped fiber amplifiers: Principles and applications*. John Wiley and Sons, 1994.

[12] H. M. Pask, R. J. Carman, D. C. Hanna, A. C. Tropper, C. J. Mackechnie, P. R. Barber, and J. M. Dawes, "Ytterbium-doped silia fiber lasers: Versatile sources for the 1-1.2 μm region," *IEEE Journal of Selected Topics in Quantum Electronics*, vol. 1, no. 1, pp. 2–13, 1995.

[13] R. Paschotta, J. Nilsson, P. Barber, J. Caplen, A. Tropper, and D. Hanna, "Lifetime quenching in Yb-doped fibres," *Optics Communications*, vol. 136, pp. 375–378, 1997.

[14] B. J. Ainslie, S. P. Craig-Ryan, S. T. Davey, J. R. Armitage, C. G. Atkins, J. F. Massicott, and R. Wyatt, "Erbium doped fibres for efficient optical ampilfiers," in *Optical Amplifiers for Communication*, vol. 137 of *IEE Proceedings Pt. J*, pp. 205–208, 1990.

[15] R. S. Quimby, W. J. Miniscalco, and B. Thompson, "Clustering in erbium-doped silica glass fibers analyzed using 980 nm excited-state absorption," *Journal of Applied Physics*, vol. 76, no. 8, pp. 4472–4478, 1994.

[16] C. Y. Chen, R. R. Petrin, D. C. Yeh, and W. A. Sibley, "Concentration-dependent energy-transfer processes in Er^{3+}- and Tm^{3+}-doped heavy-metal fluoride glass," *Optics Letters*, vol. 14, no. 9, pp. 432–434, 1989.

[17] D. L. Dexter, "A theory of seinsitized luminescense in solids," *The Journal of Chemical Physics*, vol. 21, no. 5, pp. 836–850, 1953.

[18] J. L. Philipsen, *Highly Erbium-Doped Glasses and Photonic Components*. Ph.d. thesis, Research Center COM, Technical University of Denmark, 1999.

[19] B. J. Ainslie, "A review of the fabrication and properties of erbium-doped fibers for optical amplifiers," *IEEE Journal of Lightwave Technology*, vol. 9, no. 2, pp. 220–227, 1991.

[20] E. Desurvire, J. L. Zyskind, and C. R. Giles, "Design optimisation for efficient erbium-doped fibre amplifiers," *IEEE Journal of Lightwave Technology*, vol. 8, no. 11, pp. 1730–1741, 1990.

[21] K. Arai, H. Namikwa, K. Kumata, T. Honda, Y. Ishii, and T. Handa, "Aluminium or phosphorous co-doping effects on the fluorescense and structural properties of neodymium-doped silica glass," *Journal of Applied Physics*, vol. 59, no. 10, pp. 3430–3436, 1986.

[22] Y. Yan, A. Faber, H. d. Waal, P. Kik, and A. Polman, "Erbium-doped phosphate glass waveguide on silicon with 4.1 dB/cm gain at 1.535 μm," *Applied Physics Letters*, vol. 71, no. 20, pp. 2922–2924, 1997.

[23] S. W. Martin, "Review of the structure of phosphate glasses," *European Journal of Solid State Inorganic Chemistry, t*, vol. 28, pp. 163–205, 1991.

[24] M. A. Marcus and A. Polman, "Local structure around er in silica and sodium silicate glasses," *J. Non-Crystalline Solids*, vol. 136, pp. 260–265, 1991.

[25] S. J. Gurman, R. J. Newport, M. Overluizen, and E. J. Tarbox, "Extended x-ray absorption fine structure study of the rare earth sites in a neodymium doped glass," *Physical Chemistry of Glasses*, vol. 33, no. 1, pp. 30–32, 1992.

[26] B. Pedersen, A. Bjarklev, J. H. Povlsen, K. Dybdal, and C. Larsen, "The design of erbium-doped fiber amplifiers," *IEEE Journal of Lightwave Technology*, vol. 9, no. 9, pp. 1105–1112, 1991.

[27] J. E. Townsend, W. L. Barnes, K. P. Jedrzejewski, and S. G. Grubb, "Yb^{3+} sensitized Er^{3+} doped silica optical fibre with ultrahigh transfer efficiency and gain," *Electronics letters*, vol. 27, no. 21, pp. 1958–1959, 1991.

[28] W. L. Barnes, S. B. Poole, J. E. Townsend, L. Reekie, D. J. Taylor, and D. N. Payne, "$Er^{3+}-Yb^{3+}$ and Er^{3+} doped fiber lasers," *IEEE Journal of Lightwave Technology*, vol. 7, no. 10, pp. 1461–1465, 1989.

[29] B.-C. Hwang, S. Jiang, T. Luo, L. L. Neindre, J. Watson, and N. Peyghambarian, "Characterisation of cooperative upconversion and energy trnsfer of Er^{3+} and Yb^{3+}/Er^{3+} doped phosphate

glasses," in *Proc. SPIE - Int. Soc. Opt. Eng.*, vol. 3622, pp. 10–18, 1997.

[30] V. P. Gapontsev, S. M. Matitsin, A. A. Isieev, and V. B. Kravchenko, "Erbium glass lasers and their applications," *Optics and Laser Technology*, vol. 14, no. 4, pp. 189–196, 1982.

[31] F. D. Pasquale and M. Frederighi, "Improved gain characteristics in high-concentration Er^{3+}/Yb^{3+} codoped glass waveguide amplifiers," *IEEE Journal of Quantum Electronics*, vol. 30, no. 9, pp. 2127–2131, 1994.

[32] M. A. Lieberman and A. J. Lichtenberg, *Principles of Plasma Discharges and Materials Processing.* John Wiley and Sons, 1994.

[33] R. Syms and J. Cozens, *Optical guided waves and devices.* McGraw-Hill, 1992.

[34] L. C. Feldman and J. W. Mayer, *Fundamentals of Surface and Thin Film Analysis.* North-Holland, 1986.

[35] K. Hattori, T. Kitagawa, M. Oguma, H. Okazaki, and Y. Ohmori, "Optical amplification in Er^{3+}-doped $P_2O_5--SiO_2$ planar waveguides," *Journal of Applied Physics*, vol. 80, no. 9, pp. 5301–5308, 1996.

[36] T. Kitagawa, K. Hattori, M. Shimizu, Y. Ohmori, and M. Kobayashi, "Guided-wave laser based on erbium-doped silica planar lightwave circuit," *Electronics Letters*, vol. 27, no. 4, pp. 334–335, 1991.

[37] J. Shmulovich, "Er-doped glass waveguide amplifiers on silicon," in *Proc. SPIE - Int. Soc. Opt. Eng.*, vol. 2996, pp. 143–153, 1997.

[38] D. Barbier, P. Bruno, C. Cassagnettes, M. Trouillon, R. L. Hyde, A. Kevorkian, and J. M. P. Delavaux, "Net gain of 27 db with a 8.6 cm long Er/Yb doped glass planar amplifier," in *OFC'98, Technical Digest*, 1998. Paper TuH5.

[39] J. Shmulovich, A. Bruce, P. Hansen, T. Nielsen, D. Muehlner, G. Bogert, I. Brener, E. Laskowski, A. Paunescu, I. Ryazansky,

D. Jacobson, and A. White, "Integrated planar waveguide amplifier with 15 dB net gain at 1550 nm," in *OFC-'99 Techn. Digest.*, pp. PD42–1–PD42–3, 1999.

[40] K. Shuto, K. Hattori, T. Kitagawa, Y. Ohmori, and M. Horiguchi, "Erbium-doped phosphosilicate glass waveguide amplifier fabricated by PECVD," *Electronics Letters*, vol. 29, no. 2, pp. 139–141, 1993.

[41] S. A. Guldberg-Kjær, *Planar Waveguide Amplifiers and Lasers in Erbium Doped Silica.* Ph.d. thesis, Research Center COM, Technical University of Denmark, 1999.

[42] R. M. Almeida, X. M. Du, D. Barbier, and X. Orignac, "Er^{3+}-doped multicomponent silicate glass planar waveguides prepared by Sol-Gel processing," *J. Sol-Gel Sci. Techn.*, vol. 14, pp. 209–216, 1999.

[43] X. Orignac, D. Barbier, X. M. Du, R. m. Almeida, O. McCarthy, and E. Yeatman, "Sol-gel silica/titania-on-silicon er/yb-doped waveguides for optical amplification at 1.5 μm," *Optical Materials*, vol. 12, pp. 1–18, 1999.

[44] E. M. Yeatman, M. M. Ahmad, O. McCarthy, A. Vannucci, P. Gastaldo, D. Barbier, D. Mongardien, and C. Moronvalle, "Optical gain in er-doped $SiO_2 - TiO_2$ waveguides fabricated by the sol-gel technique," *Optics Communications*, vol. 164, pp. 19–25, 1999.

[45] P. Camy, J. E. Roman, F. W. Willems, M. Hempstead, J. C. van der Plaats, C. Prel, A. Beguin, A. M. Koonen, J. S. Wilkinson, and C. Lerminaux, "Ion-exchanged planar lossless splitter at 1.5 μm," *Electronics Letters*, vol. 32, no. 4, pp. 321–323, 1996.

[46] D. Barbier, M. Rattay, N. Kreps, M. Trouillon, F. Saint-Andrè, G. Clauss, and J. M. P. Delavaux, "Lossless 1×8 splitter integrated on Er/Yb doped phosphate glass and silicate glass," in *Proc. 8th Eur. Conf. Int. Opt. (ECIO'97)*, pp. 161–164, 1997.

[47] D. Barbier, L. du Mouza, Y. Jaouën, J. M. P. Delavaux, and P. Bruno, "Eight-wavelength amplifying combiner/splitter module

based on erbium/ytterbium-doped planar technology," in *Optical Amplifiers and their Applications (OAA'99)*, 1999. Paper FC5.

[48] J. L. Philipsen, D. Barbier, A. K. C. Cassagnettes, N. Krebs, and P. Bruno, "Compact gain-block consisting of an Er^{3+}-doped waveguide amplifier (edwa) and a pump/signal multiplexer, realized by ion exchange," in *Optical Amplifiers and their Applications*, 2000. Paper OTuD2.

[49] C. Laurent-Lund, M. R. Poulsen, M. Beukema, and J. E. Pedersen, "PECVD grown multiple core planar waveguides with extremely low interface reflections and losses," *IEEE Photonics Technology Letters*, vol. 10, no. 10, pp. 1431–1433, 1998.

[50] D. L. Veasey, D. S. Funk, N. A. Sanford, and J. S. Hayden, "Arrays of distributed-bragg-reflector waveguide lasers at 1536 nm in Yb/Er codoped phosphate glass," *Applied Physics Letters*, vol. 74, no. 6, pp. 789–791, 1999.

[51] K. A. Winick and G. L. Vossler, "Erbium:ytterbium planar waveguide laser in ion-exchanged glass," in *Proceedings of the SPIE - The International Society for Optical Engineering*, vol. 2996, pp. 121–134, 1997.

[52] J. E. Román, P. Camy, M. Hempstead, W. S. Brocklesby, S. Nouh, A. Béguin, C. Lerminaux, and J. S. Wilkinson, "Ion-exchanged Er/Yb waveguide laser at 1.5 μm pumped by laser diode," *Electronics Letters*, vol. 31, no. 16, pp. 1345–1346, 1995.

[53] T. Kitagawa, F. Bilodeau, B. Malo, S. Thériault, J. Albert, D. C. Jihnson, K. O. Hill, K. Hattori, and Y. Hibino, "Single-frequency Er^{3+}-doped silica-based planar waveguide laser with integrated photo-imprinted bragg reflectors," *Electronics Letters*, vol. 30, no. 16, pp. 1311–1312, 1994.

[54] H. Kogelnik and C. V. Shank, "Coupled-wave theory of distributed feedback lasers," *Journal of Applied Physics*, vol. 43, no. 5, pp. 2327–2335, 1972.

[55] M. Yamada and K. Sakuda, "Analysis of almost-periodic distributed feedback slab waveguides via a fundamental matrix approach," *Applied Optics*, vol. 26, no. 16, pp. 3474–3478, 1987.

[56] C. Lester, A. Bjarklev, T. Rasmussen, and P. G. Dinesen, "Modelling of Yb^{3+}-sensitized Er^{3+}-doped silica waveguide amplifiers," *IEEE Journal of Lightwave Technology*, vol. 13, no. 5, pp. 740–743, 1995.

[57] T. Rasmussen, J. H. Povlsen, A. Bjarklev, O. Lumholt, B. Pedersen, and K. Rottwitt, "Detailed comparison of two approximate methods for the solution of the scalar wave equation for a rectangular optical waveguide," *IEEE Journal of Lightwave Technology*, vol. 11, no. 3, pp. 429–433, 1993.

[58] K. O. Hill, Y. Fujii, D. C. Johnson, and B. S. Kawasaki, "Photosensitivity in optical fiber waveguides: Application to reflection filter fabrication," *Applied Physics Letters*, vol. 32, no. 10, pp. 647–649, 1978.

[59] G. Melz, W. W. Morey, and W. H. Glenn, "Formation of bragg gratings in optical fibers by a transverse holographic method," *Optics Letters*, vol. 14, no. 15, pp. 823–825, 1989.

[60] P. Varming, *Optical fiber lasers.* Ph.d. thesis, Department of Electromagnetic Systems, Technical University of Denmark, 1997.

[61] A. Bjarklev, *Optical fiber amplifiers: Design and system applications.* Artech House, 1993.

[62] D. J. E. Knight, F. Minardi, P. D. Natale, and P. Laporta, "Frequency doubling of a fibre-amplified 1083 nm DBR laser," *Eur. Phys. J. D*, vol. 3, pp. 211–216, 1998.

[63] R. Paschotta, D. C. Hanna, P. D. Natale, G. Modugno, M. Inguscio, and P. Laporta, "Power amplifier for 1083 nm using ytterbium doped fibre," *Optics Communications*, vol. 136, pp. 243–246, 1997.

[64] M. Bashkansky, M. D. Duncan, L. Goldberg, J. P. Koplow, and J. Reintjes, "Characteristics of a yb-doped superfluorescent fiber source for use in optical coherence tomography," *Optics Express*, vol. 3, no. 8, pp. 305–310, 1998.

[65] Y. Ohishi, T. Kanamori, T. Kitagawa, S. Takahashi, E-Snitzer, and G. Sigel, "Pr^{3+}-doped fluoride fiber amplifier operating at 1.31μm," *Optics Letters*, vol. 16, no. 22, pp. 1747–1749, 1991.

[66] H. M. Pask, A. C. Tropper, and D. C. Hanna, "A Pr^{3+}-doped ZBLAN fibre upconversion laser pumped by an Yb^{3+}-doped silica fibre laser," *Optics Communications*, vol. 134, pp. 139–144, 1997.

[67] P. R. Barber, H. M. Pask, C. J. Mackechnie, D. C. Hanna, A. C. Tropper, J. Massicott, S. T. Davey, and D. Szebesta, "Improved laser performance of Tm^{3+} and Pr^{3+}-doped ZBLAN fibres," in *CLEO Europe'94*, 1994. Paper CMF3.

[68] J. Qiu, M. Shojiya, Y. Kawamoto, and K. Kadono, "Energy transfer process and Tb^{3+} up-conversion luminescense in Nd^{3+}-Yb^{3+}-Tb^{3+} co-doped fluorozirconate glasses," *Journal of Luminescence*, vol. 86, pp. 23–31, 2000.

[69] H. W. Etzel, H. W. Gandy, and R. J. Ginther, "Stimulated emission of infrared radiation from ytterbium activated glass," *Applied Optics*, vol. 1, pp. 534–536, 1962.

[70] R. Allen and L. Esterowitz, "CW tunable ytterbium YAG laser pumped by titanium sapphire," *Electronics letters*, vol. 31, pp. 639–641, 1995.

[71] C. Hönninger, R. Paschotta, M. Graf, F. Morier-Genoud, M. Zhang, M. Moser, S. Biswal, J. Nees, A. Braun, G. A. Mourou, I. Johannsen, A. Giesen, W. Seeber, and U. Keller, "Ultrafast ytterbium-doped bulk lasers and amplifiers," *Applied Physics B*, vol. 69, pp. 3–17, 1999.

[72] D. C. Hanna, R. M. Percival, I. R. Perry, R. G. Smart, P. J. Suni, J. E. Townsend, and A. C. Trooper, "Continuous-wave oscillation of a monomode ytterbium-doped fiber laser," *Electronics Letters*, vol. 24, no. 17, pp. 1111–1113, 1988.

[73] J. Y. Allain, J. F. Bayon, M. Monerie, P. Bernage, and P. Niay, "Ytterbium-doped silica fibre laser with intracore bragg gratings operating at 1.02 μm," *Electronics Letters*, vol. 29, no. 3, pp. 309–310, 1993.

[74] C. Florea and K. A. Winick, "Ytterbium-doped glass waveguide laser fabricated by ion exchange," *IEEE Journal of Lightwave Technology*, vol. 17, no. 9, pp. 1593–1601, 1999.

[75] D. L. Veasey, D. S. Funk, P. M. Peters, N. A. Sanford, G. E. Obarski, N. Fontaine, M. Young, A. P. Peskin, W.-C. Liu, S. N. Houde-Walter, and J. S. Hayden, "Yb/Er-codoped and Yb-doped waveguide lasers in phosphate glass," *Journal of Non-Crystalline Solids*, vol. 263&264, pp. 369–381, 2000.

[76] S. Magne, Y. Ouerdane, M. Druetta, J. P. Goure, P. Ferdinand, and G. Monnom, "Cooperative luminescense in an ytterbium-doped silica fibre," *Optics Communications*, vol. 111, pp. 310–316, 1994.

[77] E. Montoya, O. Espeso, and L. E. Bausá, "Cooperative luminescense in Yb^{3+}:$LiNbO_3$," *Journal of Luminescense*, vol. 87–89, pp. 1036–1038, 2000.

[78] R. Paschotta, J. Nilsson, A. C. Tropper, and D. C. Hanna, "Ytterbium-doped fiber amplifiers," *IEEE Journal of Quantum Electronics*, vol. 33, no. 7, pp. 1049–1056, 1997.

[79] J. Capmany, E. Montoya, V. Bermúdez, D. Callejo, E. Diéguez, and L. E. Bausá, "Self-frequency doubling in Yb^{3+} doped periodically poled $LiNbO_3$:MgO bulk crystal," *Applied Physics Letters*, vol. 76, no. 11, pp. 1374–1376, 2000.

[80] D. E. McCumber, "Theory of phonon-terminated optical masers," *Physical Review*, vol. 134, pp. A299–A306, 1964.

[81] J.-M. Jouanno, J. Hübner, J. E. Pedersen, R. Kromann, T. Feuchter, and M. Kristensen, "Strong bragg gratings for WDM devices in non-sensitised low-loss Ge-doped waveguides," *Electronics Letters*, vol. 32, no. 23, pp. 2151–2152, 1996.

[82] L. Hofmann, A. Klehr, F. Bugge, H. Wenzel, V. Smirnitski, J. Sebastian, and G. Erbert, "180 mW DBR lasers with first-order grating in GaAs emitting at 1062 nm," *Electronics Letters*, vol. 36, no. 6, pp. 534–535, 2000.

[83] V. C. Lauridsen, J. H. Povlsen, and P. Varming, "Optimising erbium-doped DFB fibre laser length with respect to maximum output power," *Electronics Letters*, vol. 35, no. 4, pp. 300–302, 1999.

[84] J. Canning, M. G. Sceats, H. I. Inglis, and P. Hill, "Transient and permanent gratings in phoshposilicate fibers produced by the flash condensation technique," *Optics Letters*, vol. 20, no. 21, pp. 1–3, 1995.

[85] C. Montero, C. Gomez-Reino, and J. Brebner, "Planar bragg gratings made by excimer-laser modification of ion-exchanged waveguides," *Optics Letters*, vol. 24, no. 21, pp. 1487–1489, 1999.

[86] D. Geraghty, D. Provenzano, W. Marshall, S. Honkanen, A. Yariv, and N. Peyghambarian, "Gratings photowritten in ion-exchanged glass channel waveguides," *Electronics Letters*, vol. 35, no. 7, pp. 585–587, 1999.

[87] J. Hübner, *Index Engineering with Excimer Light.* Ph.d. thesis, Mikroelektronik Centeret, Technical University of Denmark, 1998.

[88] J. R. Armitage, "Spectral dependence of the small-signal gain around 1.5 μm in erbium doped silia fiber amplifiers," *IEEE Journal of Quantum Electronics*, vol. 26, no. 3, pp. 423–425, 1990.

[89] O. Lumholt, T. Rasmussen, and A. Bjarklev, "Modelling of extremely high concentration erbium.doped silica waveguides," *Electronics Letters*, vol. 29, no. 5, pp. 495–496, 1993.

[90] J. Nilsson, P. Scheer, and B. Jaskorzynska, "Modeling and optimisation of short Yb^{3+}-sensitised Er^{3+}-doped fiber amplifiers," *IEEE Photonics Technology Letters*, vol. 6, no. 3, pp. 383–385, 1994.

[91] M. Federighi and F. D. Pasquale, "The effect of pair-induced energy transfer on the performance of silica waveguide amplifiers with high Er^{3+}/Yb^{3+} concentrations," *IEEE Photonics Technology letters*, vol. 7, no. 3, pp. 303–305, 1995.

[92] W. Huang and R. R. A. Syms, "Analysis of folded erbium-doped planar waveguide amplifiers by the method of lines," *IEEE Journal of Lightwave Technology*, vol. 17, no. 12, pp. 2658–2664, 1999.

[93] L. Dong, W. H. Loh, J. E. Caplen, J. D. Minelly, K. Hsu, and L. Reekie, "Efficient single-frequency fiber lasers with novel photosensitive er/yb optical fibers," *Optics Letters*, vol. 22, no. 10, pp. 694–696, 1997.

[94] W. H. Loh, B. N. Samson, L. Dong, G. J. Cowle, and K. Hsu, "High performance single frequency fiber grating-based erbium:ytterbium-codoped fiber lasers," *IEEE Journal of Lightwave Technology*, vol. 16, no. 1, pp. 114–118, 1998.